

博士論文

**Long term change of sunshine duration in Nepal as influenced by
the atmospheric brown clouds and biomass burning**

(大気の色雲とバイオマス燃焼によって生じたネパール
における日照時間の長期的変化)

ニーラム ニロウラ

Doctoral Thesis

博士論文

**Long term change of sunshine duration in Nepal as influenced by
the atmospheric brown clouds and biomass burning**

(大気の色雲とバイオマス燃焼によって生じたネパール
における日照時間の長期的変化)

Neelam NIROULA

ニーラム ニロウラ

Department of Global Agricultural Sciences,
Graduate School of Agricultural and Life Sciences,
The University of Tokyo
1-1-1 Yayoi, Bunkyo-ku, Tokyo, 113-8657 Japan

Acknowledgement

This dissertation would not have been possible without the guidance and help of many individuals and organizations who in one way or another contributed and extended their valuable assistance in the preparation and completion of this study. I am very grateful for all the help and support. It is a pleasure to extend my cordial appreciation to all of them.

First of all, I want to thank my supervisor, Professor Kazuhiko Kobayashi, for his guidance and immeasurable support throughout the course of my research work and stay in Japan. Prof. Kobayashi has been a father figure who always encouraged and assisted me in my study.

I am heartily thankful to Dr. Jianqing Xu at Center for Research in Isotopes and Environmental Dynamics (CRiED) for her knowledgeable guidance while seeding this research. I would also like to extend my sincere appreciation to Dr. Kooiti Masuda at JAMSTEC, Yokohama. His expertise concerning data related to cloudiness was very valuable for the progression of this study. I am very thankful to Mr. Ram Chandra Karki at the Department of Hydrology and Meteorology (DHM), Nepal, for the support and cooperation in obtaining the meteorological data. I would also like to extend my sincere appreciation to Assoc. Prof. Kae Miyazawa and Assoc. Prof. Mark Lieffering for their thoughtful suggestions.

Special thanks to Ms. Harumi Uwai for the lab assistance throughout my stay in Japan, in particular for coping with my lack of Japanese proficiency. I would also like to appreciate the invaluable support and encouragement from my colleagues and seniors, especially Ms. Shen Yinyue.

My sincere gratitude to the Government of Japan for the Monbukagakusho (MEXT) Scholarship that supported me the whole time. I would also like to acknowledge Dr. Sunil Adhikari for the words of advice to pursue my higher studies in Japan.

I would also like to acknowledge all the data sources for their immense work in putting together the scientific data I have used for this study. Thank you DHM, Nepal for the meteorological data; NASA/LANCE - FIRMS for the MODIS active fire and burnt area products; ESA GlobCover 2009 Project for the landuse product; and NASA Langley

Research Center Atmospheric Science Data Center for The GEWEX Radiative Flux Assessment data.

Finally, I would like to express my gratitude towards my friends and families for their endless love, support and understanding. I am blessed to have my mother Ms. Sumitra Devi and my father Mr. Nayan Kumar Niroula as my parents, who nurtured me with quality education and good values and are responsible for making me the person who I am today.

Last but not the least, I don't have enough words to thank my husband, Uttam Paudel, whose immense love, support and encouragement throughout my study period has enabled me to accomplish my dream of holding a doctoral degree. Thank you very much.

Neelam Niroula

Tokyo, Japan

March, 2015

Summary

Chapter 1. Introduction: Background and objectives of study.

Solar radiation (SR) at earth's surface is the primary energy source for life on our planet. Over the past decades, there had been significant reduction in SR referred to as 'global dimming' in regions with high concentrations of anthropogenic aerosols such as India and China. These aerosols are produced as a result of large scale combustion of fossil fuels and biomass burning and have significant impacts on hydrological cycle, monsoon circulation and regional climate change.

In Nepal, the Himalayas in the north act as a barrier that separates a region of abundant aerosols in the Indo-Gangetic plains (IGP). These aerosols transform into thick, persistent layers of haze known as 'atmospheric brown clouds' (ABC) and are transported to as far as the Himalayas. In addition to the trans-boundary air pollution, local pollution has increased drastically in major urban cities of Nepal. Despite such evidences of local and regional air pollution, no study on change in SR has been reported for Nepal. In this thesis, I elucidated long term changes in SR by analyzing temporal changes in sunshine duration (SSD) over an extended period in Nepal and identified the major drivers of the observed changes in SSD. I also identified the sources contributing to the major drivers with particular focus on aerosol emissions from different combustion sources and the influence of trans-boundary air pollution.

Chapter 2. Long term trends of sunshine duration in Nepal for the period 1987-2010.

In this chapter, I analyzed temporal changes of SSD in Nepal across its three physiographic regions: plains, low-hills (LH) and high-hills and mountains (HHM) for the period 1987-2010 with the records at 13 meteorological stations. I found declining trends in SSD, i.e. solar dimming, across the country at a rate of -0.20% per year with the highest decline in post-monsoon season (-0.33% per year) followed by pre-monsoon season (-0.24% per year). A close look at the individual stations indicated that the declines in pre-monsoon and post-monsoon seasons are common regional phenomena. By region, the dimming was pronounced (-0.56% per year) in the plains (<300 m a.s.l.) and gradually diminishes with an increase in elevation. The decline in the stations in the

plains closely matched the decreasing trends observed at the stations lying in IGP confirming the persistence of dimming over the region.

Chapter 3. Possible drivers of the decline in sunshine duration in Nepal.

In this chapter, I identified the major drivers of the decline in SSD by analyzing trends in SSD on clear days (S_{clear}) to understand the role of aerosols and trends in SSD on cloudy days (S_{cloudy}) to understand the influence of clouds across the period 1987-2007. A significant decline was found in S_{clear} trends at a rate of -0.42% per year, with intense dimming at the stations located in the plains and Kathmandu, suggesting direct effect of aerosols. Seasonally, the decline in S_{clear} was evident in all the dry seasons (October to May) in the plains, with highest dimming at a rate of -1.27% per year in the winter season. On the other hand, the trends in S_{cloudy} showed intense dimming at a rate of -3.27% per year with strong decline in all the three regions. Seasonally, the highest decline in S_{cloudy} occurred in monsoon followed by pre-monsoon seasons.

The 8 times higher decline in S_{cloudy} compared to S_{clear} indicated that clouds play much larger role in the observed dimming than aerosols which could be likely due to the increasing trends in cloud amount. Trends in total rainfall (R) did not show any significant increase which could explain an increase in cloud amount rather a significant decline was observed in total number of rainy days (NRD). Analysis of light rainfall ($R \leq 10\text{mm}$, $\text{NRD} \leq 10\text{mm}$) and heavy rainfall ($R \geq 45\text{mm}$, $\text{NRD} \geq 45\text{mm}$) revealed significant decline in light rainfall while moderate increase was observed in heavy rainfall. Such anomalies in light and heavy rainfall occurrences suggested the role of indirect effect of aerosols, in which the aerosols could interact with the clouds to suppress light rainfall from shallow clouds but could increase the rainfall from deep clouds in the later stage. The aerosols induced increase in shallow and deep clouds as reflected by the decrease in light rainfall and increase in heavy rainfall could be the most plausible explanation for the high dimming observed in S_{cloudy} in Nepal.

Hence, both direct and indirect effects of aerosols have been identified as the major driver of the dimming in plains while aerosol indirect effect plays a crucial role in the dimming in LH and HHM.

Chapter 4. Influence of biomass burning and long-range transport of pollutants on aerosol variations in Nepal.

As aerosols were identified as the major driver of the decline in SSD, major sources of aerosols were sought out in this chapter. Among the two major divisions of aerosol sources: biomass burning and fossil fuel combustion, the emissions from biomass burning were estimated to be approximately three times the emissions from fossil fuel combustion, contributing on average to 74% of the total emissions (black carbon and SO₂) in Nepal. To understand aerosol variations and its relation to biomass burning, Moderate Resolution Imaging Spectroradiometer (MODIS) derived firecounts and aerosol optical depth (AOD) were analyzed for the period 2005-2010. The highest mean AOD values (0.495) and maximum firecounts (53% of total firecounts) both occurred in April and were found to be in peak values in pre-monsoon season. Acute pollution (AP) events characterized by significant increase in AOD values were identified for two locations: Simara and Kathmandu. A coupling of air mass backward trajectory analysis with MODIS firecounts identified 55% of the AP events in Simara and 60% of the AP events in Kathmandu, respectively, to be influenced by biomass burning referred to as 'biomass burning (BB) pollution events'. Regional frequency of firecounts for different seasons during BB pollution events suggested that biomass burning occurring in Nepal could strongly influence the occurrence of highest AOD in pre-monsoon season, while trans-boundary biomass burning was dominant in all the other seasons.

Cluster analysis of air mass backward trajectories arriving at Kathmandu showed that air masses from highly polluted IGP were carried by the prevailing winds, and caused peak AOD in the winter season. The peak AOD in the pre-monsoon season was significantly contributed by air masses originating in the North-eastern states of India, Meghalaya, dominated by slash and burn agriculture; and air masses from Punjab, characterized by wheat residue burning. The air masses originating in the Bay of Bengal indicated the pathway of the Indian summer monsoon (ISM) circulation, which brings pollutants in early monsoon causing peak AOD in June. Weakening of ISM, known as 'break' periods, dominated by westerly circulations also contributed to peak AOD in June. The polluted smoke of rice residue burning occurring on a large scale in Punjab of the northern IGP caused peak AOD in post-monsoon season despite its negligible contribution in total trajectories.

Chapter 5. Synthesis and implications.

In this chapter, I synthesized the findings in previous chapters. A significant decline was observed in SSD particularly in the plains of Nepal. Seasonal analysis of the trends revealed intense dimming in plains in all the dry seasons under clear days. While intense dimming under cloudy days occurred in all the three regions particularly in the monsoon season. Aerosols released from biomass burning during pre-monsoon season in Nepal and transport of air pollutants from Indian subcontinent were identified as the major determinants of peak AOD in Nepal.

The observed dimming and peak AOD concentrations will have large implications on agriculture in Nepal. The main growing season (November to April) of wheat and dry season rice in the plains, coincides with the peak AOD values and significant dimming in S_clear, observed in the winter and pre-monsoon seasons. Similarly the significant dimming observed in S_cloudy in monsoon season coincides with the rice growing season (July to October) in both plains and LH. The observed reduction in SR would significantly reduce the photosynthetic rate of the crops and other vegetation (forests, grasslands and shrublands) and lower productivity, influencing the livelihood and food security of a large population base.

Such impacts of dimming and the ABC on agriculture calls for immediate action to mitigate aerosol emissions both at national and international levels. The mitigation efforts could include controlled fires in protected areas, use of improved cooking stoves, and awareness about the implications of forest fires to reduce emissions from biomass burning. A larger international collaboration and cooperation will be required to fix the problem of trans-boundary air pollution. It is important to understand that the mitigation efforts to reduce aerosol emissions represent a rewarding step for the food security and regional climate.

Table of contents

Acknowledgement.....	i
Summary	iii
Table of contents	vii
Lists of tables	x
List of figures	xi
List of acronyms.....	xiii
Chapter 1	1
1. INTRODUCTION: BACKGROUND AND OBJECTIVES OF STUDY	1
1.1. Background	1
1.1.1. Solar radiation and sunshine duration.....	1
1.1.2. Modifiers of solar radiation: Clouds and aerosols	2
1.1.3. Atmospheric brown clouds and its sources: biomass burning and fossil fuel combustion	2
1.1.4. Atmospheric brown clouds and its impacts on regional climate change ..	3
1.2. Scope of this study	4
1.3. Outline of the thesis	6
Chapter 2	8
2. LONG TERM TRENDS OF SUNSHINE DURATION IN NEPAL FOR THE PERIOD 1987-2010	8
2.1. Introduction.....	8
2.2. Materials and methods	8
2.2.1. The study area.....	8
2.2.2. Weather records and analysis	9
2.3. Results.....	11
2.3.1. Individual stations, regional and all-Nepal annual sunshine duration trends	11
2.3.2. Seasonal sunshine duration trends and distribution across regions	14
2.4. Discussions.....	17
Chapter 3	20
3. POSSIBLE DRIVERS OF THE DECLINE IN SUNSHINE DURATION IN NEPAL	20
3.1. Introduction.....	20
3.2. Materials and methods	21

3.2.1.	Sunshine duration.....	21
3.2.2.	Total cloud fraction.....	21
3.2.3.	Calculation of sunshine duration on clear days and sunshine duration on cloudy days.....	22
3.2.4.	Rainfall records.....	22
3.3.	Results.....	23
3.3.1.	Trends in sunshine duration on clear days and sunshine duration on cloudy days.....	23
3.3.1.1.	Inter annual trends in sunshine duration on clear days and sunshine duration on cloudy days (1987-2007)	23
3.3.1.2.	Seasonal trends in sunshine duration on clear days and sunshine duration on cloudy days (1987-2007)	25
3.3.2.	Trends in rainfall and number of rainy days.....	27
3.3.2.1.	Trends in total rainfall and total number of rainy days (1980-2009).....	27
3.3.2.2.	Trends in light rainfall (1980-2009).....	29
3.3.2.3.	Trends in heavy rainfall (1980-2009).....	32
3.3.3.	Seasonal trends in light rainfall and its relation to sunshine duration on cloudy days.....	35
3.4.	Discussion	37
3.4.1.	Contribution of atmospheric brown clouds to “aerosols direct effect” ...	37
3.4.2.	Contribution of atmospheric brown clouds to “aerosols indirect effect”	38
3.4.2.1.	Aerosol - clouds interactions in pre-monsoon season.....	38
3.4.2.2.	Aerosol - clouds interactions in monsoon season	39
3.4.2.3.	Winter rainfall	41
3.4.3.	Sources and transportation of atmospheric brown clouds	42
Chapter 4	43
4.	INFLUENCE OF BIOMASS BURNING AND LONG-RANGE TRANSPORT OF POLLUTANTS ON AEROSOL VARIATIONS IN NEPAL	43
4.1.	Introduction	43
4.2.	Data	44
4.2.1.	MODIS aerosol optical depth	44
4.2.2.	MODIS active fire and burnt area products	44
4.2.3.	Land cover data.....	45

4.2.4.	GDAS meteorological data.....	46
4.3.	Methods.....	46
4.3.1.	Estimation of aerosol emissions	46
4.3.2.	Estimation of influence of biomass burning	48
4.3.2.1.	Selection of study area	48
4.3.2.2.	Identification of acute pollution events	49
4.3.2.3.	Calculation of air mass backward trajectory	49
4.3.2.4.	Identification of the acute pollution events affected by biomass burning	50
4.3.2.5.	Cluster analysis for long-range transport of pollutants	50
4.4.	Results.....	51
4.4.1.	Aerosols (Black carbon and SO ₂) emissions (1995-2009)	51
4.4.2.	Temporal and spatial variations of aerosols and biomass burning	54
4.4.2.1.	Variations in aerosol optical depth (2005-2010).....	54
4.4.2.2.	Variations in MODIS active firecounts (2005-2010).....	55
4.4.3.	Influence of biomass burning in aerosol variations	58
4.4.4.	Influence of long distance transport of polluted air mass on aerosol variations	64
4.5.	Discussion	67
4.5.1.	Aerosol optical depth variations in Nepal.....	67
4.5.2.	Contribution of biomass burning to aerosol optical depth.....	68
4.5.3.	Contribution of atmospheric circulations and long range transport of pollutants to aerosol optical depth.....	69
4.6.	Conclusion	71
Chapter 5	72
5. SYNTHESIS AND IMPLICATIONS.....	72
5.1.	Dimming and its possible drivers.....	72
5.2.	Major sources of aerosols, biomass burning and long-range transport of air pollutants.....	73
5.3.	Implications of dimming and atmospheric brown clouds on agriculture in Nepal.....	75
References:	78
Appendices.....	97

Lists of tables

Table 2-1 Details of the observation records of sunshine duration.	10
Table 2-2 All-Nepal annual mean of daily total sunshine duration (SSD, hour), monthly total SSD (hour) and inter-annual trends (%/year) in SSD across the stations and physiographic regions for the period 1987-2010 (SSD).	12
Table 2-3 Inter-annual trends in sunshine duration (SSD) and interaction between stations and years in the three physiographic regions for the period 1987-2010.	14
Table 2-4 Regional and all-Nepal trends in sunshine duration (SSD, %/year) by season for the period 1987-2010.	15
Table 3-1 All-Nepal inter-annual trends (%/yr) in annual mean SSD on clear days (S_clear) and SSD on cloudy days (S_cloudy) across the stations and physiographic regions for the period 1987-2007.	24
Table 3-2 Regional and all-Nepal trends in sunshine duration on clear days (S_clear, %/year) by season for the period 1987-2007.	26
Table 3-3 Regional and all-Nepal trends in sunshine duration on cloudy days (S_cloudy, %/year) by season for the period 1987-2007.	26
Table 3-4 All-Nepal mean annual total and inter-annual trends in total rainfall and total number of rainy days (NRD) across the stations and physiographic regions for the period 1980-2009.	28
Table 3-5 Inter-annual trends in rainfall less than 10mm per day ($R \leq 10$) and number of rainy days with rainfall less than 10mm per day ($NRD \leq 10$) across the stations and physiographic regions for the period 1980-2009.	30
Table 3-6 Inter-annual trends in rainfall more than 45mm per day ($R \geq 45$) and number of rainy days with rainfall more than 45mm per day ($NRD \geq 45$) across the stations and physiographic regions for the period 1980-2009.	33
Table 3-7 Regional and all-Nepal trends in heavy rainfall ($R \geq 45$ mm per day) and number of rainy days with light rainfall ($NRD \geq 45$ mm per day) by season for the period 1987-2009.	35
Table 3-8 Regional and all-Nepal trends in light rainfall ($R \leq 10$ mm per day) and number of rainy days with light rainfall ($NRD \leq 10$ mm per day) by season for the period 1987-2009.	36
Table 4-1 Emission factors in g/kg for different aerosols for different fuel types.	47
Table 4-2 Emission factors in g/kg for different aerosols for different vegetation types.	48
Table 4-3 Correlation coefficients between monthly total fire-counts (FC) and monthly mean aerosol optical depth (AOD) in different physiographic regions for pre-monsoon season (2005-2010).	57
Table 4-4 Seasonal frequency of each cluster reaching Kathmandu in 2005-2010.	64

List of figures

Figure 2-1 Map of Nepal, showing location of the meteorological stations, the three physiographic regions and five development regions. The names of the stations are abbreviated with the first three characters except for the station Dhankuta (DHK).....	9
Figure 2-2 Estimated trends in annual mean monthly total sunshine duration (SSD, hour/month) at individual stations in plains (a), low-hills (b), and high-hills and mountains (c) for the period from 1987 to 2010. Symbols are the observations and lines are the linear model fit.	13
Figure 2-3 Monthly mean sunshine duration (SSD, hour/day) averaged across the 13 stations for the period from 1987 to 2010.....	15
Figure 2-4 Trends (%/year) in annual and seasonal means of sunshine duration in Nepal over the period from 1987 to 2010. (\square -plains, \star -low-hills and Δ -high-hills and mountains)	16
Figure 2-5 Monthly total sunshine duration in Kathmandu averaged across two decades 1991 to 2000 and 2001 to 2010.	18
Figure 3-1 Trends in annual total (average of 13 stations) rainfall and number of rainy days (NRD) for the period 1980-2009. Symbols are the observations and lines represent trend.	29
Figure 3-2 Trends in annual total (average of 13 stations) (a) rainfall less than 5mm per day ($R \leq 5$) and 10mm per day ($R \leq 10$) and (b) number of rainy days with rainfall less than 5mm per day ($NRD \leq 5$) and 10mm per day ($NRD \leq 10$) for the period 1980-2009. Symbols are the observations and lines represent trend.	31
Figure 3-3 Trends in annual total (average of 13 stations) (a) rainfall more than 40mm per day ($R \geq 40$) and 45mm per day ($R \geq 45$) and (b) number of rainy days with rainfall more than 40mm per day ($NRD \geq 40$) and 45mm per day ($NRD \geq 45$) for the period 1980-2009. Symbols are the observations and lines represent trend.....	34
Figure 4-1 Study area (in red border) selected to detect the influence of biomass burning within and outside the boundary of Nepal (in thin black border). The red dots indicate MODIS active firecounts and the symbols (in black) indicates the location of Simara and Kathmandu.	48
Figure 4-2 Total burnt areas in different vegetation types derived from Globcover 2009 and MODIS burnt area product from 2005 to 2010.....	51
Figure 4-3 Black carbon (BC) emissions from fossil fuel combustion and biomass burning in Nepal from 1995 to 2009. Note that the contribution from open burning of 'Forest and Savanna' and 'Crop residue' is accounted for only from 2000/2001 on...	52
Figure 4-4 Sulfur dioxide (SO_2) emissions from fossil fuel combustion and biomass burning in Nepal from 1995 to 2009. Note that the contribution from open burning of 'Forest and Savanna' and 'Crop residue' is accounted for only from 2000/2001 on...	53

Figure 4-5 Total emissions (sum of BC and SO ₂) from fossil fuel combustion and biomass burning in Nepal from 1995 to 2009. Note that the contribution from open burning of ‘Forest and Savanna’ and ‘Crop residue’ is accounted for only from 2000/2001 on.	53
Figure 4-6 Monthly mean aerosol optical depth (AOD) for Nepal averaged across 2005 to 2010.	54
Figure 4-7 Annual mean aerosol optical depth (AOD) in different physiographic regions from 2005 to 2010.....	55
Figure 4-8 Monthly mean MODIS active firecounts for Nepal averaged across 2005 to 2010.....	56
Figure 4-9 Annual total MODIS active firecounts in different physiographic regions from 2005 to 2010.....	56
Figure 4-10 Density map of MODIS active firecounts showing biomass burning in pre-monsoon seasons in Nepal from 2005-2010. Symbols indicate location of field survey.	58
Figure 4-11 Time series of daily mean aerosol optical depth (AOD) and acute pollution events in (a) Simara and (b) Kathmandu from 2005 to 2010.	59
Figure 4-12 Monthly variations in firecounts intercepted by the trajectories arriving at (a) Simara and (b) Kathmandu from 2005 to 2010.....	60
Figure 4-13 Number of acute pollution events possibly influenced by biomass burning in the region (a) Simara and (b) Kathmandu for the period 2005-2010.	62
Figure 4-14 Regional frequency (%) of firecounts for different seasons during biomass burning (BB) pollution events (a) Simara and (b) Kathmandu across the observation period (2005-2010). Numbers at the top of each column indicate the total number of firecounts intercepted during BB pollution events.	63
Figure 4-15 Mean backward trajectories for clusters 1 to 6 arriving at Kathmandu (KAT) across the period 2005-2010. See Appendix Fig. 3 for all the trajectories in each cluster.	64
Figure 4-16 Monthly variation in mean AOD by trajectory clusters in Kathmandu in 2005-2010	65
Figure 4-17 Mean backward trajectories for clusters 1 to 6 arriving at Simara (SIM) across the period 2005-2010.	66

List of acronyms

ABC	Atmospheric Brown Clouds
AERONET	Aerosol Robotic NETwork
AOD	Aerosol Optical Depth
AP	Acute Pollution
ARL	Air Resources Laboratory
ASDC	Atmospheric Science Data Center
BB	Biomass Burning
BC	Black Carbon
CALIPSO	Cloud-Aerosol LiDAR and Infrared Pathfinder Satellite Observation
CBS	Central Bureau of Statistics, Nepal
CCN	Cloud Condensation Nuclei
DHM	Department of Hydrology and Meteorology
EEA	European Environmental Agency
EMEP	European Monitoring and Evaluation Program
EOS	Earth Observing System
ESA	European Space Agency
ESRI	Environmental Systems Research Institute
FC	Fire-Counts
FIRMS	Fire Information for Resource Management System
GCM	Global Circulation Model
GDAS	Global Data Assimilation System
GEWEX	Global Energy and Water Cycle Experiment
GJ	Giga Joule
GRIB	GRIdded Binary
HDF	Hierarchical Data Format
HHM	High-Hills and Mountains
HKHT	Hindu Kush-Himalayan-Tibetan
HYSPLIT	Hybrid Single Particle Lagrangian Integrated Trajectory Model
IGP	Indo-Gangetic Plains
IPCC	Intergovernmental Panel on Climate Change
ISM	Indian Summer Monsoon
JAMSTEC	Japan Agency for Marine-Earth Science and Technology
LANCE	Land Atmosphere Near real-time Capability for EOS
LH	Low-Hills

LPG	Liquefied Petroleum Gas
MERIS	Medium-Resolution Imaging Spectrometer (ESA - Envisat)
MEXT	Ministry of Education, Culture, Sports, Science and Technology, Japan
MODIS	Moderate Resolution Imaging Spectroradiometer (EOS)
NASA	National Aeronautics and Space Administration
NCEP	National Center for Environmental Prediction
NCO-P	Nepal Climate Observatory-Pyramid
NOAA	National Oceanic and Atmospheric Administration
NRD	Number of Rainy Days
OC	Organic Carbon
SD	Sunshine Duration
SDS	Scientific Data Sets
SR	Solar Radiation
SRB	Surface Radiation Budget
SSD	Sunshine Duration
SST	Sea Surface Temperature
TCC	Total Cloud Cover
TCF	Total Cloud Fraction
TRMM	Tropical Rainfall Measuring Mission
UTC	Coordinated Universal Time
WECS	Water and Energy Commission Secretariat
WMO	World Meteorological Organization

Chapter 1

1. INTRODUCTION: BACKGROUND AND OBJECTIVES OF STUDY

1.1. Background

1.1.1. Solar radiation and sunshine duration

Solar radiation (SR) is the ultimate source of energy for life on Earth and governs a wide range of physical and ecological processes such as surface energy exchange, snow and glacier melt, photosynthesis and associated plant growth (Wild, 2009). On a more applied level, knowledge of SR is crucial for solar energy technologies and agricultural production. Therefore, a substantial change in the availability of SR on earth's surface can have profound impacts on our environment. Such changes are identified through worldwide networks of pyranometers, the measurement devices that record SR. However, in regions with scarce networks of pyranometers, SR can be measured by its proxies such as sunshine duration (SSD), cloud cover, pan-evaporation or reference evapotranspiration. Among these proxies, SSD is one of the oldest and most robust measures for use as a proxy of SR (WMO, 2003).

Long-term observations of SR flux at the ground surface across the globe have revealed a widespread reduction: global dimming, between 1950s and late 1980s (Alpert, 2005; Liepert, 2002; Stanhill and Cohen, 2001) and a partial recovery: global brightening, between late 1980s to 2000 (Wild, 2012, 2009; Wild et al., 2005). Increase in the concentration of man-made aerosols and the subsequent change in the optical properties of the atmosphere, particularly of clouds and aerosol-cloud interactions are considered as the most probable cause of the global dimming (Norris and Wild, 2007; Stanhill and Cohen, 2001), whereas global brightening is attributed to the implementation of air quality management measures in industrialized countries as well as to the major economic crises (Wild, 2012). The trends after the year 2000 however show mixed tendencies as brightening continues at sites in United States and Europe but levels off in Japan, while there are some indications of renewed dimming in China after a phase of stabilization during the 1990s and persistent dimming throughout India, in

association with their growing economy and respective aerosol emissions (Norris and Wild, 2009; Padma Kumari et al., 2007; Wild, 2012; Wild et al., 2009).

1.1.2. Modifiers of solar radiation: Clouds and aerosols

Broadly speaking, there are two major modifiers of SR: clouds and atmospheric aerosols. Firstly, cloud cover has been identified as the primary modulator of SR or SSD as it reflects the downward solar flux back to space (Dessler, 2010), therefore SR and cloud cover show inverse relations implying that increase in cloudiness results in decrease in SR and vice-versa, referred as “cloud effect”. Indeed, some investigators found that the dimming/brightening coincides with the increase/decrease of cloud cover in different regions (Abakumova et al., 1996; Liepert, 2002; Norris and Wild, 2009).

Secondly, atmospheric aerosols from anthropogenic air pollution have been considered an important contributor to the dimming observed in different parts of the world (Jhajharia and Singh, 2011; Kaiser and Qian, 2002; Li et al., 2011; Norris and Wild, 2007; Qian et al., 2006; Soni et al., 2012). In addition, Streets et al. (2006) found that the inter-annual global trends in SR between 1980 and 2000 were consistent with the trend in primary emissions of SO₂ and black carbon (BC), which contributes to about one-third of global average aerosol optical depth (AOD). Aerosols can largely reduce incoming SR from reaching the earth’s surface either by scattering or absorbing SR referred to as the “aerosols direct effect”. Aerosols also reflect more SR through their ability to act as a cloud condensation nuclei (CCN), thereby increasing cloud reflectivity and lifetime and suppressing rainfall. Such aerosol-cloud interactions is referred as “aerosols indirect effect” (Haywood and Boucher, 2000; Ramanathan et al., 2001; Rosenfeld, 2000).

1.1.3. Atmospheric brown clouds and its sources: biomass burning and fossil fuel combustion

Aerosols are not restricted to local emissions, rather there are evidences of long range transport of man-made aerosols and the transformation of the urban haze into regional and continental-scale brown clouds known as “**atmospheric brown clouds**” (ABC). The Indo-Asian haze enveloping most of South Asia and northern Indian ocean, the Arctic haze, the east Asian dust and haze travelling across the Pacific ocean and dust plumes and haze in North Africa (Sahara and Sahel regions) are examples of typical

ABC observed across the world (Ramanathan et al., 2001). Presence of 3 km-thick brownish haze in the Indo-Gangetic plains (IGP) and Himalayan foothills during the dry seasons from October to May is well documented (Bonasoni et al., 2010; Ramanathan and Ramana, 2005; Ramanathan et al., 2005).

Important sources of ABC in the IGP and Himalayan region include the **combustion of biofuels** used in cooking and heating, agricultural residue burning and forest fires (collectively known as biomass burning) and **fossil fuels** used broadly throughout diverse economic activities. Emissions from fossil fuels, biofuels and crop residue burning is dominant in the IGP associated with growing population and its demands (Lu et al., 2011; Vadrevu et al., 2011) while emissions from forest fires are prevalent in the low-elevation regions of the Himalayas (Vadrevu et al., 2012). A conspicuous feature of the Asian ABC is its unusually high content of BC particles (Lelieveld et al., 2001). Two-third of the BC in the Asian ABC is contributed by biomass burning (Gustafsson et al., 2009) occurring on a wide scale in the IGP. Of major concern is the widespread crop residue burning in the western states of IGP (Punjab, Haryana) which is considered as a serious threat to air quality and regional climate change (Singh and Kaskaoutis, 2014).

1.1.4. Atmospheric brown clouds and its impacts on regional climate change

While ABC reflects the SR and causes surface cooling, one of the component of ABC, BC absorbs SR causing atmospheric heating. Estimates have suggested that ABC induced dimming cools the surface, masking as much as 50% of the global warming due to the recent rise in green-house gases (GHGs) (net radiative forcing due to GHGs is 3 W/m^2 , while the net radiative forcing of ABC is -1.4 W/m^2) (Forster et al., 2007; Ramanathan and Carmichael, 2008; Ramanathan et al., 2005). Of particular importance is BC, whose warming potential is approximately 55% of that due to CO_2 (top of the atmospheric forcing of BC is $+0.9$ vs $+1.6 \text{ W/m}^2$ for CO_2) (Carmichael et al., 2009; Ramanathan and Carmichael, 2008). Several studies have highlighted the fact that atmospheric solar heating by BC in ABC may be as much important as warming by CO_2 in GHGs, in causing the faster retreat of Himalayan glaciers observed in recent decades (Bonasoni et al., 2010; Ramanathan and Carmichael, 2008; Ramanathan et al., 2007b). An additional concern regarding BC is significant soot deposition in the Hindu Kush-

Himalayan-Tibetan (HKHT) glaciers and snow packs; this darkening of snow also speeds the melting process by lowering the reflectivity of the snow-covered land surface. Recent studies suggest that this is also one of the important contributors to the melting of Himalayan glaciers (Bolch et al., 2012; Yasunari et al., 2013).

In addition to the impacts mentioned above, ABC have great potential to modify the hydrological cycle through different mechanisms. According to global circulation model (GCM) simulation results, ABC played a significant role to modify the Indian summer monsoon (ISM) circulation and caused decrease in rainfall in South Asia by approximately 5% from 1930 to 2000 (Ramanathan and Carmichael, 2008; Ramanathan et al., 2005). Liepert et al. (2004) also highlighted the importance of aerosol-cloud interactions and its ability to slow down the hydrological cycle through surface energy budget modifications and subsequent reduction in evaporation. Collectively, ABC have given rise to major areas of concern, the most critical for South Asia being the observed decrease in the ISM rainfall and the accelerated retreat of the HKHT glaciers. Both of these have led to negative effects on water resources and crop yields in Asia (Ramanathan et al., 2007a)

1.2. Scope of this study

While Nepal, my home country, contributes to the global GHGs emissions to a negligible extent, it is one of the most vulnerable countries to the anthropogenic climate variability and change (Lohani and Eco, 2007; Maplecroft, 2010). It is also evident that the ABC emissions from the Indian sub-continent will further aggravate Nepal's vulnerability in terms of climate and hydrological resources. The location of Nepal between the two rapidly developing nations and the position of the Himalayas plays a vital role in this. The Himalayas acts as a barrier that separates a region of abundant aerosols in the IGP from the region of pristine air at high altitude in the Tibetan Plateau (Gautam et al., 2009b). The accumulations of aerosols and its transformation to ABC is evident in IGP but regional scale circulations modulated by topography also plays an important role in its long distance transport. In recent years, presence of high concentrations of ABC have been recorded by ABC observatories in the foothills region of the lower Himalayas in Kathmandu valley (Ramanathan et al., (2007) and in the foothills of Mt Everest by Nepal Climate Observatory Pyramid, NCO-P (Bonasoni et al.

2008). Recent investigations at NCO-P provided clear evidence that, Himalayan valleys represent a direct channel for the transport of the brown clouds pollutants from the foothills up to as high as 5000 meters above sea level (m a.s.l.) in Nepal (Bonasoni et al., 2010).

In addition to the trans-boundary pollution, local air pollution has also increased in major urban cities of Nepal. Vehicular emission in urban areas has for example increased drastically as there has been 20 times increase in the number of vehicles from 1990 to 2013 (Department of Transport Management, 2014) (Figure 1-1). Another important contributor to the emissions is the extensive biomass burning occurring every year in the low-elevation regions of Nepal, which is believed to pose a serious threat to Himalayas through BC emissions.

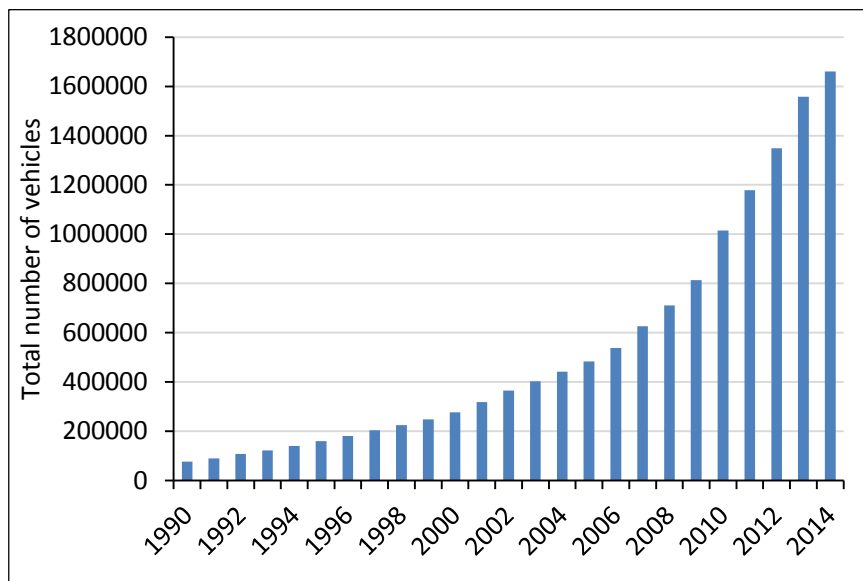


Figure 1-1 Total number of vehicles in urban areas in Nepal from 1990 to 2014.

Despite several evidences of dimming due to increased air pollution (Qian et al., 2007; Soni et al., 2012), no study on long term change in SR has been reported for Nepal under the intensifying local and regional air pollution. The changes in SR, if any, are particularly crucial for a country like Nepal where the livelihood of a majority of the population depends on the local ecosystem provisions and the solar input is the sole energy source. In addition, the impacts of ABC on regional climate is critical for Nepal in terms of water resources, which largely depends on the river water fed by the

Himalayan glaciers and ISM rainfall to sustain the agrarian economy and livelihood of a large population base.

This study is the first scientific effort that elucidated the long-term changes of SR in Nepal. It consists of three major activities, viz.

- to detect any long term changes in SR by analyzing temporal changes in SSD over an extended period,
- to identify the major drivers of the changes in SSD, whether it is clouds, aerosols or aerosol-cloud interactions, and
- to identify sources contributing to the major drivers with particular focus on aerosol emissions from different combustion sources and the influence of trans-boundary air pollution.

1.3. Outline of the thesis

This thesis consists of 5 chapters including this chapter for introduction. The subsequent 3 chapters represent the major activities as noted above. In Chapter 2, I quantified long term temporal changes in SSD in Nepal by analyzing SSD records from 13 meteorological stations distributed across the country for the period 1987-2010. As the results in Chapter 2 confirmed strong dimming in Nepal, I identified the major drivers of the observed dimming by analyzing long term trends in SSD on clear days and SSD on cloudy days to understand the role of aerosols and clouds respectively (Chapter 3). To further understand the role of aerosol cloud interactions, I studied changes in rainfall and number of rainy days.

The results in Chapter 3 indicated aerosols to be the major driver of the decline in SSD, and hence, in Chapter 4, I identified the major sources of aerosols in Nepal by estimating the emissions of aerosols from biomass burning as well as fossil fuel combustion within the territory of Nepal. As the emissions from biomass burning far exceeded the emissions from fossil fuels, I further analyzed the influence of open biomass burning on the aerosols variations by analyzing AOD and firecounts data captured by satellites. To understand the influence of trans-boundary air pollution, major source regions for the aerosols transportation to Nepal were identified through trajectory analysis of wind data (Chapter 4).

In the concluding Chapter 5, I synthesized the findings across the previous chapters along with the findings in the literature. I also discussed the implications of the findings with the main focus on impacts of the dimming and ABC on agriculture in Nepal.

Chapter 2

2. LONG TERM TRENDS OF SUNSHINE DURATION IN NEPAL FOR THE PERIOD 1987-2010

2.1. Introduction

The global dimming/brightening has been mainly evidenced by measurements of solar radiation (SR), but has also been confirmed using its proxies such as sunshine duration (SSD), cloud cover, pan-evaporation or reference evapotranspiration in different regions of the world (Kitsara et al., 2012; Raichijk, 2012; Sanchez-Lorenzo et al., 2008; Wang et al., 2013). Among these proxies, SSD, defined as the time during which the direct solar irradiance exceeds 120 W m^{-2} on each day (WMO, 2003), is one of the oldest and most robust measures for use as a proxy of SR. The advantage of SSD, in relation to other variables, is that it is less subjective than visibility and cloudiness observations (Xia, 2010). In addition, it can be recorded without electricity or automatic data loggers, and, hence, its observation has been done far more prevalently than that of SR in developing countries like Nepal.

In this chapter, I studied long term temporal changes in SR by analyzing SSD records for the period 1987-2010 to quantify changes, if any, in SR in Nepal. SSD records at 13 meteorological stations were analyzed across three physiographic regions: plains, low-hills, and high-hills and mountains and four seasons: winter, pre-monsoon, monsoon and post-monsoon seasons of Nepal.

2.2. Materials and methods

2.2.1. The study area

Located at 26.25° - 30.5° North and 80.0° - 88.25° East, Nepal is a landlocked mountainous country in South Asia with the Himalayas as its northern boundary with China and borders with India in all other sides (**Error! Reference source not found.**). Elevation across Nepal ranges from 65 m a.s.l. in the plains to over 8000 m a.s.l. in the High-Himalaya including the Everest (8848 m a.s.l.). Mountains covering about 83% of the total land area play a vital role in the Indian summer monsoon (ISM) environment by guarding the Indian subcontinent from the dry, cold air masses of central Asia and blocking the warm, moist airflow from the Indian Ocean (Shrestha et al., 2012). This

monsoon is crucial for the climate and agriculture of the country. Nepal experiences four distinct seasons: winter (December of the previous year, January, and February), pre-monsoon (March-May), monsoon (June-September), and post-monsoon (October and November) seasons.

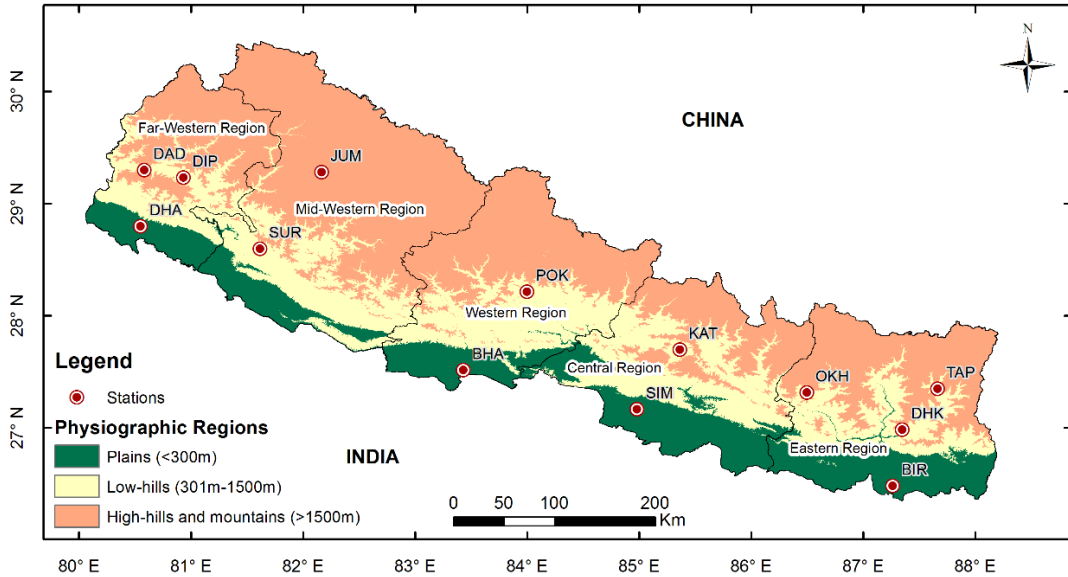


Figure 2-1 Map of Nepal, showing location of the meteorological stations, the three physiographic regions and five development regions. The names of the stations are abbreviated with the first three characters except for the station Dhankuta (DHK).

2.2.2. Weather records and analysis

SSD records from the start of measurement in the year 1987 to 2010 were obtained for 16 meteorological stations from the Department of Hydrology and Meteorology (DHM), Nepal. In this study, I used the data at 13 out of the 16 stations with three stations being omitted (**Error! Reference source not found.**). The omission was due to short length of observation period in Nepalgunj and Khumaltar, and to obstruction in the sunshine observation by trees surrounding the Ghorai station. The length of records varies by stations and because of a limited number of stations; I have used all the data irrespective of the length of the observation period (Table 2-1). The SSD data used in this study were available as daily total of SSD in hours.

As a preliminary quality control, the 13 stations SSD data series were inspected to (1) remove gross errors (e.g. SSD registered more than maximum possible duration), (2) check the consistency of calendar dates (days per annum or month); and (3) remove

suspicious values, for example negative or continuous values of 0 or 0.1 for the whole month. For the study period, there were some gaps in the SSD data records (Table 2-1) which ranged from a few days to a few years in some records. For the months with complete daily values, monthly SSD was calculated as the sum of the daily values (WMO, 2011). However, for the months with missing daily values, a tolerance of up to two missing daily values was considered with reference to Good (2009). The monthly total was adjusted to account for the missing day(s) by using the average SSD across all the other days in the month. The monthly total was then calculated as a sum of the available daily values and the filled missing values. The months with more than two missing daily values were excluded and considered missing.

Table 2-1 Details of the observation records of sunshine duration.

Station names	Elevation (m a.s.l.)	Latitude (degree decimal North)	Longitude (degree decimal East)	Duration of SSD record	Fraction of missing data in SSD
Biratnagar	72	26.48	87.27	1990-2010	23%
Bhairawaha	109	27.52	83.43	1997-2010	28%
Simara	130	27.17	84.98	1997-2010	6%
Dhangadi	187	28.80	80.55	1994-2010	17%
Dipayal	720	29.23	80.93	1997-2010	26%
Surkhet	720	28.60	81.62	1991-2010	19%
Pokhara	827	28.22	84.00	1987-2010	24%
Dhankuta	1210	26.98	87.35	1991-2009	31%
Kathmandu	1337	27.70	85.37	1991-2010	2%
Okhaldhunga	1720	27.32	86.50	1991-2010	24%
Taplejung	1732	27.35	87.67	1991-2010	26%
Dadeldhura	1848	29.30	80.58	1991-2010	30%
Jumla	2300	29.28	82.17	1988-2010	26%

SSD: sunshine duration; m a.s.l.: meters above sea level

For the geographical analysis of this study, I classified the study area into three physiographic regions on the basis of elevation: plains (0-300 m a.s.l.), low-hills (LH; 301-1500 m a.s.l.) and high-hills and mountains (HHM; above 1500 m a.s.l.) as shown

in Figure 2-1. The division by elevation is adapted from Water and Energy Commission Secretariat (2010), which is most widely accepted among similar divisions proposed for Nepal. All the stations were then categorized into one of these physiographic regions by their elevation. The trend analysis was carried out for individual stations and physiographic regions across all the four seasons. The statistical analysis was performed using JMP statistical software (SAS Institute, Cary, USA). Monthly total values of SSD were used to generate annual, regional and seasonal trends by fitting linear models. The significance of the trends was tested at the P-value of 0.05. While fitting the model, the interaction between stations and years was tested. Lack of significant interaction suggested a common trend across the stations while significant interaction suggested a difference in the trends among the stations. The trends were finally expressed as percentage changes in SSD. The maps presented in this study were created using ArcGIS 10.1 (ESRI, 2011). Kriging interpolation technique was applied to create the distribution maps. Kriging was used as the best interpolation algorithm for environmental variables when the known values are less than 100 and missing values are relatively more (Fortner, 1995).

2.3. Results

2.3.1. Individual stations, regional and all-Nepal annual sunshine duration trends

Annual mean of daily total, monthly total and inter-annual trends are presented for all individual stations, three physiographic regions and for all-Nepal in Table 2-2. For individual stations, daily total SSD varied from 6.1 hours at Taplejung in HHM to 7.4 hours at Simara in plains. Regionally, daily total and monthly total SSD were highest in plains, followed by those in LH and HHM. The all-Nepal values for daily total and monthly total SSD were found to be 6.9 hours and 209.1 hours respectively.

Most stations showed decreasing trends in monthly total SSD, while a few showed increasing trends. Among the stations, Biratnagar and Dhangadi in plains and Surkhet and Kathmandu in LH showed maximum decline; with the highest decrease rate of -0.95% per year in Dhangadi. On the other hand, Jumla in HHM had a significant increasing trend. Regionally, the highest decline in SSD was observed in the plains followed by the LH; the HHM showed rather increasing trends. These regional trends indicated that a reduction in SSD was prominent in the plains and the decline gradually

diminished with increasing elevation. From 1987-2010, Nepal on average experienced a significant decline in SSD at a rate of -0.20% per year.

Table 2-2 All-Nepal annual mean of daily total sunshine duration (SSD, hour), monthly total SSD (hour) and inter-annual trends (%/year) in SSD across the stations and physiographic regions for the period 1987-2010 (SSD).

Regions	Station name	Mean daily total SSD (hour)	Mean monthly total SSD (hour)	Inter-annual trend of monthly total SSD (%/year) ^a
	Biratnagar	7.0	212.9	-0.71**
	Bhairawaha	7.2	220.3	-0.35
	Simara	7.4	224.8	-0.19
	Dhangadi	7.2	217.9	-0.95***
Plains		7.2	219.0	-0.56***
	Dipayal	6.9	210.8	0.53
	Surkhet	7.4	223.9	-0.36**
	Pokhara	6.5	198.1	-0.06
	Dhankuta	6.8	207.3	-0.17
	Kathmandu	6.1	186.1	-0.32*
Low-hills		6.7	205.3	-0.09
	Okhaldhunga	6.2	188.7	-0.3
	Taplejung	6.1	185.4	-0.03
	Dadeldhura	7.3	221.5	0.09
	Jumla	7.1	216.4	0.31*
High-hills & mountains		6.7	203.0	0.05
All-Nepal		6.9	209.1	-0.20***

^a. Statistical significance of the trends are shown by *** for P<0.001, ** for P<0.01, and * for P<0.05. Trends with no asterisks were not significantly different from zero.

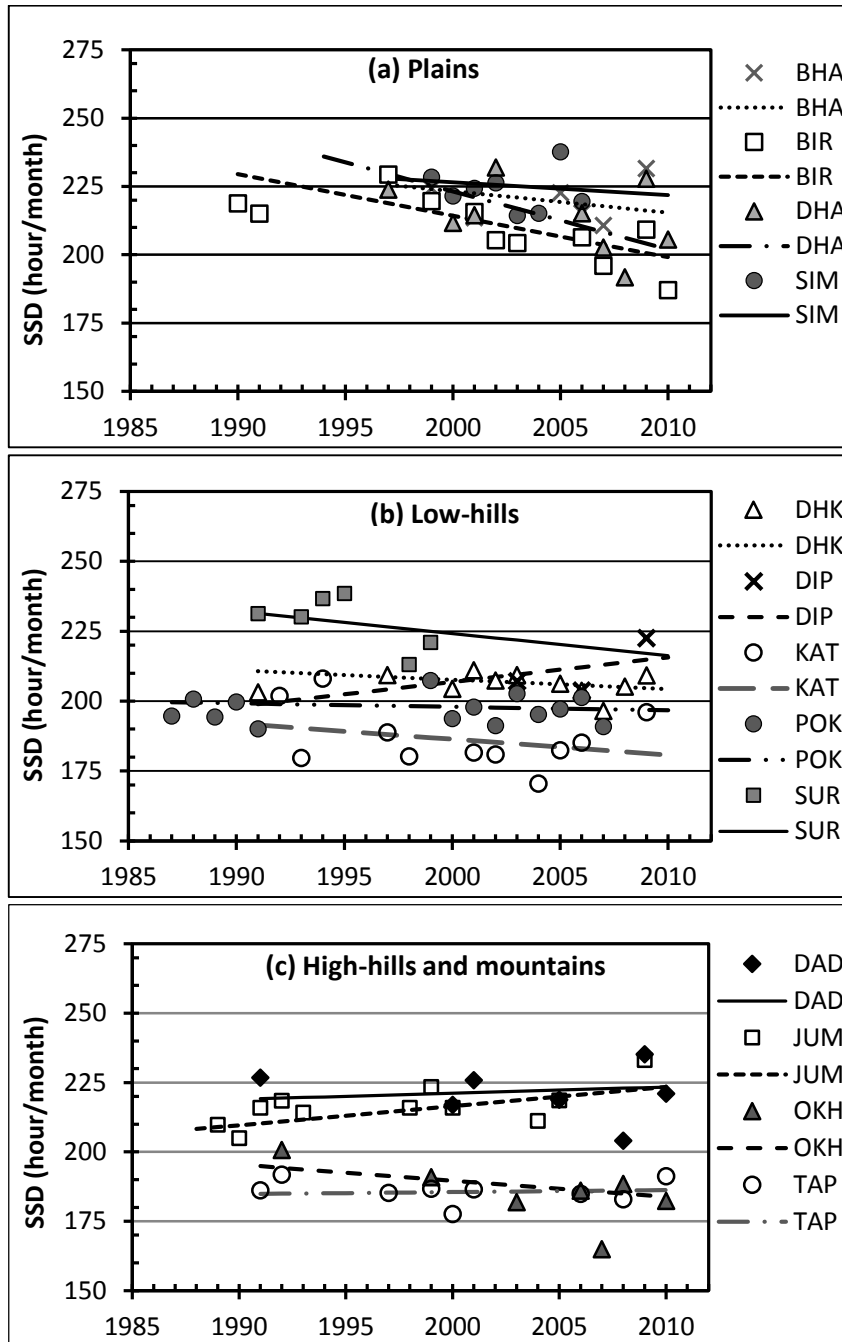


Figure 2-2 Estimated trends in annual mean monthly total sunshine duration (SSD, hour/month) at individual stations in plains (a), low-hills (b), and high-hills and mountains (c) for the period from 1987 to 2010. Symbols are the observations and lines are the linear model fit.

Note: BHA- Bhairawaha, BIR- Biratnagar, DHA- Dhangadi, SIM- Simara, DHK- Dhankuta, DIP- Dipayal, KTM- Kathmandu, POK- Pokhara, SUR- Surkhet, DAD- Dadeldhura, JUM- Jumla, OKH- Okhaldhunga and TAP- Taplejung.

The stations in the plains and the LH showed a common declining trend (Figure 2-2a and Figure 2-2b), which lacked a significant interaction between years and stations in the plains (P=0.088) and the LH (P=0.076) (Table 2-3). This explains that the decline in SSD at the stations in plains and LH are influenced by a phenomenon occurring at a regional scale rather than local one. On the contrary, a significant interaction was observed in the HHM, suggesting a difference in the temporal trends among the stations (Figure 2-2c). In HHM, Okhaldhunga showed a significant decline while Jumla showed a significant increase.

Table 2-3 Inter-annual trends in sunshine duration (SSD) and interaction between stations and years in the three physiographic regions for the period 1987-2010.

Regions	Inter-annual SSD trend (%/year) ^a	P-value for year-by-station interaction
Plains	-0.56 ^{***}	0.088
Low-hills	-0.09	0.076
High-hills & mountains	0.05	0.048
All-Nepal	-0.20 ^{***}	<0.0001

^a. Statistical significance of the trends are shown by *** for P<0.001, ** for P<0.01, and * for P<0.05. Trends with no asterisks were not significantly different from zero.

2.3.2. Seasonal sunshine duration trends and distribution across regions

A significant variation in SSD was observed in all the months across Nepal. Mean daily total SSD ranged from 4.5 hours in July to a peak of 8.4 hours in April (Figure 2-3). All-Nepal and regional SSD trends varied from season to season (Table 2-4). For all-Nepal, a dimming was observed in all the seasons with an exception in the winter season; whereas among the regions, the plains experienced a decreasing trend in all the seasons. Overall, the dimming was pronounced in the post- and pre-monsoon seasons. The gradual shift from a negative to a positive trend as we moved from the plains to the high altitude regions was distinct in the winter season. The significant positive trend in the winter season also contributed to the regional positive trend in HHM. For the monsoon season, a decline in SSD was seen in all the regions but neither of the trends was significant. As observed in regional trends, the station-by-year interaction for seasonal

trends were also non-significant, which suggested that the changes in SSD observed in different seasons might also be induced by a common regional phenomenon.

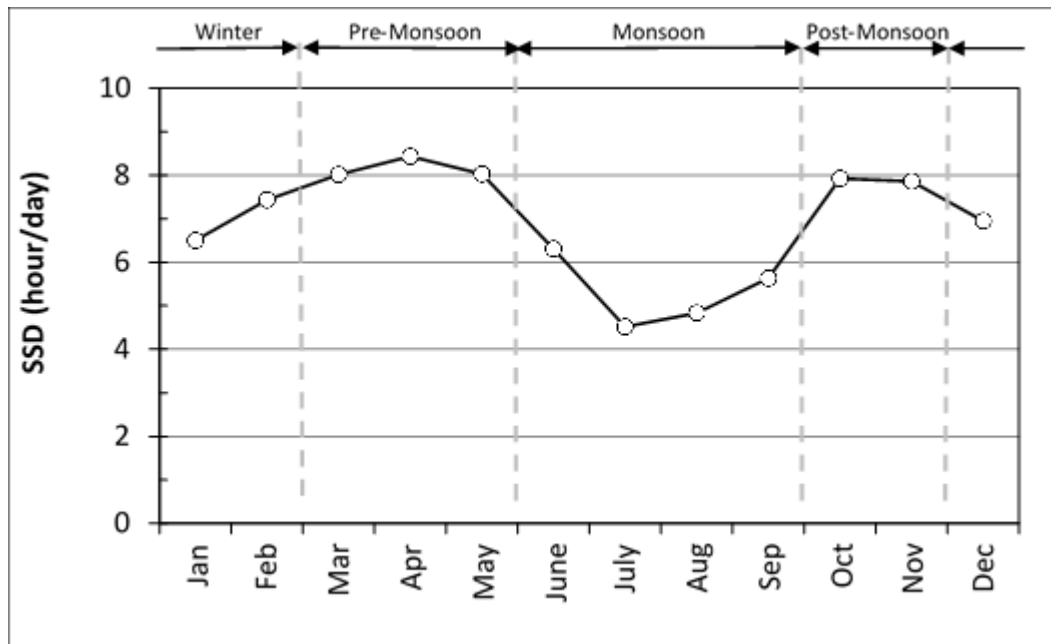


Figure 2-3 Monthly mean sunshine duration (SSD, hour/day) averaged across the 13 stations for the period from 1987 to 2010.

Table 2-4 Regional and all-Nepal trends in sunshine duration (SSD, %/year) by season for the period 1987-2010.

Regions	SSD trends by season (%/y) ^a			
	Winter	Pre-monsoon	Monsoon	Post-monsoon
	Dec-Feb	Mar-May	Jun-Sep	Oct-Nov
Plains	-0.80 ^{**}	-0.51 ^{***}	-0.31	-0.70 ^{**}
Low-hills	0.26	-0.21	-0.24	-0.16
High-hills & mountains	0.54 [*]	0.02	-0.27	-0.17
All-Nepal	0.05	-0.24 ^{***}	-0.28	-0.33 ^{***}

^a. Statistical significance of the trends are shown by *** for P<0.001, ** for P<0.01, and * for P<0.05. Trends with no asterisks were not significantly different from zero.

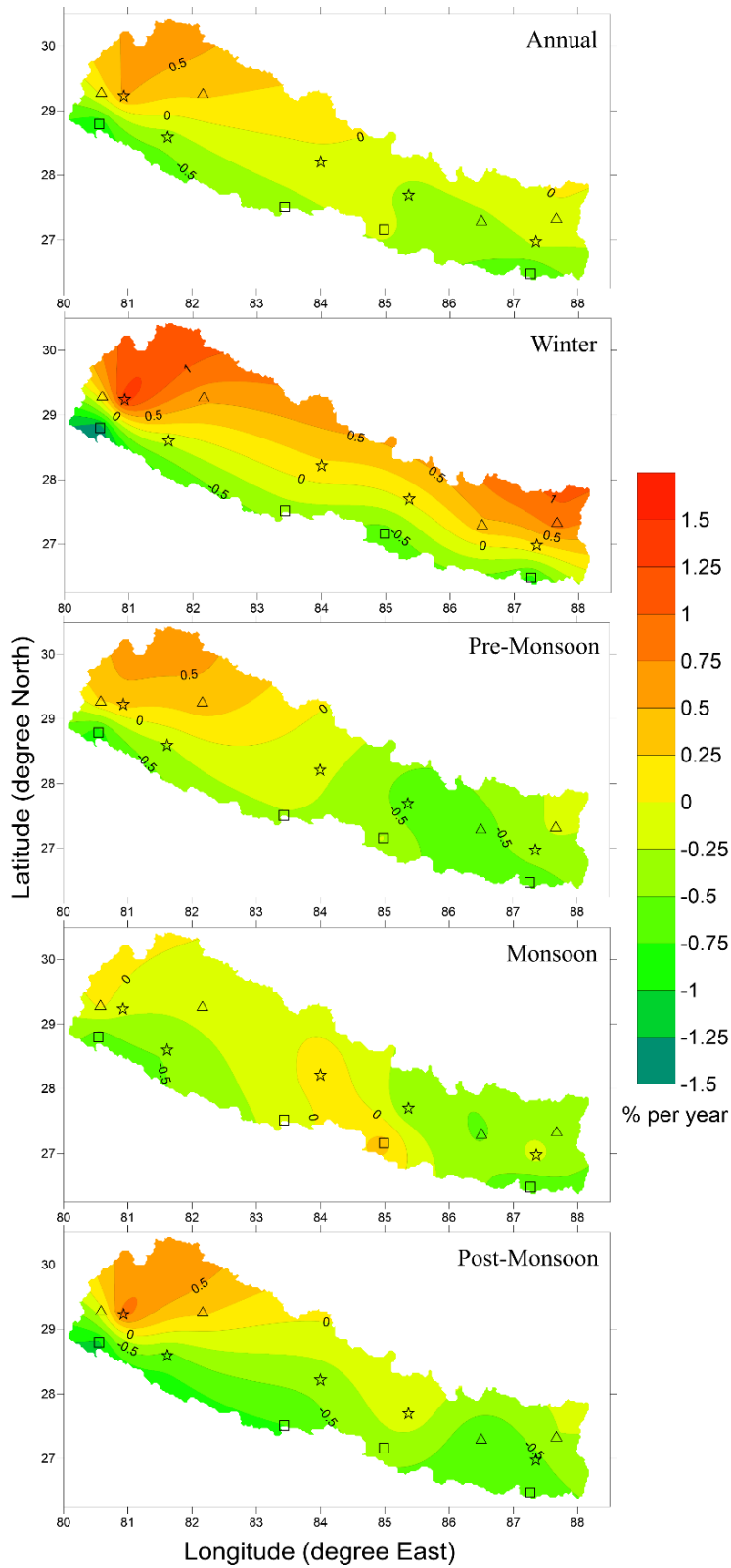


Figure 2-4 Trends (%/year) in annual and seasonal means of sunshine duration in Nepal over the period from 1987 to 2010. (□-plains, ☆-low-hills and Δ-high-hills and mountains)

The spatial distribution of the SSD trends over the period 1987-2010 is presented in Figure 2-4. Mean annual SSD showed dimming trends greater than -0.25% per year in most of the regions in plains and LH. Anomalously high decline of SSD ($< -0.70\%$ per year) was observed in Dhangadi and Biratnagar, both of which are located in the plains. Within the HHM, an increasing SSD trend ($> 0.25\%$ per year) was observed in the far-western and mid-western mountain regions while declining trends were observed for the major part of the eastern and central mountain regions. The contrast in SSD trends between the regions was prominent for winter season (Figure 2-4). The SSD trend distribution for pre-monsoon and post-monsoon closely resembled that of the annual SSD distribution, while the post-monsoon season showed maximum rate of decline. The monsoon SSD trend was strikingly different from that of the other seasons as negative and positive trends were observed in both the plains and the LH (Figure 2-4).

2.4. Discussions

Despite the partial recovery from the dimming across the world (Wild, 2009), our study showed the continuing decline in SSD, which is consistent with the reports for India. A study by Soni et al. (2012) found that the decline in SSD in India averaged across 12 stations for 1971-2005 is about 0.28% per year and the decline in SR ranged from 0.03 to 0.90 $W m^{-2}$ per year for the same period. In a similar study by Padma Kumari et al. (2007) for the period 1981-2004, decline in SR ranged from 0.17 to 1.44 $W m^{-2}$ per year. Both studies found that the dimming has been more intense in recent decades; SR declining at an average of 5% per two decades (Padma Kumari et al., 2007). In this study, we analyzed SSD in Kathmandu (a station with 98% data availability) for two decades (1991-2010) and found a reduction of 3.5% (Figure 2-5). The significant decline in SSD observed in cities such as Biratnagar, Dhangadi, Kathmandu and Surkhet (Table 2-2) are also comparable to the SSD declines reported for major cities of India such as Delhi (0.63% per year), Kolkata (0.35% per year), Visakhapatnam (0.57% per year) among others (Soni et al., 2012). This study hence confirms the persistence of the dimming in Nepal at a rate similar to that in India.

Similar dimming rate implies that like India, aerosols of anthropogenic origin is the most likely cause of the dimming. Emission of pollutants in an area is a function of

population density and the level of its economic development (Alpert, 2005), on which Kathmandu tops the list of cities in Nepal.

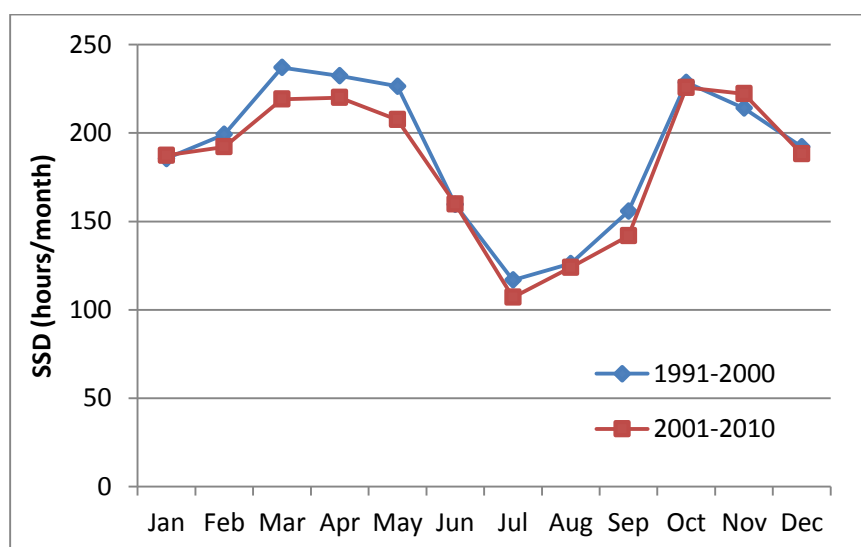


Figure 2-5 Monthly total sunshine duration in Kathmandu averaged across two decades 1991 to 2000 and 2001 to 2010.

Nevertheless, the SSD decline was two times greater in Biratnagar and Dhangadi than Kathmandu. These smaller cities are notably located in the plains, the northern most extension of the Indo-Gangetic plain (IGP), a vast stretch of land in South Asia extending from west to east across Pakistan, India, Nepal and Bangladesh (Abrol et al., 2002) and IGP is one of the most polluted and densely populated regions of the world (Guttikunda et al., 2003). At the same time, the decline in SSD (-0.60 % per year) observed over the IGP by Jaswal (2009) for a longer period of 1970-2006 is comparable to -0.56 % per year decline in SSD observed in this study for the plains. Studies have reported a continuous increase in the emission of BC and sulfates over the IGP during 1990s and 2000s (Lu et al., 2011; Sahu et al., 2008). Thus, the reductions in SSD in plains might be explained by the increasing loading of aerosols and large-scale pollution across the IGP.

Air pollution in Nepal is largely controlled by seasonal cycles of local urban-industrial pollutants and aerosol loading by regional air mass. During post-monsoon and winter seasons, local emissions are aggravated by the air pollution in IGP and air mass flowing from the north and north-west, bringing finer continental aerosols (Singh, 2004). These aerosols transformed into ABC have caused a reduction in SR by approximately

32 (± 5) W m^{-2} in IGP and Himalayan foothills during the dry season from October to May in the year 2001-2003 (Ramanathan and Ramana, 2005) and 25 Wm^{-2} in Kathmandu valley during winter season in 2003 (Ramana et al., 2004). During pre-monsoon season, burning of open vegetation and agricultural fires occur in low elevation regions of Nepal, and may make significant contribution to aerosols (Vadrevu et al., 2012). A change in SR could alter diurnal temperature range by influencing the maximum temperature (Padma Kumari et al., 2007; Ye et al., 2009). The increasing trend in maximum temperatures during winter season in the Himalayan regions (Shrestha et al., 1999) is therefore consistent with the increasing trends of SSD in HHM regions in this study.

The mechanisms of the SSD trends are yet to be understood. Studies on SSD and SR trends under clear sky as compared with cloudy sky conditions would help the understanding of the influence of aerosols and clouds on SR, which is the main objective of the next chapter.

Chapter 3

3. POSSIBLE DRIVERS OF THE DECLINE IN SUNSHINE DURATION IN NEPAL

3.1. Introduction

As the results of Chapter 2 confirmed a strong decline in sunshine duration (SSD), I tried in this chapter to identify the major drivers of the observed dimming. As mentioned earlier, there are two major drivers to reduce solar radiation (SR) from reaching the earth's surface through different mechanisms. The first driver is the clouds which can directly reflect incoming SR and reduces its amount in surface, referred as "cloud effect". The second driver is the atmospheric aerosols, which can largely reduce incoming SR from reaching the earth's surface either by scattering or absorbing SR referred as "aerosols direct effect" hereafter referred as "direct effect". While most of the aerosols have the ability to scatter SR, carbonaceous aerosols are identified as playing a major role in absorption (Hansen et al., 1997). Aerosols also reflect more SR through their ability to act as a cloud condensation nuclei (CCN), in which aerosols could generate more clouds by increase in droplet number concentration but with small drop sizes. Such polluted clouds have longer lifetime and less precipitation efficiency, which leads to suppression of rainfall particularly drizzle or light rainfall from shallow and short-lived clouds (Radke et al., 1989). Therefore, aerosols does not only reflect more SR by increasing clouds lifetime but also suppresses rainfall, giving rise to the so-called "aerosols indirect effect" hereafter referred as 'indirect effect' (Haywood and Boucher, 2000; Ramanathan et al., 2001; Rosenfeld, 2000). Several studies have highlighted the importance of aerosol-cloud interactions and its ability to reduce rainfall particularly in regions with heavy aerosols concentrations (Qian et al., 2009; Rosenfeld, 2000; Rosenfeld et al., 2007).

In this chapter, I posed two questions: "Is the decline in SSD entirely caused by aerosols direct effect, or is the cloud effect also involved?" and "Could some of the changes in the clouds be due to interactions with the aerosols indirect effect?"

To answer these questions, I analyzed temporal changes in SSD on clear days (S_{clear}) to understand the role of aerosols direct effect and those in SSD on cloudy

days (S_{cloudy}) for the influence of cloud effect. The segregation of SSD into S_{clear} and S_{cloudy} is important to differentiate the influence of aerosols and clouds on the observed dimming. It is based on the following idea. Any changes in SR under clear (cloudless) skies are attributed to the presence of atmospheric aerosols, which directly reduces SR, i.e. direct effect. If, on the other hand, the change in SR is observed under cloudy skies, SR is reduced by the clouds which could be due to cloud effect or indirect effect (Padma Kumari and Goswami, 2010). I further analyzed trends in rainfall and number of rainy days (NRD) to understand the changes in S_{cloudy} contributed by the interactions between aerosols and clouds through indirect effect.

3.2. Materials and methods

3.2.1. Sunshine duration

The SSD records from 13 stations used in this chapter are similar to that explained in Chapter 2, but daily SSD has been further segregated into S_{clear} and S_{cloudy} . For this segregation, cloudiness data was used and the method is explained in section 3.2.3.

3.2.2. Total cloud fraction

Cloudiness data used in this study is based on satellite observation produced by NASA Langley Research Center as part of their SRB (Surface Radiation Budget) project (<http://gewex-srb.larc.nasa.gov/>). The particular data set is SRB REL3.0 Cloud Properties 3 Hourly Averages (https://eosweb.larc.nasa.gov/project/srb/3hourly_cloud_binary_table). It covers a time period from July 1983 to December 2007 and the values are given on a 1 degree latitude x 1 degree longitude grid. The dataset contains 47 various surface and cloud properties (ASDC, 2014); the ‘Total Cloud Fraction’ (TCF) variable at the grid boxes corresponding to Nepal was extracted for this study using FORTRAN codes from the data provider. The original 3-hourly values of TCF (at 03, 06, 09, 12, 15, 18, 21, 24 UTC) were then averaged for the daily values (Total Cloud Cover, TCC). TCC for each of the 13 stations was then extracted from the corresponding grids. The valid values of TCC ranged from 0 to 1.

The end date of December 2007 dictated the range of analysis concerning clear/cloudy days.

3.2.3. Calculation of sunshine duration on clear days and sunshine duration on cloudy days

This analyses was restricted to 1987-2007 by the start and end dates of SSD and TCC respectively. Firstly, the days within the analysis period were classified into clear or cloudy days using TCC data extracted for each of the stations. Clear days were defined as the days in a year with daily mean TCC less than or equal to the 10th percentile value of the annual TCC distribution. Similarly, cloudy days were defined as the days in a year with daily mean TCC greater than or equal to 90th percentile value of the TCC distribution. This is a modification to the method used by Qian et al. (2006), where clear days were simply defined by assigning days with daily mean TCC less than 0.10 and cloudy days were defined by assigning days with daily mean TCC larger than 0.90. The hilly and mountainous topography of Nepal gives rise to frequent orographic lifting of air and formation of clouds in the hilly regions when compared to plains. Such orographic effect in the hilly regions limits the number of clear days with daily mean TCC less than 0.10 (Qian et al., 2006) and did not allow a reliable estimate of the trend under clear sky conditions. The modifications to the previous definitions of clear/cloudy days by the use of percentile made sure that there were at least 36 days of both clear and cloudy days each year to estimate the trends. In this case, therefore, a clear day in the LH and HHM may not be an actual representation of clear day and may have some influence of clouds. SSD corresponding to clear and cloudy days were defined as S_clear and S_cloudy respectively. From daily total S_clear and S_cloudy composites for each of the 13 stations from 1987-2007, annual and seasonal means were computed for all the stations. The time series of annual and seasonal means of S_clear and S_cloudy from 1987 to 2007 were analyzed for individual stations and physiographic regions across all four seasons by fitting linear models as explained in Chapter 2.

3.2.4. Rainfall records

Changes in rainfall is an important indicator of the aerosols indirect effect where under intense air pollution, aerosols interact with the clouds to suppress rainfall (Rosenfeld, 2000; Rosenfeld et al., 2007). Therefore, temporal changes in total rainfall amount and total number of rainy days (NRD) were analyzed to understand the influence of aerosol-cloud interactions in the observed dimming. Daily rainfall records from the year 1980 to 2009 were obtained from Department of Hydrology and Meteorology

(DHM), Nepal for all the 13 stations. In this study, a rainy day is defined as a day with > 0 mm rainfall or measurable precipitation. Firstly, for each station, the rainy days were categorized into days with daily rainfall ≤ 2 mm, 5 mm, or 10 mm, and rainfall days with daily rainfall ≥ 10 mm, 15 mm, 20 mm, 30 mm, 35 mm, 40 mm, 45 mm, or 50 mm. Annual sum of rainfall amount (R) and number of rainy days (NRD) were calculated for the various categories of rainy days. Inter-annual trends for R and NRD were estimated using linear model across each of the stations, regions and all-Nepal (Appendix Table 1 & 2). Among different categories of rainy days, trends were highly significant for two particular categories (daily rainfall ≤ 10 mm) and (daily rainfall ≥ 45 mm), which were termed as days with 'light rainfall' and 'heavy rainfall', respectively. Detail analysis of trends in total rainfall, light rainfall and heavy rainfall were conducted for individual stations and physiographic regions across all the four seasons. There were no gaps in the rainfall data, and annual total values of rainfall and NRD were used to generate annual, regional and seasonal trends by fitting linear models. The statistical analysis was performed using JMP statistical software (SAS Institute, Cary, USA). The significance of the trends was tested at the P-value of 0.05.

3.3. Results

3.3.1. Trends in sunshine duration on clear days and sunshine duration on cloudy days

3.3.1.1. Inter annual trends in sunshine duration on clear days and sunshine duration on cloudy days (1987-2007)

The annual mean of daily total and linear trends in S_{clear} and S_{cloudy} across the stations in the three physiographic regions and all-Nepal are given in Table 3-1. Most stations showed decreasing trends in S_{clear} except the three stations: Pokhara, Taplejung and Jumla (see Table 3-1 for statistical significance of the trends). Among the stations with the decline in S_{clear} , Bhairawaha, Simara and Dhangadi, all located in the plains, showed maximum declines varying from -0.55% to -2.14% per year. Among the LH and HHM regions, the decline was highly significant only for Kathmandu (-1.02% per year), the urban-industrialized city with 9.5% of the total population. Regionally the highest decline in S_{clear} occurred in the plains, followed by LH and HHM and the decline gradually diminished with increasing elevation in a similar manner as observed in total SSD trends in Chapter 2. Therefore, dimming under

clear skies represent the direct effect of aerosols, which is prominent in the plains and the capital city of Kathmandu.

Table 3-1 All-Nepal inter-annual trends (%/yr) in annual mean SSD on clear days (S_clear) and SSD on cloudy days (S_cloudy) across the stations and physiographic regions for the period 1987-2007.

Regions	Stations	Mean daily total S_clear (hour)	Inter-annual trends of annual mean S_clear (%/yr) ^a	Mean daily total S_cloudy (hour)	Inter-annual trends of annual mean S_cloudy (%/yr) ^a
	Biratnagar	8.8	-0.29	2.6	-3.89**
	Bhairawaha	9.1	-1.36*	2.3	-1.04
	Simara	9.2	-0.55**	2.6	-4.96
	Dhangadi	8.6	-2.14***	2.6	-1.81
Plains		8.9	-1.02***	2.5	-3.32**
	Dipayal	7.6	-0.46	2.3	-2.02
	Surkhet	8.8	-0.20	2.4	-4.00**
	Pokhara	8.2	0.64	2.6	-3.86**
	Dhankuta	9.0	-0.06	2.4	-4.42**
	Kathmandu	7.4	-1.02***	3.1	-3.19***
Low-hills		8.2	-0.24	2.6	-3.61***
	Okhaldhunga	9.5	-0.25	1.8	-5.27*
	Taplejung	8.4	0.07	2.3	-3.75**
	Dadeldhura	9.1	-0.03	2.0	-3.29
	Jumla	9.2	0.15	2.7	-2.23
High-hills & mountains		9.1	-0.02	2.2	-3.64***
All-Nepal		8.7	-0.42***	2.5	-3.27***

^a. Statistical significance of the trends are shown by *** for P<0.001, ** for P<0.01, and * for P<0.05. Trends with no asterisks were not significantly different from zero.

It can be explained by the increasing trend of anthropogenic aerosols in the surrounding region of Indo-Gangetic plains (IGP) (Kaskaoutis et al., 2012; Sahu et al., 2008) and

rapidly growing population (the population in Kathmandu has more than doubled in a span of two decades: 1991-2011) and air pollution in Kathmandu (CBS, 2013). It should be noted that the daily total S_{clear} is highest for the HHM (9.1 hours) in comparison to the LH and plains which also indicates lesser aerosols in the remote mountain region (Table 3-1). The average dimming observed for Nepal under clear sky conditions is found to be -0.42% per year.

Similarly, the linear trends in S_{cloudy} showed strong decline at all the stations (see Table 3-1 for statistical significance of the trends) varying from -1.04% to -5.27% per year. In contrast to S_{clear} trends, trends in S_{cloudy} showed maximum decline at the stations located in LH and HHM, with the highest decrease rate of -5.27% per year occurring in Okhaldhunga. Among stations in the plains, only Biratnagar showed a significant decline. Regionally, the highest decline in S_{cloudy} occurred in the HHM followed by LH and plains. The average dimming observed for Nepal under cloudy sky conditions is found to be -3.27% per year. If we compare the average dimming observed for Nepal between clear and cloudy skies, it is noteworthy that the dimming under cloudy skies is approximately 8 times the dimming under clear skies on a relative rate basis. On the basis of absolute number of hours, the dimming under cloudy sky is approximately 3 times that in clear sky, since S_{cloudy} is less than S_{clear} . This indicates that clouds play a greater role in the observed dimming than aerosols which could be likely due to the increasing trends in cloud amount. To further understand the seasonal variations in dimming, seasonal trends in S_{clear} and S_{cloudy} were analyzed.

3.3.1.2. Seasonal trends in sunshine duration on clear days and sunshine duration on cloudy days (1987-2007)

All-Nepal and regional S_{clear} trends varied from season to season (Table 3-2). A strong dimming was evident in all the dry seasons (winter, pre-monsoon and post-monsoon) in the plains, with highest dimming occurring in winter (-1.27% per year). This suggests the presence of high aerosol loading in all the clear days, thereby reducing SR through direct effect. In the monsoon season, the air pollutants are reduced by the Indian summer monsoon (ISM) rainfall (washout effect) resulting in lesser aerosols and clearer days. The decline in S_{clear} despite the washout effect in the plains is an indication of the increasing local and regional air pollution. During the post-monsoon

season, the dimming extends from the plains to LH as well. In contrast, a positive trend in S_clear was observed during winter in HHM. For all-Nepal, a significant decline in S_clear occurred only in the post-monsoon season.

Table 3-2 Regional and all-Nepal trends in sunshine duration on clear days (S_clear, %/year) by season for the period 1987-2007.

Regions	S_clear trends by season (%/yr) ^a			
	Winter	Pre-monsoon	Monsoon	Post-monsoon
	Dec-Feb	Mar-May	Jun-Sep	Oct-Nov
Plains	-1.27***	-0.65**	-0.35	-0.84***
Low-hills	0.11	0.31	0.35	-0.59*
High-hills & mountains	0.41*	-0.27	0.52	-0.15
All-Nepal	-0.22	-0.18	0.15	-0.53***

^a Statistical significance of the trends are shown by *** for P<0.001, ** for P<0.01, and * for P<0.05. Trends with no asterisks were not significantly different from zero.

Table 3-3 Regional and all-Nepal trends in sunshine duration on cloudy days (S_cloudy, %/year) by season for the period 1987-2007.

Region	S_cloudy trends by season (%/yr) ^a			
	Winter	Pre-monsoon	Monsoon	Post-monsoon
	Dec-Feb	Mar-May	Jun-Sep	Oct-Nov
Plains	-1.94	-3.07**	-5.52*	0.96
Low-hills	-0.16	-1.31*	-4.74***	-1.15
High-hills & mountains	0.73	-0.49	-3.88**	0.02
All-Nepal	-0.47	-1.77***	-4.67***	-0.19

^a Statistical significance of the trends are shown by *** for P<0.001, ** for P<0.01, and * for P<0.05. Trends with no asterisks were not significantly different from zero.

Table 3-3 presents the regional and all-Nepal trends in S_cloudy across the seasons. Maximum decline occurred in the monsoon followed by pre-monsoon seasons under cloudy days in all the regions while winter and post-monsoon season revealed mixed

trends and did not show any significant changes. The average decline in S_cloudy for all-Nepal is highest in the monsoon season at a rate of -4.67% per year. Since clouds are the largest modifiers of SR, changes in SR under cloudy skies is expected. However, it is not obvious why it should show an intense dimming. Such a strong decline under cloudy skies could occur if there is an increase in the cloud amount which could reflect larger amount of SR (cloud effect). More clouds implies more rainfall, therefore long term trends in rainfall were analyzed to detect changes in cloud amount.

3.3.2. Trends in rainfall and number of rainy days

3.3.2.1. Trends in total rainfall and total number of rainy days (1980-2009)

Rainfall in Nepal is largely influenced by the abundant moisture brought by the south-easterly inflows of air mass associated with the ISM (Shrestha et al., 2012), which contributes to about 80 % of total rainfall occurring in monsoon season (Shrestha et al., 2000). The annual total rainfall in Nepal (average of 13 stations across 30 years period) is 1725.8 mm, and varies from 1843.6 mm in the plains to 1488.2 mm in HHM (Table 3-4). The station with highest annual total rainfall is Pokhara in LH (3896.1 mm) and least rainfall occurs in Jumla in HHM (817.3 mm). In contrast, the annual total NRD in Nepal (average of 13 stations across 30 years period) is 119 days, and varies from 96 days in the plains to 137 days in HHM (Table 3-4). The station with highest annual total NRD is Taplejung in HHM (170 days) and least NRD occurs in Dhangadi and Biratnagar in the plains (90 days). These results are consistent with the observation from Tropical Rainfall Measuring Mission (TRMM), which showed that less number of rainy days with heavy rainfall are dominant in the plains while high number of rainy days with relatively weak but persistent rainfall is dominant in the higher elevation regions of Nepal (Shrestha et al., 2012).

Table 3-4 also shows the inter-annual trends in total rainfall and total NRD across the stations and physiographic regions respectively. From 1980-2009, the stations revealed mixed tendencies in total rainfall trends with no significant change in any of them but most stations showed a declining trend in total NRD. A maximum decline in total NRD occurred in the LH regions particularly at two stations: Surkhet (-0.72% per year or 0.81 days per year) and Dhankuta (-0.62% per year or 0.66 days per year).

Table 3-4 All-Nepal mean annual total and inter-annual trends in total rainfall and total number of rainy days (NRD) across the stations and physiographic regions for the period 1980-2009.

Regions	Stations	Mean annual total rainfall (mm)	Trends in total rainfall (%/yr) ^a	Mean annual total NRD (days)	Trends in total NRD (%/yr) ^a
	Biratnagar	1890.5	0.05	108	0.15
	Bhairawaha	1719.2	-0.43	90	-0.18
	Simara	1904.1	0.22	94	-0.25
	Dhangadi	1860.8	0.62	90	0.30
Plains		1843.6	0.13	96	0.01
	Dipayal	1123.5	-0.43	99	-0.32
	Surkhet	1646.3	-0.03	112	-0.72***
	Pokhara	3896.1	0.15	166	-0.11
	Dhankuta	992.4	-0.17	107	-0.62***
	Kathmandu	1450.2	0.24	131	-0.16
Low-hills		1821.7	0.03	123	-0.35***
	Okhaldhunga	1758.9	0.43	139	-0.06
	Taplejung	1978.8	-0.12	170	-0.02
	Dadeldhura	1397.6	-0.37	117	-0.42
	Jumla	817.3	-0.61	122	-0.27
High-hills & mountains		1488.2	-0.08	137	-0.17
All-Nepal		1725.8	0.03	119	-0.20***

^a. Statistical significance of the trends are shown by *** for P<0.001, ** for P<0.01, and * for P<0.05. Trends with no asterisks were not significantly different from zero.

Figure 3-1 shows the time series of annual total rainfall and NRD (averaged across 13 stations) respectively for 1980-2009. The linear trends in total rainfall amount did not show any significant change while total NRD showed significant decline at a rate of -0.20% per year or 0.24 days per year. Long term trends in total rainfall and total NRD did not justify the assumption that strong dimming in S_cloudy was caused by increase

in cloud effect. Rather a different phenomenon referred to as indirect effect of aerosols could have played a crucial role by enhancing cloud lifetime thereby reflecting more SR, but at the same time suppressing rainfall and NRD. To understand the role of indirect effect of aerosols, trends were analyzed in light rainfall and heavy rainfall as defined in section 3.2.4.

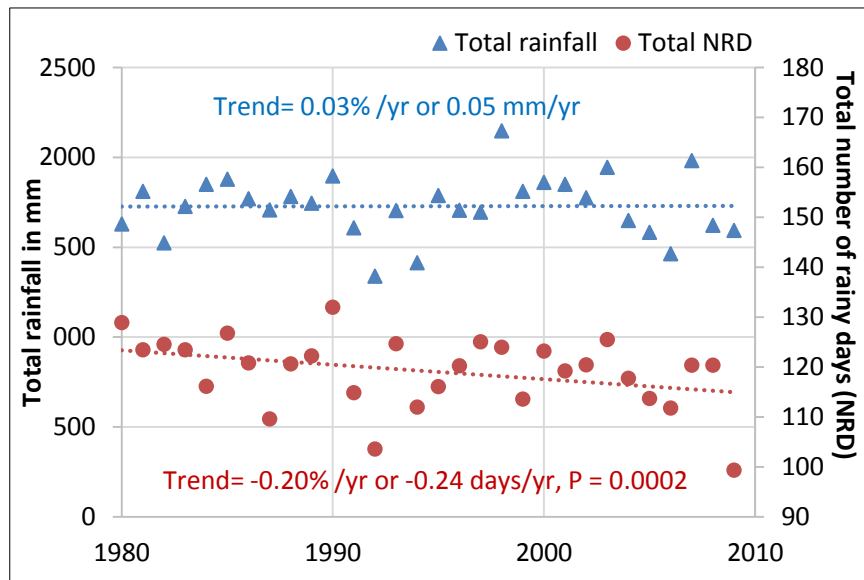


Figure 3-1 Trends in annual total (average of 13 stations) rainfall and number of rainy days (NRD) for the period 1980-2009. Symbols are the observations and lines represent trend.

3.3.2.2. Trends in light rainfall (1980-2009)

Table 3-5 shows the inter-annual trends in light rainfall: $R \leq 10\text{mm}$ and $\text{NRD} \leq 10\text{mm}$ respectively. Though the calculations were done in detail for different categories of light rainfall days ($R, \text{NRD} \leq 2\text{mm}$, $R, \text{NRD} \leq 5\text{mm}$, $R, \text{NRD} \leq 10\text{mm}$) as shown in Appendix Table 1 & 2; the explanation here is with regard to $R \leq 10\text{mm}$ and $\text{NRD} \leq 10\text{mm}$. Whereas the contribution of light rainfall accounts for only 14% of annual rainfall amount, the NRD with light rainfall accounts for around 61% of the total NRD in a year. Therefore, a majority of the rainy days are with light rainfall in Nepal. Unlike the trends in total rainfall that displayed no significant long term changes as shown in Table 3-4, trends in $R \leq 10\text{mm}$ showed a significant decline in the LH and HHM regions at a rate of -0.32% per year and -0.23% per year respectively. The trends in the plains revealed no significant change. Likewise, the trends in $\text{NRD} \leq 10\text{mm}$

revealed similar trends as those $R \leq 10$ mm but with a stronger decline rate of -0.48% per year in LH but less decline in HHM.

Table 3-5 Inter-annual trends in rainfall less than 10mm per day ($R \leq 10$) and number of rainy days with rainfall less than 10mm per day ($NRD \leq 10$) across the stations and physiographic regions for the period 1980-2009.

Regions	Stations	Inter-annual trends in $R \leq 10$ mm (%/yr)	Inter-annual trends in $NRD \leq 10$ mm (%/yr)
	Biratnagar	0.18	0.33
	Bhairawaha	-0.05	-0.12
	Simara	0.06	-0.55 [^]
	Dhangadi	-0.01	0.50
Plains		0.05	0.04
	Dipayal	-0.83*	-0.15
	Surkhet	-0.55 [^]	-1.23***
	Pokhara	0.09	-0.04
	Dhankuta	-0.40	-0.79***
	Kathmandu	-0.05	-0.27
Low-hills		-0.32*	-0.48***
	Okhaldhunga	0.02	-0.21
	Taplejung	-0.20	0.06
	Dadeldhura	-0.83*	-0.34
	Jumla	-0.30	-0.14
High-hills & mountains		-0.23*	-0.14
All-Nepal		-0.23*	-0.23***

^a. Statistical significance of the trends are shown by *** for $P < 0.001$, ** for $P < 0.01$, * for $P < 0.05$ and [^] for $P < 0.10$. Trends with no asterisks were not significantly different from zero.

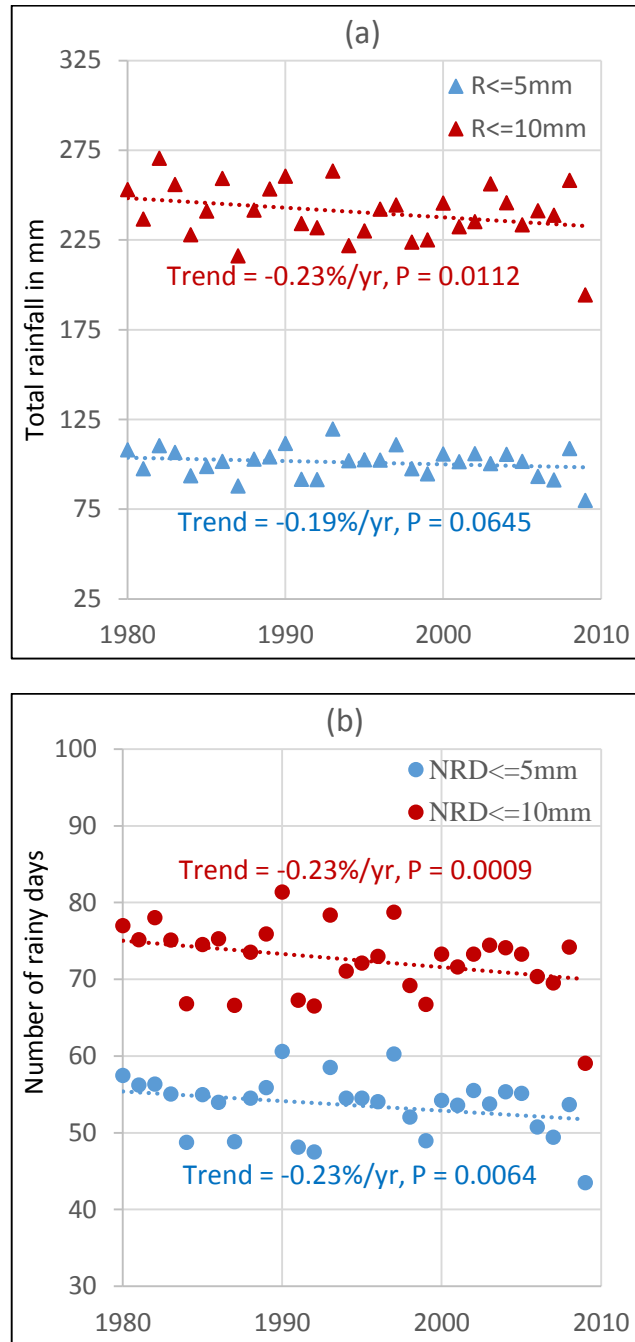


Figure 3-2 Trends in annual total (average of 13 stations) (a) rainfall less than 5mm per day ($R \leq 5$) and 10mm per day ($R \leq 10$) and (b) number of rainy days with rainfall less than 5mm per day ($NRD \leq 5$) and 10mm per day ($NRD \leq 10$) for the period 1980-2009. Symbols are the observations and lines represent trend.

The stations which showed significant negative trends in either of the light rainfall (R or NRD) are Simara in plains; Dipayal, Surkhet and Dhankuta in LH; and Dadeldhura in HHM. Furthermore, for the light rainfall with $R \leq 2$ mm and $NRD \leq 2$ mm (Appendix

Table 1 & 2), along with the above mentioned stations, Kathmandu showed a significant decline in both light rainfall days ($R \leq 2\text{mm} = -0.81\%$ per year, $\text{NRD} \leq 2\text{mm} = -0.67\%$ per year). These results imply that the decline in light rainfall was highest in the LH followed by HHM. Figure 3-2 shows the time series of light rainfall days (averaged across 13 stations) from 1980-2009, which clearly indicated a significant decrease in light rainfall occurring at a rate of -0.23% per year each for $R \leq 10\text{mm}$ and $\text{NRD} \leq 10\text{mm}$ respectively.

3.3.2.3. Trends in heavy rainfall (1980-2009)

Table 3-6 shows the inter-annual trends in heavy rainfall: $R \geq 45\text{mm}$ and $\text{NRD} \geq 45\text{mm}$ respectively. The linear trends for heavy rainfall showed an increasing trend in all the regions but neither of them was significant except for few stations such as Dhangadi in plains and Okhaldhunga in HHM. However it is noteworthy that the rate of increase of heavy rainfall days is higher when compared to light rainfall days implying that heavy rainfall has become more severe and frequent.

Table 3-6 Inter-annual trends in rainfall more than 45mm per day ($R \geq 45$) and number of rainy days with rainfall more than 45mm per day ($NRD \geq 45$) across the stations and physiographic regions for the period 1980-2009.

Regions	Stations	Inter-annual trends in $R \geq 45$ mm (%/yr)	Inter-annual trends in $NRD \geq 45$ mm (%/yr)
	Biratnagar	-0.01	0.00
	Bhairawaha	-0.93	-0.93
	Simara	0.41	0.85
	Dhangadi	1.22 [^]	1.21 [*]
Plains		0.21	0.33
	Dipayal	-0.23	-0.84
	Surkhet	-0.08	0.48
	Pokhara	0.38	0.18
	Dhankuta	0.48	0.36
	Kathmandu	1.03	1.09
Low-hills		0.32	0.26
	Okhaldhunga	1.34 [^]	1.43 [^]
	Taplejung	0.00	0.19
	Dadeldhura	0.89	0.26
	Jumla	-0.16	-0.03
High-hills & mountains		0.79	0.70
All-Nepal		0.34	0.37 [^]

^a. Statistical significance of the trends are shown by *** for $P < 0.001$, ** for $P < 0.01$, * for $P < 0.05$ and [^] for $P < 0.10$. Trends with no asterisks were not significantly different from zero.

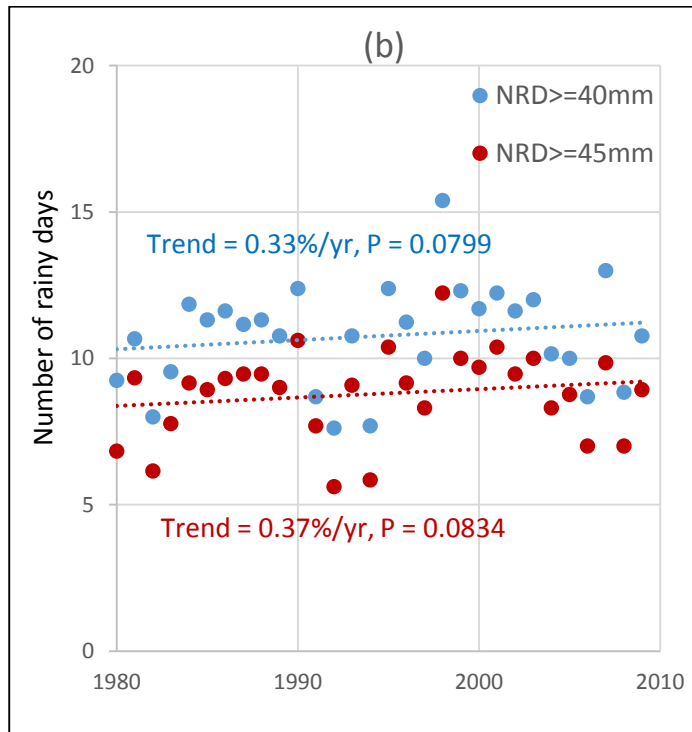
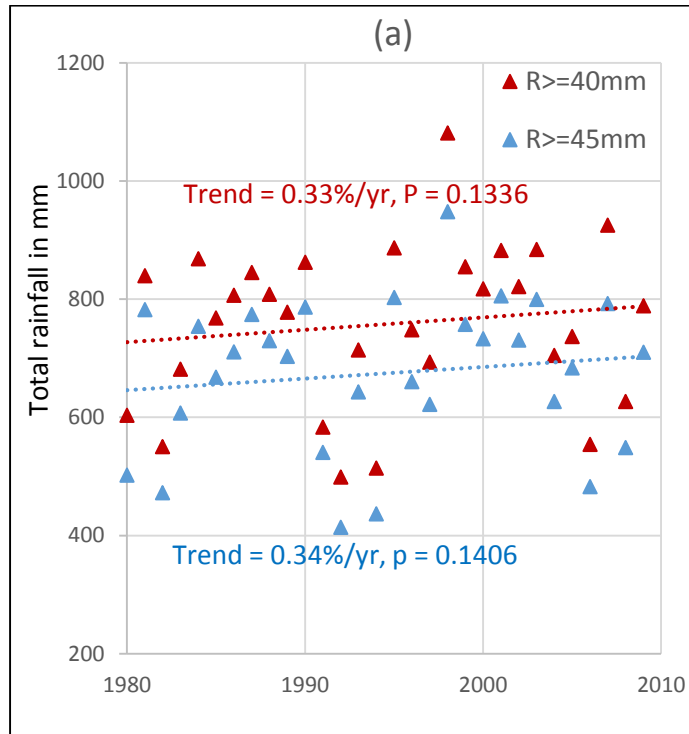


Figure 3-3 Trends in annual total (average of 13 stations) (a) rainfall more than 40mm per day ($R \geq 40$) and 45mm per day ($R \geq 45$) and (b) number of rainy days with rainfall more than 40mm per day ($NRD \geq 40$) and 45mm per day ($NRD \geq 45$) for the period 1980-2009. Symbols are the observations and lines represent trend.

Figure 3-3 shows the time series of heavy rainfall (averaged across 13 stations) from 1980-2009, which displays an increasing trend for all-Nepal heavy rainfall. The linear trends for NRD with heavy rainfall was indeed increasing at a rate of 0.37% per year for $NRD \leq 45\text{mm}$ with a P-value less than 0.10. Seasonal trends in heavy rainfall ($R \geq 45\text{mm}$, $NRD \geq 45\text{mm}$) showed significant increase in monsoon season in the HHM (Table 3-7). These evidences suggest that together with the significant reduction in light rainfall, there is a shift in rainfall rate from light to heavy rainfall.

Table 3-7 Regional and all-Nepal trends in heavy rainfall ($R \geq 45\text{mm}$ per day) and number of rainy days with light rainfall ($NRD \geq 45\text{mm}$ per day) by season for the period 1987-2009.

Region		Rainfall and $NRD \geq 45\text{mm}$ trends by season (%/yr)			
		Winter	Pre-monsoon	Monsoon	Post-monsoon
		Dec-Feb	Mar-May	Jun-Sep	Oct-Nov
Plains	R	2.65	1.30	0.06	2.07
	NRD	1.23	1.34	0.21	1.46
Low-hills	R	0.45	1.09	0.18	2.46
	NRD	-0.34	1.00	0.14	1.74
High-hills & mountains	R	-2.08	-4.01*	1.19*	1.94
	NRD	-2.49	-3.60*	1.10*	2.14
All-Nepal	R	0.45	0.16	0.27^	2.20
	NRD	-0.44	0.11	0.34^	1.72

^a. Statistical significance of the trends are shown by *** for $P < 0.001$, ** for $P < 0.01$, * for $P < 0.05$ and ^ for $P < 0.10$. Trends with no asterisks were not significantly different from zero.

3.3.3. Seasonal trends in light rainfall and its relation to sunshine duration on cloudy days

Significant reduction in light rainfall gives an indication that increase in anthropogenic aerosols might have made a significant contribution to the reduction of light rainfall through indirect effect and coherently contributed to the observed dimming in S_{cloudy} through increased cloud lifetime. To further clarify this issue, I analyzed the seasonal trends in light rainfall amount $R \leq 10\text{mm}$ and frequency $NRD \leq 10\text{mm}$ and compared them with the seasonal trends in S_{cloudy} .

Seasonal trends in light rainfall exhibited significant decline in winter and monsoon seasons in LH followed by HHM (Table 3-8). Among these two seasons, the decrease in winter was about 3-5 times higher than the decrease in monsoon season (for all-Nepal). It is interesting to note that the decrease occurred in the two major rainy seasons. While monsoon season is influenced by ISM brought by the south-easterly flows and is the major source of rainfall in Nepal, winter is marked by winter monsoon dominated by westerly circulations (Bolch et al., 2012; Shrestha et al., 2000; Sigdel and Ikeda, 2012). Here, it is important to understand that atmospheric circulations contributing moisture required for rainfall play a crucial role in the observed changes in rainfall.

Table 3-8 Regional and all-Nepal trends in light rainfall ($R \leq 10$ mm per day) and number of rainy days with light rainfall ($NRD \leq 10$ mm per day) by season for the period 1987-2009.

		Rainfall and $NRD \leq 10$ mm trends by season (%/yr)			
		Winter	Pre-monsoon	Monsoon	Post-monsoon
Region		Dec-Feb	Mar-May	Jun-Sep	Oct-Nov
Plains	R	0.49	0.47	-0.10	0.00
	NRD	-0.08	0.19	0.02	-0.06
Low-hills	R	-1.21***	-0.28 [^]	-0.20	-0.72
	NRD	-1.76***	-0.45 [^]	-0.33**	-0.34
High-hills & mountains	R	-1.37*	0.23	-0.50**	0.83
	NRD	-1.01*	0.11	-0.22 [^]	0.58
All-Nepal	R	-0.91*	0.06	-0.29**	0.10
	NRD	-1.11***	-0.10	-0.20*	0.11

^a. Statistical significance of the trends are shown by *** for $P < 0.001$, ** for $P < 0.01$, * for $P < 0.05$ and [^] for $P < 0.10$. Trends with no asterisks were not significantly different from zero.

Comparing seasonal trends between light rainfall (Table 3-8) and S_{cloudy} (Table 3-3), the decrease in light rainfall in pre-monsoon (in LH) and monsoon seasons (in LH and HHM) were found consistent with the dimming observed in S_{cloudy} in the same but it could not explain the strong dimming in S_{cloudy} observed in the plains. In HHM, which has a remote and pristine environment in comparison to LH and plains, a positive trend is observed in both S_{clear} and S_{cloudy} during winter. The significant decrease

in light rainfall in HHM implies decrease in clouds and could explain the positive trends observed in S_clear and S_cloudy in HHM.

3.4. Discussion

3.4.1. Contribution of atmospheric brown clouds to “aerosols direct effect”

Increased activity of biomass combustion, industrial as well as vehicular emissions associated with growing population and urbanization, all contributed to identify IGP (which includes the plains of Nepal) as one of the major hotspots of atmospheric brown clouds (ABC) (Ramanathan and Carmichael, 2008). An important feature of the aerosols in IGP is that the aerosols from local pollution such as BC from biomass burning are added to natural aerosols such as mineral dusts and carbonaceous aerosols (Dey, 2004; Vadrevu et al., 2012). The declining trends in S_clear observed at the stations located in the plains (Table 3-1) are likely due to the increasing trend of the anthropogenic aerosols in the IGP (Lu et al., 2011; Sahu et al., 2008), causing a reduction in SR under clear days by scattering and absorbing SR through direct effect. In addition to the stations in the plains, the decrease in S_clear was observed for Kathmandu, the capital city. Ramana et al. (2004) found the average clear sky aerosol optical depth (AOD) value at Kathmandu to be 0.34, which is typical for the polluted areas. Studies suggested that the high-altitude peak aerosol layers in Kathmandu are attributed to the boundary layer mixing and transport of aerosols from the IGP while the low-altitude peak is caused by local pollution within the valley (Ramana et al., 2004; Ramanathan and Ramana, 2005). Increasing trends in vehicular emissions and population in Kathmandu valley are consistent with the declining trends in S_clear.

The decline in S_clear was observed in all the dry seasons in the plains as shown in **Error! Reference source not found.** This can be explained by the seasonal variations in aerosols from different sources, which converts the local emissions into persistent thick brownish haze evident in the dry seasons from October to May in this region (Bonasoni et al., 2010; Ramanathan and Ramana, 2005). Increased wintertime fog as shown by the declining trends in visibility (Jaswal et al., 2013) and increasing trends in AOD in IGP (Kaskaoutis et al., 2012) are consistent with high dimming observed during winter and post-monsoon seasons in this study. During the pre-monsoon season, dry dust particles carried by the westerly air mass from the Thar-desert and as far as Sahara

desert makes the highest contribution to aerosols in IGP (Dey, 2004; El-Askary et al., 2006; Sarkar et al., 2006; Singh, 2004). However, the influence of dust loading significantly diminished in eastern IGP than western IGP, rather presence of strongly absorbing carbonaceous aerosols was observed in foothill/elevated Himalayan slopes of Nepal (Gautam et al., 2011; Putero et al., 2014), indicating the presence of aerosols released from biomass burning. In a study of vegetation fires in the Himalayan region, Vadrevu et al. (2012) found March-June (pre-monsoon) to be the peak period of biomass burning with maximum AOD value of 0.5-0.7 in the month of May, suggesting that peak values of aerosols occurs during pre-monsoon season in Nepal.

3.4.2. Contribution of atmospheric brown clouds to “aerosols indirect effect”

Aerosols serve as cloud condensation nuclei (CCN) and hence have a substantial effect on clouds and the initiation of precipitation. Because all cloud droplets must form on pre-existing aerosol particles that act as CCN, increased aerosols also change the composition of clouds (i.e., size and number of cloud droplets), which in turn determines to a large extent the precipitation-forming processes (Rosenfeld et al., 2008). However, it is difficult to establish clear relationships between aerosols and precipitation because changes in the ambient meteorological conditions can also influence precipitation (Levin and Cotton, 2009). Therefore, aerosols-clouds-precipitation interactions have been recognized as major area of uncertainties in future climate projections (IPCC, 2001).

3.4.2.1. Aerosol - clouds interactions in pre-monsoon season

The pre-monsoon is the key season when the aerosol concentrations peaks over the IGP as well as the elevated slopes of the Himalayas (Gautam et al., 2011; Marinoni et al., 2010; Pant et al., 2006). As mentioned in the previous section, the atmosphere is loaded with high levels of anthropogenic pollutants enhanced by the strong influence of dust transport and biomass burning in this season. Investigations at Nepal Climate Observatory-Pyramid (NCO-P), located at 5079 m a.s.l., provided clear evidence that the Himalayas are directly influenced by the ABC transported from the IGP and lowlands through the Himalayan valleys, resulting in AOD values greater than 0.4 in the pre-monsoon season (Bonasoni et al., 2010). These high values of AOD reveal that

during the pre-monsoon season, the ABC prevailed across Nepal from the plains to HHM of Nepal.

Several observations have revealed that in heavily polluted areas, aerosols through their indirect effects on clouds increase cloud amount (increase in droplet concentration and decrease in droplet size) and lifetime, and tend to suppress precipitation from shallow clouds (Ackerman, 2003; Qian et al., 2009; Radke et al., 1989; Rosenfeld, 2000). Twomey (1977) pointed out that such polluted clouds formed from aerosol-cloud interactions are more reflective, reducing more SR from reaching the ground. In a study by Lau et al. (2008), Moderate Resolution Imaging Spectroradiometer (MODIS) images showed polluted and bright (more reflective) clouds over IGP during episodes of increased pollution in pre-monsoon season. They also found that such polluted clouds had smaller droplet size (less than 10 μm) and greater AOD values providing evidence of the indirect effect. In addition, Tripathi et al. (2007) examined the AOD and cloud droplet size derived from MODIS from 2001-2005 during pre-monsoon season over the IGP. The greater AOD values were associated with increased cloud cover and reduced droplet size, which demonstrated indirect effect of aerosols. In a recent study in the Himalayan region, Shrestha and Barros (2010) provided further evidence of the indirect effect. In an area centering on Central Nepal, the regions of aerosol buildup during the pre-monsoon season were collocated with the areas of high rainfall/cloudiness during the monsoon season, which suggested aerosol-cloud-rainfall interaction. In this study, a significant decline in S_{cloudy} and coincident decline in light rainfall were observed in the LH during the pre-monsoon season (Table 3-3 and Table 3-8). As the above mentioned studies suggest, the decline observed in S_{cloudy} in the pre-monsoon season could be due to increase in polluted clouds, which suppressed the number of light rainfall through the indirect effect of aerosols.

3.4.2.2. Aerosol - clouds interactions in monsoon season

As the air pollution is becoming increasingly acute in South Asia, the aerosol radiative forcing may influence the summer monsoon cycle through different mechanisms. The solar dimming induced by ABC cools the surface and reduces evapotranspiration, an important source of water vapor for monsoon rainfall (Liepert et al., 2004; Ramanathan et al., 2001). It has been demonstrated that the aerosol solar

absorption causes atmospheric warming and surface cooling leading to weakened meridional sea surface temperature (SST) gradient in the northern Indian ocean and an increase in atmospheric stability (Chung and Ramanathan, 2007; Ramanathan et al., 2005). Both the mechanisms may weaken monsoon circulation and reduce monsoon rainfall in South Asia leading to a greater possibility of droughts in the region. On the other hand, Lau and Kim (2006) showed that the enhanced mixture of dust and carbonaceous aerosols in the IGP during the pre-monsoon season can act as an elevated heat source in the troposphere, and that the monsoon over northern India (IGP and Himalayan foothills) could be intensified due to the greater tropospheric land-sea thermal gradient in the pre-monsoon season. Recent study by Gautam et al. (2009a) supported the findings of Lau and Kim (2006) and found an increasing trend in early summer monsoon (June) rainfall over India for the period 1950-2004. Nevertheless, in this study, the rainfall in Himalayan foothills did not show any significant trends, which is consistent with the findings of Ichiyanagi et al. (2007). These authors analyzed precipitation anomalies from 1987 to 1996 using data from a dense network of 274 rain gauge stations distributed throughout Nepal, and found no trends across the period of study.

The studies related to indirect effects of aerosols have, so far, focused on non-monsoon seasons. However, Lau et al. (2008) pointed out that high aerosol concentrations prior to monsoon onset or during monsoon break periods could interact with the clouds, further affecting the subsequent evolution of the monsoon water cycle. Rosenfeld et al. (2008) proposed a model and explained that the aerosol-induced suppression of rainfall from shallow clouds could increase the rainfall from deep clouds through increase in effective convective potential energy. Results from modeling studies also demonstrated the delay of early rain by aerosols which resulted in greater amount of cloud water and heavy rainfall at the later stage of the cloud (Philips et al., 2007; Tao et al., 2007). Similar results of decrease in light rainfall and increase in heavy rainfall during monsoon season, under high aerosol conditions, have been reported for rainfall records in China by Qian et al. (2009). This mechanism may likely explain the decreasing trends in light rainfall and increasing trends in heavy rainfall in monsoon season observed in this study (Table 3-7 and Table 3-8). Interestingly, Bookhagen and Burbank (2010) observed that high rainfall intensities in Himalayan region have shifted

several dozen kilometers northward which is consistent with the significant increasing trend in heavy rainfall in HHM in monsoon season (Table 3-7). Despite the complexities of aerosol-cloud-rainfall interactions, the increase in shallow and deep clouds as reflected by the decrease in light rainfall and increase in heavy rainfall could be the most plausible explanation for the high dimming observed in S_cloudy in the monsoon season in Nepal. In a similar study for India, Padma Kumari and Goswami (2010) found increasing trends in amount of deep clouds to cause decline in SR under cloudy skies over the Indian monsoon region.

As mentioned earlier, studies have documented high aerosol loading in the plains, yet the suppression of light rainfall through aerosol indirect effect was more distinct in LH in comparison to the plains (Table 3-5). Much of the rainfall at the LH is generated by the orographic uplift of the air from upwind polluted plains. In a study in central China, decreasing trends of 10 to 25% in the precipitation ratio between stations at Mt. Hua (downwind) and urban and industrial lowlands (upwind) was observed, indicating the influence of air pollution on orographic precipitation (Rosenfeld et al., 2007). Similar studies reported reductions of precipitations by 10 to 25% in the past half century in much of the mountain ranges in United States, downwind of major urban and industrial areas (Griffith et al., 2005; Jirak and Cotton, 2006; Rosenfeld and Givati, 2006). Evidences from these studies support our findings of greater decline in orographic rainfall in LH than in the plains.

3.4.2.3. Winter rainfall

Winter in Nepal is marked by winter monsoon, dominated by westerly circulations that enter from the west and deliver markedly increasing precipitation with increasing elevation (Bolch et al., 2012; Shrestha et al., 2000; Sigdel and Ikeda, 2012). This moisture for winter precipitation usually originates over the Mediterranean Sea and the Atlantic Ocean (Guhathakurta and Rajeevan, 2008). The significant trends of decreasing light rainfall in LH and HHM are consistent with the significant declining trends in moderate rainfall in the north-western Himalayan region of India (Dash et al., 2009). During winter, the decrease in temperature results in lower boundary layer height, which favors the accumulation of pollutants near the surface (Singh and Kaskaoutis, 2014) and reduces the transport of ABC from the plains to the mountainous regions (Bonasoni et

al., 2010). This suggests less influence of aerosols in the observed decline, though the actual mechanisms are not well understood. The increasing trends in S_clear and S_cloudy in HHM (Table 3-2 and Table 3-3) are also consistent with the declining trends in light rainfall observed in the same.

3.4.3. Sources and transportation of atmospheric brown clouds

In summary, the declining trends in S_clear is largely caused by increase in anthropogenic aerosols by direct effect of absorbing and scattering SR. On the other hand, the decline in S_cloudy could be partly explained by the indirect effect of aerosols. Significant reduction in light rainfall gives an indication that increase in anthropogenic aerosols might have made a significant contribution in increasing cloud cover and lifetime through indirect effect and coherently contributed to the observed dimming in S_cloudy. Therefore, it appeared crucial to identify the major sources of aerosols in Nepal. The transport of ABC from the Indian subcontinent up to the Himalayas might also contribute to the aerosols. In this regard, in Chapter 4, I tried to identify the major source regions for the aerosols transportation to Nepal.

Chapter 4

4. INFLUENCE OF BIOMASS BURNING AND LONG-RANGE TRANSPORT OF POLLUTANTS ON AEROSOL VARIATIONS IN NEPAL

4.1. Introduction

The results in Chapter 3 indicated that aerosols are likely the major driver of the decline in sunshine duration (SSD). Therefore, in this chapter, I studied aerosol variations in Nepal and identified its major sources: biomass burning or fossil fuel combustion. The aerosol components contributing to atmospheric brown clouds (ABC) in this region include soot or black carbon (BC), sulfates, organics, dust, among others (Carmichael et al., 2009). Of these components, sulfates and the primary carbonaceous aerosols, BC and organic carbon (OC) together, account for more than 60% of the change in aerosol optical depth (AOD; a measure of aerosol concentration from space) observed in South Asia (Streets et al., 2009). Further, they are important variables, needed to constrain the role of atmospheric particles in the Earth's radiation budget, both directly and indirectly through cloud condensation nuclei (CCN) activation (Marinoni et al., 2010). Hence, I estimated the emissions of BC and sulfur dioxide (SO₂) from both biomass burning and fossil fuel combustion to identify the major contributor to aerosols. A conspicuous feature of the Asian ABC is its unusually high content of BC particles (Lelieveld et al., 2001). Gustafsson et al. (2009) found that two-thirds of the BC in the Asian ABC is contributed by biomass burning occurring on a wide scale in the Indo-Gangetic plains (IGP) and the Himalayan region. Consistent with their findings, the emissions from biomass burning far exceeded the emissions from fossil fuels in Nepal (as shown below in section 4.4.1), therefore, I further analyzed the influence of biomass burning on the aerosols variation by analyzing AOD and firecounts data captured by Moderate Resolution Imaging Spectroradiometer (MODIS).

Along with the emissions of aerosols within Nepal, trans-boundary air pollution caused by the transport of ABC from IGP (Bonasoni et al., 2010; Putero et al., 2014) also influences the amount of aerosol over Nepal. Bonasoni et al. (2007) also acknowledged the role of large-scale atmospheric circulations (Indian summer monsoon circulations during monsoon season and westerly circulations during dry seasons) in the

distribution of aerosols in the region. To understand the influence of long-range transport of pollutants, I also analyzed 5-day backward trajectory using the HYbrid Single Particle Lagrangian Integrated Trajectories model (HYSPLIT) and wind direction data from Global Data Assimilation System (GDAS).

4.2. Data

4.2.1. MODIS aerosol optical depth

In this study, I used satellite-derived information about aerosol distribution collected by MODIS. The aerosol concentration from space is measured as aerosol optical depth (AOD, a dimensionless number). It is a measure of the amount of aerosols (dust, smoke, pollution) over the observation location obstructing the solar beam from reaching the Earth's surface (Kaufman et al., 1997; Ramanathan et al., 2001).

I used daily MODIS Collection 6 Level 3 (MYD08_D3; <http://ladsweb.nascom.nasa.gov/data/search.html>) AOD data provided at the spatial resolution of 1 degree to characterize the aerosol variations. I chose the AOD_550_Dark_Target_Deep_Blue_Combined_Mean data set for the information regarding AOD for the period 2005 to 2010. The combined dataset takes retrievals from either or both the Dark Target and Deep Blue algorithms based on regional and seasonal climatologies and provides a complete estimate of AOD (Blue et al., 2014; Levy et al., 2013). Marine Geospatial Ecology Tools (Roberts et al., 2010) was used to convert the data provided in Scientific Data Sets (SDS) in each Hierarchical Data Format (HDF) file format to ArcGIS raster. Daily rasters were resampled (nearest neighbor) to 0.025 degree prior to the extraction of information for Nepal. The resampling was required in order to minimize the loss of data due to incomplete inclusion of some 1 degree cells within the political boundary. Only days with more than 50% AOD information coverage over Nepal were considered for analysis. A zonal analysis of AOD values for plains, low-hills (LH) and high-hills and mountains (HHM) was also carried out according to the elevation classified in Figure 2-1.

4.2.2. MODIS active fire and burnt area products

I used in this study MODIS Fire locations (MCD14ML; <https://earthdata.nasa.gov/node/5323>) collected by Aqua and Terra satellites, processed by the University of

Maryland, and distributed by the Land Atmosphere Near real time Capability for EOS (LANCE), Fire Information for Resource Management System (FIRMS). The firecounts as ESRI shape-files were obtained for the period 2005-2010. The Collection 5 product used in this study has a spatial resolution of 1 km but includes fires as small as 50 m². If thermal anomalies/active fires are detected within the 1km pixel, the center of the pixel is flagged by the fire detection algorithm (Giglio et al., 2003) as containing one or more fires within the pixel. To avoid the false detection possibility for daytime active fires (Kaufman et al., 1998), we only used firecounts with detection confidence above 50%, which was suggested by Tang et al. (2013) as a reasonable mid-point between the accuracy and efficiency in detecting the small-scale fires.

The MODIS burnt area product (MCD45A1; Collection 5.1, level-3) for the period 2005-2010 was used in this study. The dataset was obtained as ESRI shape-files from the University of Maryland (<http://modis-fire.umd.edu>). It had been processed using both the Terra- and Aqua-derived daily surface reflectance inputs and a MODIS algorithm to analyze the spectral, temporal, and structural changes. The algorithm maps the spatial extent (at 500 m resolution) of recent fires (excluding previous occurrences) by locating the occurrence of rapid changes in daily surface reflectance time series data (Boschetti et al., 2013; Justice et al., 2006; Roy et al., 2005). The subset window 18 (Appendix Fig. 1) was used to collect the burnt area data for this study.

4.2.3. Land cover data

We used GlobCover 2009 (Bontemps et al., 2011; <http://due.esrin.esa.int/globcover/>) for characterizing the land cover over the study area. The high resolution (300 m) dataset is derived by an automatic and regionally-tuned classification of a time series of global MEidium-spectral Resolution Imaging Spectrometer (MERIS) fine resolution mosaics for the year 2009. The global land cover map counts 22 land cover classes defined with the United Nations Land Cover Classification System (Bontemps et al. 2011). MERIS was one of the main instruments on board the European Space Agency's Envisat (March, 2002 – April, 2012) platform. The land cover was used together with the MODIS active fires and burnt area products to analyze the fire regimes. ArcGIS 10.1 (ESRI, 2011) was used to overlay the datasets for the analyses.

4.2.4. GDAS meteorological data

Air-mass backward trajectory calculations were made using the meteorological data from the National Centers for Environmental Prediction's (NCEP; <http://www.ncep.noaa.gov/>) Global Data Assimilation System (GDAS). GDAS adds the following types of observations to a gridded, 3-D, model space: surface observations, balloon data, wind profiler data, aircraft reports, buoy observations, radar observations, and satellite observations. NCEP generates the 3-hourly GDAS GRIdded Binary (GRIB) files four times daily (at 00, 06, 12, and 18 UTC) with 1° latitude/longitude global grid (181 ×360). The GDAS archive accessed from the National Oceanic and Atmospheric Administration's (NOAA) Air Resources Laboratory (ARL) was used for this study. The ARL archiving program produces weekly files of 3-hourly, global dataset which is made available online at an ftp site (<ftp://arlftp.arlhq.noaa.gov/pub/archives/gdas1>). A total of 358 GDAS 7-day archive files covering a period of 6 years from December 2004 to December 2010 were used for this study.

4.3. Methods

4.3.1. Estimation of aerosol emissions

A recent study indicated that the relative abundance of BC and sulfates is the main determinant of overall aerosol radiative forcing (Ramana et al., 2010). Therefore, I analyzed BC and SO₂ emissions from fossil fuels combustion and biomass burning to estimate their contribution to aerosol loading in Nepal. Emissions from fossil fuels were estimated for various fuel types such as coal and fuel oil used mainly in factories and industries; kerosene and liquid petroleum gas (LPG) used for domestic purposes; and gasoline and diesel used in automobiles. The emissions from biomass burning were grouped into two: the first group included emissions from the combustion of biofuels such as fuel wood, agricultural residues and animal dung for domestic purposes; whereas the second group represented the emissions from open biomass burning in agricultural fields (crop residues), forests and savannah. Methods of emission estimation differed between the two groups of biomass burning.

BC and SO₂ emissions from both fossil fuels and the first group of biomass burning were estimated following European Monitoring and Evaluation Program/ European Environmental Agency (EMEP/EEA) air pollutant emission inventory guidebook 2013,

which gives a technical guidance to prepare national emission inventories (EEA, 2013) as:

$$E = ED * EF,$$

where E is the emissions (in grams), ED is the energy consumption data for different fuel types (in GJ) and EF is the emission factor (in g/GJ). The energy consumption data were derived from Water and Energy Commission Secretariat (WECS), Nepal for the period from 1995 to 2009 (WECS, 2010) and BC and SO₂ emission factors were derived from Bond et al. (2004) and EEA (2013) as shown in Table 4-1.

Table 4-1 Emission factors in g/kg for different aerosols for different fuel types.

Aerosols/ Fueltypes	Coal	Fuel oil	Kerosene	LPG	Gasoline	Diesel	Fuelwood	Agricultural residues	Animal dung
SO ₂	900	47	60	0.22	3.6	8.79	11	20.83	20.83
BC	6.91	1.12	21(a)	4.34(a)	9.39(a)	79.12(a)	57.4	36.46	36.46

(a) Values are from Bond et al. (2004)

Others are derived from EMEP/EEA air pollutant emission inventory guidebook 2013.

BC and SO₂ emissions from the second group of biomass burning, i.e. open biomass burning, were estimated following Seiler and Crutzen (1980) as:

$$E = A * B * \beta * EF,$$

where E is the emissions (in grams), A is the total land area burned annually (m²/yr), B is the average biomass/ fuel load (in kg dry matter/m²), β is the combustion efficiency of the above-ground biomass and EF is the emission factor (in g/kg). At first, the vegetation types subjected to open biomass burning were identified using GlobCover 2009. The burnt areas for identified vegetation types were derived using MODIS burnt area product from 2000 to 2009. The average biomass/ fuel load and combustion efficiency for the vegetation types were taken from Vadrevu et al. (2011, 2012) who did a similar study in the Himalayan region. BC and SO₂ emission factors were derived from Andreae and Merlet (2001); Akagi et al. (2011) and Yokelson et al. (2013) as shown in Table 4-2.

Table 4-2 Emission factors in g/kg for different aerosols for different vegetation types.

Aerosols	Agricultural residue	Tropical forest	Temperate forest	Savannah
SO ₂	0.40 ^a	0.40 ^b	1.06 ^c	0.48 ^b
BC	0.75 ^b	0.52 ^b	0.56 ^b	0.37 ^b

^a. Values are from Andreae and Merlet (2001)

^b. Values are from Akagi et al. (2011)

^c. Values are from Yokelson et al. (2013)

4.3.2. Estimation of influence of biomass burning

4.3.2.1. Selection of study area

MODIS firecounts within the 21°-40°N and 65°-98°E domain (Figure 4-1) were used to understand the possible influence of biomass burning within and outside the boundary of Nepal. The study area included all of Nepal, Bhutan and Bangladesh as well as parts of India, China, Myanmar, Pakistan, Afghanistan, Uzbekistan, Tajikistan, Kyrgyzstan and Turkmenistan.

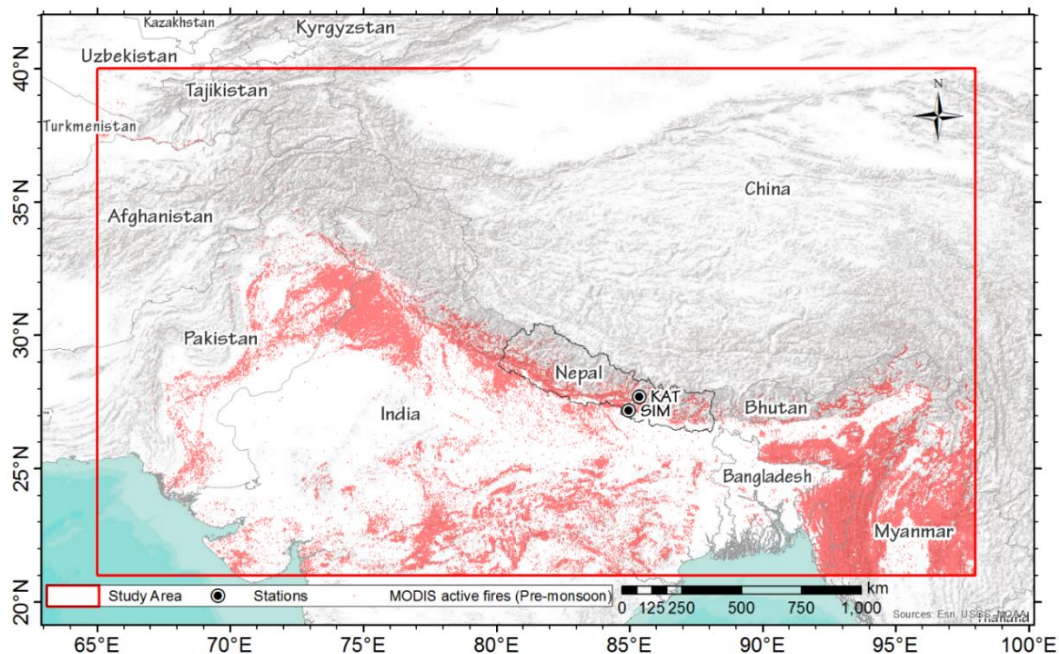


Figure 4-1 Study area (in red border) selected to detect the influence of biomass burning within and outside the boundary of Nepal (in thin black border). The red dots indicate MODIS active firecounts and the symbols (in black) indicates the location of Simara and Kathmandu.

I further chose two stations: Simara and Kathmandu, as representatives of the stations located in the plains and LH, respectively, to perform the air mass backward trajectory analysis.

4.3.2.2. Identification of acute pollution events

Acute pollution (AP) events were identified for Simara and Kathmandu by analyzing MODIS AOD values extracted for the grids corresponding to Simara and Kathmandu for the period 2005-2010. AP events, defined as the days characterized by significant AOD increase against the seasonal cycle, were identified using the method described by Marinoni et al. (2013) for estimating AP events for BC. Firstly, the normal seasonal cycle of AOD was calculated by averaging the six smoothed yearly cycle resulting from the application of three-time repeated iteration of a 21-day running mean to the daily mean AOD time series. This was followed by the calculation of the residuals of the original daily time series from the normal values. AP events were selected as the days on which the daily AOD values exceeded the 75th percentile of the positive residual population (Marinoni et al., 2013).

4.3.2.3. Calculation of air mass backward trajectory

In order to determine the transport pattern of air masses reaching the study locations, 5-day backward trajectories were calculated using the Hybrid Single Particle Lagrangian Integrated Trajectories model (HYSPLIT 4; Draxler and Hess, 1997).

HYSPLIT is a tool for quick response to atmospheric emergencies, diagnostic case studies, or climatological analyses using gridded meteorological data (Draxler and Hess, 1998). It has been used extensively in both global and regional pollutant transport studies (e.g., McGowan and Clark, 2008; Wang et al., 2010; Tang et al., 2013). HYSPLIT generates a simple trajectory of the time integrated advection of each particle using the three-dimensional wind field (Draxler and Hess 1997), represented in this study by the GDAS meteorological dataset.

The length of the back trajectories is restricted in many ways by the distances between source regions and the destination zone (Jorba et al., 2004). The selection of 5-day backward trajectories was done so that it represented the long-range transport of aerosols from the source regions as well as their residence time.

Daily ensembles of the 5-day backward trajectories were created for the period from January, 2005 through to December, 2010 every 6 h (at 00, 06, 12, 18 UTC), all starting at 100 meters above ground level (m a.g.l.) of the study locations. For the calculation of the trajectories, we considered 3 km as the maximum possible extent of biomass burning plume height. Putero et al. (2014) analyzed the upper extension of the aerosol layer for the detected fires using Cloud-Aerosol LiDAR and Infrared Pathfinder Satellite Observation (CALIPSO) and suggested the height to be appropriate for this study area. Their findings regarding the extent of biomass plume height are also consistent with the suggestions made by Vadrevu et al., (2012). Accordingly, any trajectory moving above 3000 m a.g.l. was truncated. A screen capture of HYSPLIT with the model parameters is included in Appendix Fig. 2.

TrajStat (Wang et al., 2009), an application for the visualization and statistical analysis of trajectories, was used to change the HYSPLIT derived trajectory paths to ESRI 'PolylineZ' shape file format. TrajStat was also used for the cluster analysis of the trajectories.

4.3.2.4. Identification of the acute pollution events affected by biomass burning

In order to identify the AP events possibly affected by biomass burning, we coupled the 5-day air mass backward trajectory ensembles with the occurrences of fires from MODIS active fire product for the study area as defined in section 4.3.2.1. First, we calculated the trajectory ensembles using HYSPLIT. The trajectory ensemble for any particular day was considered to be influenced by biomass burning if at least one member of the ensemble overpassed an active fire within the 5-day period. A buffer of 0.05° (both sides) was considered for each member of the ensemble while locating the underlying fire events. Finally, the trajectory ensembles under the influence of biomass burning were geotagged (as within-Nepal or outside-Nepal) to the location contributing maximum number of fire events in each case. An iterative ArcGIS model was created to complete the calculation for the period 2005-2010.

4.3.2.5. Cluster analysis for long-range transport of pollutants

Cluster analysis is conducted to identify the general patterns of air mass backward trajectories as well as the frequency of each pattern (Su et al., 2015). These clusters represent air mass from different sources and distinct transport pathways. Appendix Fig.

3 shows all daily 5-day backward trajectories of air masses arriving Kathmandu for the period 2005-2010. The trajectories were grouped into 6 clusters for further analysis. The clusters were limited to six because higher number of clustering resulted in indistinct pathways that originated more or less in the same regions. The manageable number of unique clusters was also helpful in the interpretation of the results.

The backward trajectories were clustered using the K-means clustering technique (maximizing between-cluster variance while minimizing within-cluster variance) in TrajStat (Sirois and Bottenheim, 1995; Wang et al., 2009). Here, Euclidean distance was used to compute the distance between the trajectories while clustering. Similar approach for cluster analysis of backward trajectories was also used by Tang et al. (2013) and Abdalmogith and Harrison (2005).

4.4. Results

4.4.1. Aerosols (Black carbon and SO₂) emissions (1995-2009)

Figure 4-2 details the vegetation types subjected to open biomass burning and their burnt areas derived from GlobCover 2009 and MODIS burnt area product.

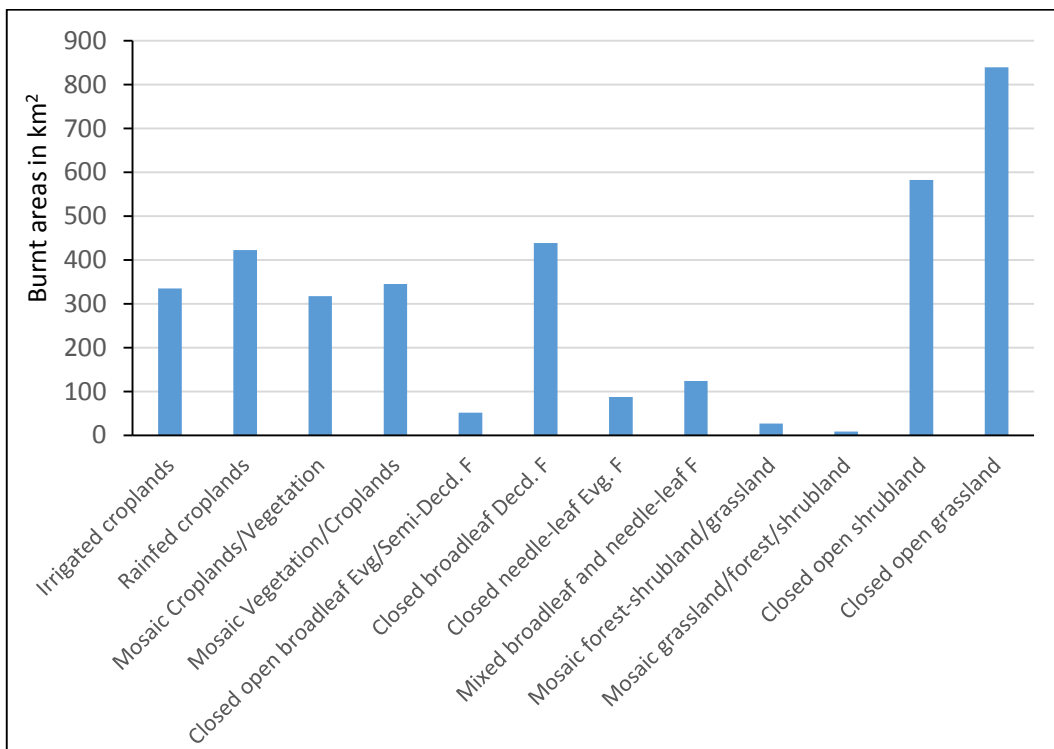


Figure 4-2 Total burnt areas in different vegetation types derived from Globcover 2009 and MODIS burnt area product from 2005 to 2010.

From 2005 to 2010, the average burnt area was estimated to be 298 km². Among the different vegetation types, burnt areas were dominated by *closed to open grassland* (23.47%) followed by *closed to open shrubland* (16.28%), *closed broadleaf deciduous forest* (12.26%) and *rain-fed croplands* (11.80%). For simplification, the emissions from different vegetation types were grouped into two categories: ‘crop residues’ for emissions from croplands; and ‘forest and savannah’ for emissions from different forests, mosaic vegetation including *open to closed grassland/ shrubland*.

Emissions of BC and SO₂ from the combustion of various fuel types (all included in section 4.3.1) were combined to get the total aerosol emission estimates for Nepal (Figure 4-3 and Figure 4-4). The average BC and SO₂ emissions from 1995 to 2009 were estimated to be 18.12 and 10.15 Gg (giga-grams) per year respectively which implies that BC emissions exceeded the emissions of SO₂ in Nepal. A steady increase is observed in the emission of BC for the observed period and fuel wood is the major contributor with the average equaling 86% of the total BC emissions. For SO₂ emissions, coal is the dominant fuel type contributing on average by 53% to the total emissions followed by fuel wood (30%).

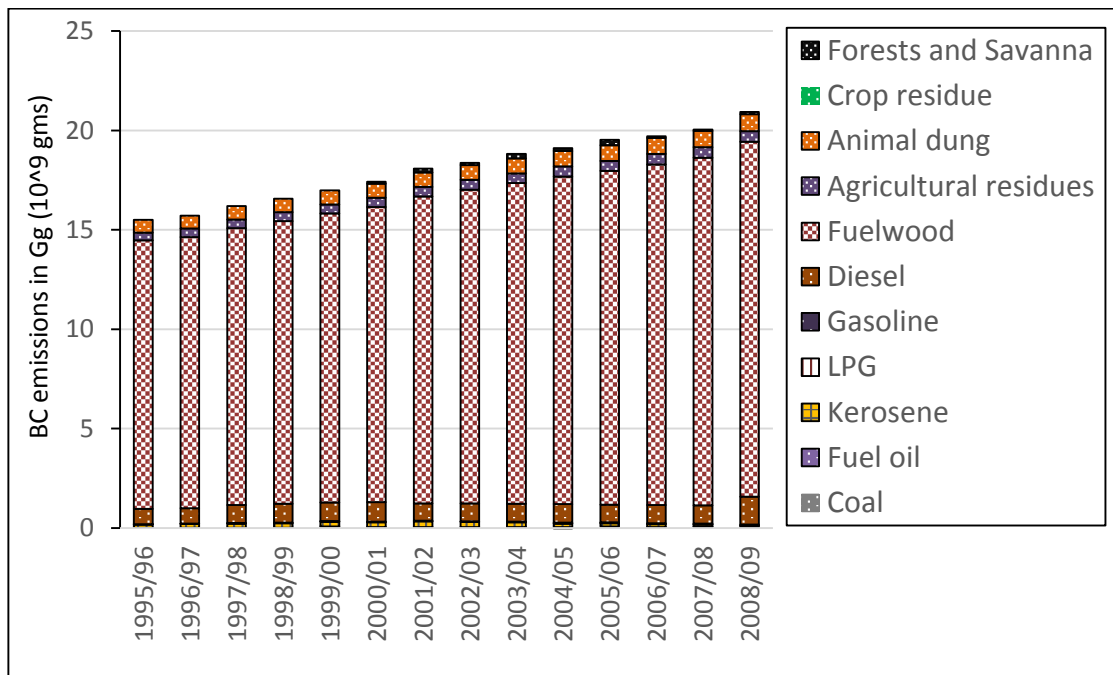


Figure 4-3 Black carbon (BC) emissions from fossil fuel combustion and biomass burning in Nepal from 1995 to 2009. Note that the contribution from open burning of ‘Forest and Savanna’ and ‘Crop residue’ is accounted for only from 2000/2001 on.

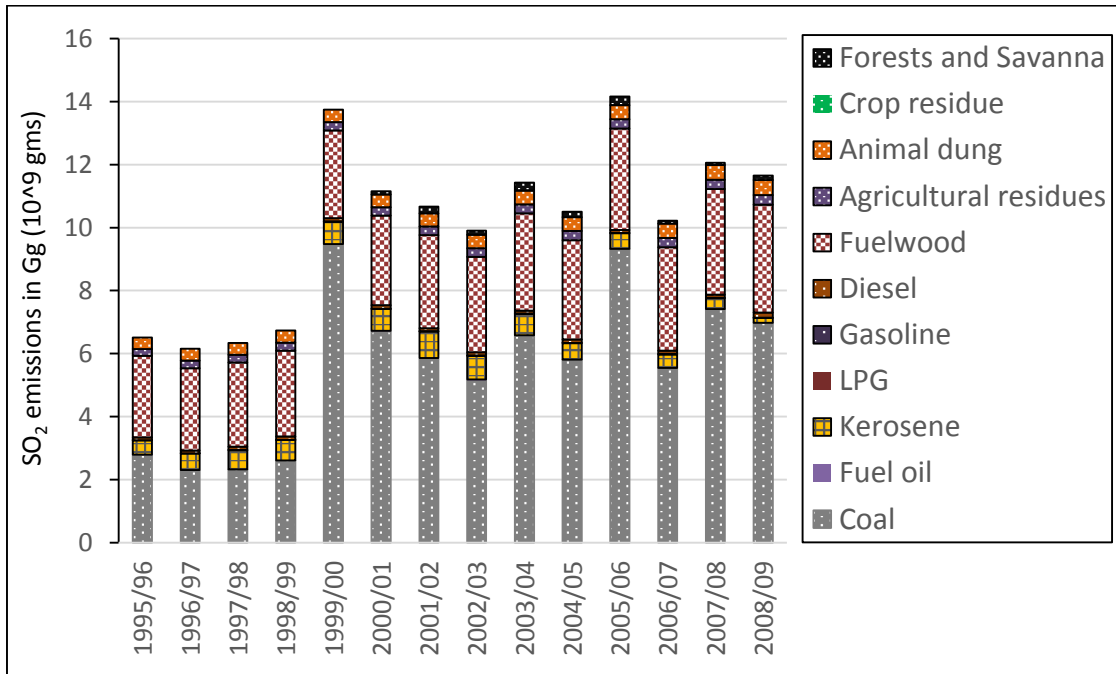


Figure 4-4 Sulfur dioxide (SO₂) emissions from fossil fuel combustion and biomass burning in Nepal from 1995 to 2009. Note that the contribution from open burning of ‘Forest and Savanna’ and ‘Crop residue’ is accounted for only from 2000/2001 on.

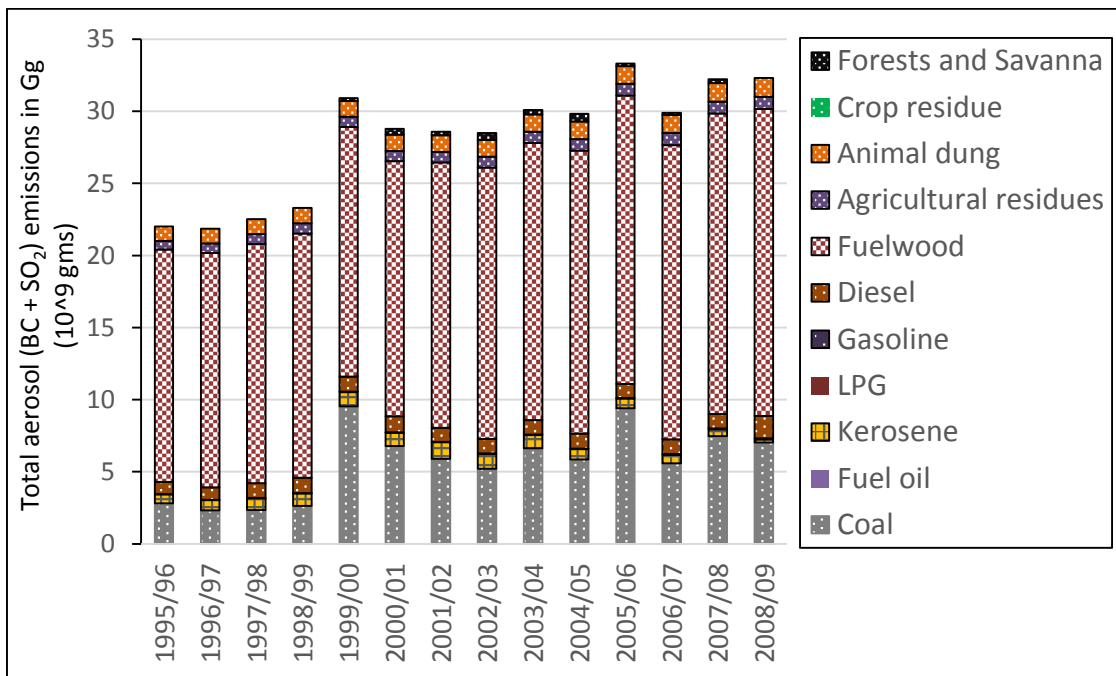


Figure 4-5 Total emissions (sum of BC and SO₂) from fossil fuel combustion and biomass burning in Nepal from 1995 to 2009. Note that the contribution from open burning of ‘Forest and Savanna’ and ‘Crop residue’ is accounted for only from 2000/2001 on.

For total aerosol emissions for the observed period as shown in Figure 4-5, the emissions from biomass burning were estimated to be approximately three times the emissions from fossil fuel combustion, contributing on average by 74% to the total emissions. This suggests that biomass burning is the major source to aerosols in Nepal. Although emissions from open biomass burning is negligible in comparison to other sources, seasonal occurrences of open fires are responsible for peak concentrations of aerosols significantly influencing the air-quality and regional climate (Bonasoni et al., 2012; Putero et al., 2014). Hence, in the next section, I studied aerosol variations and open biomass burning hereafter referred to as ‘biomass burning’ pattern in Nepal.

4.4.2. Temporal and spatial variations of aerosols and biomass burning

4.4.2.1. Variations in aerosol optical depth (2005-2010)

The variation of aerosols in Nepal was studied using MODIS AOD values extracted for the grids corresponding to Nepal. Figure 4-6 shows the variations in monthly mean AOD for Nepal averaged across 2005-2010. The average value of AOD for the whole observation period was 0.35. The maximum values of AOD occurred in the months of June (0.50) and April (0.495) whereas the minimum AOD values occurred in September (0.25). The monthly variations in AOD reflects the washout effect of the Indian summer monsoon (ISM) showing least AOD values in the months following June.

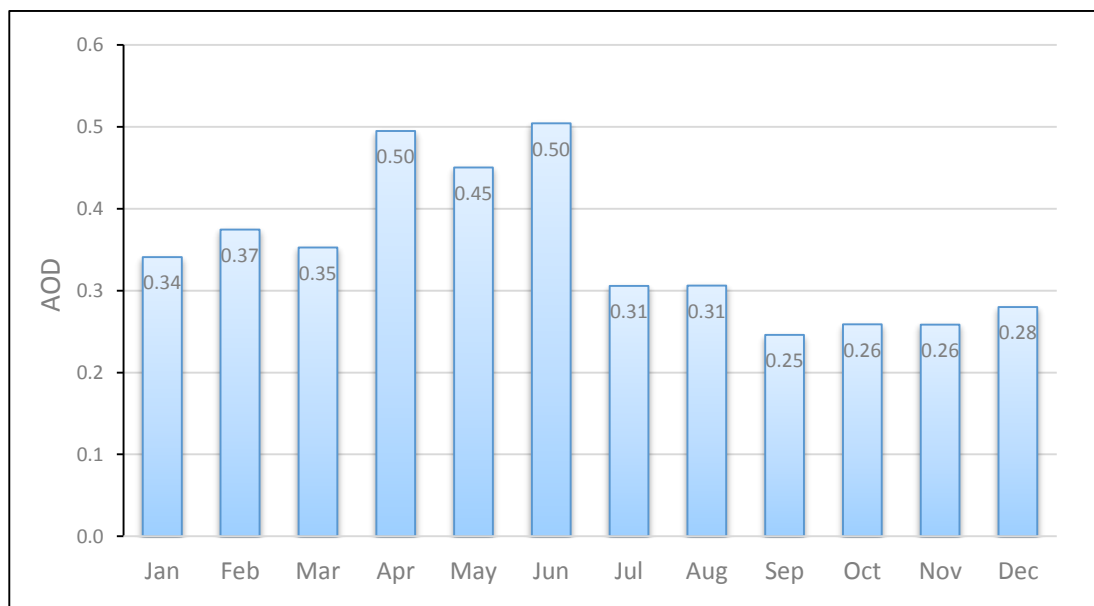


Figure 4-6 Monthly mean aerosol optical depth (AOD) for Nepal averaged across 2005 to 2010.

The seasonal maxima in AOD were observed in pre-monsoon season (0.43) followed by monsoon (0.38) and winter seasons (0.36). Across the 6 years, 771 days exceeded the standard AOD value of 0.3.

Figure 4-7 shows variations in annual mean AOD from 2005 to 2010 in different physiographic regions as classified in Chapter 2. Among the physiographic regions, the average of annual mean AOD across the observation period showed the maximum in the plains (0.48) and gradually decreased with increasing elevation, with 0.35 in LH and 0.23 in HHM, suggesting intense pollution in the plains and LH in comparison to HHM.

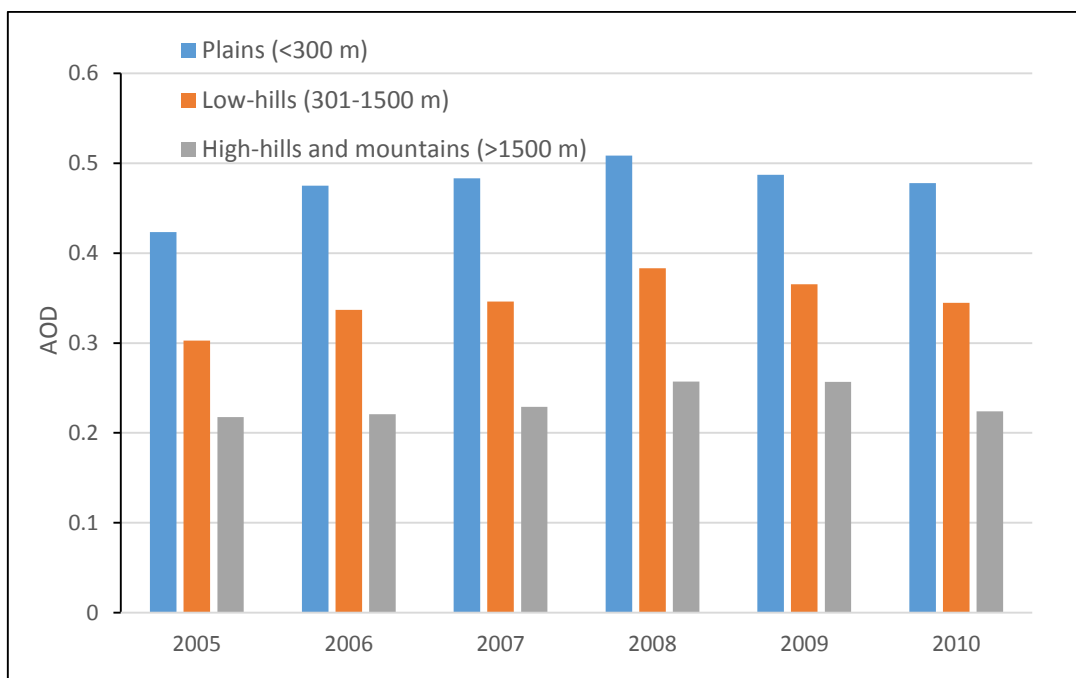


Figure 4-7 Annual mean aerosol optical depth (AOD) in different physiographic regions from 2005 to 2010.

4.4.2.2. Variations in MODIS active firecounts (2005-2010)

To study biomass burning pattern in Nepal, firecounts derived from MODIS active fire product within the boundary of Nepal was used. Figure 4-8 shows the variations in monthly mean firecounts in Nepal averaged across 2005-2010. The average number of firecounts for the whole observation period was 1989. Pre-monsoon season from March to May is the biomass burning season in Nepal which accounts for 86.2% of the total fires. April is the peak burning month with 53% of firecounts followed by March (26.6%).

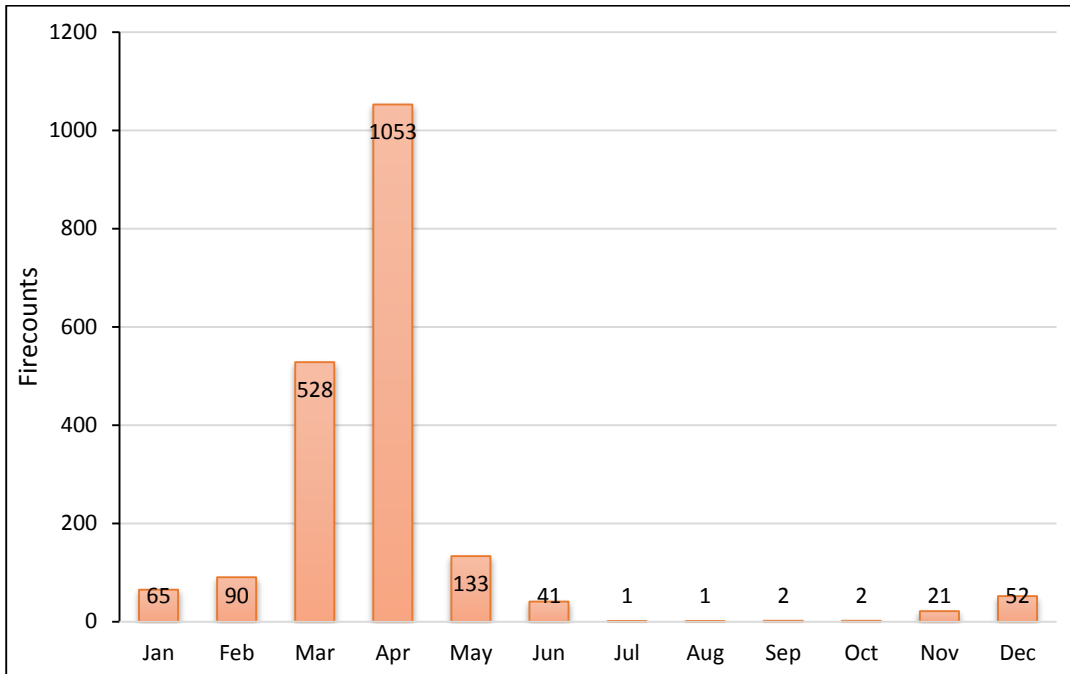


Figure 4-8 Monthly mean MODIS active firecounts for Nepal averaged across 2005 to 2010.

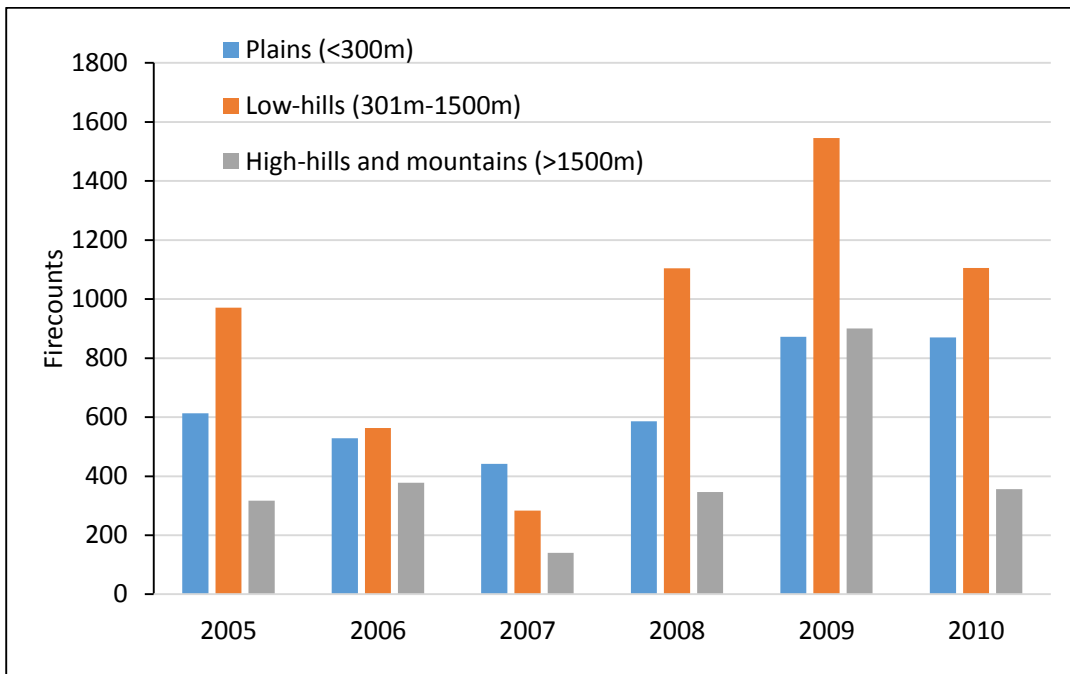


Figure 4-9 Annual total MODIS active firecounts in different physiographic regions from 2005 to 2010.

Figure 4-9 shows the annual total firecounts in different physiographic regions from 2005 to 2010. The number of firecounts showed year to year variation with the highest

occurrence of 3318 firecounts in 2009. Occurrence of biomass burning was maximum in the LH with an average of 929 firecounts, followed by plains (652) and HHM (406). The high AOD values and maximum firecounts in the pre-monsoon season suggested that biomass burning could affect the aerosol variations in the atmosphere. Therefore, I compared the monthly total firecounts and monthly mean AOD over the plains, LH and HHM from 2005 to 2010 (Table 4-3). The correlation coefficients were significant between AOD and firecounts for LH ($r = 0.65$) and between firecounts in LH and AOD in HHM ($r = 0.72$). The latter correlation suggests an influence of biomass burning in LH on the aerosol variations in HHM.

Table 4-3 Correlation coefficients between monthly total fire-counts (FC) and monthly mean aerosol optical depth (AOD) in different physiographic regions for pre-monsoon season (2005-2010).

AOD / FC	FC Plains	FC Low-hills	FC High-hills
AOD Plains	0.083	0.387	0.254
AOD Low-hills	0.277	0.648	0.443
AOD High-hills	0.283	0.719	0.487

Figure 4-10 presents the density map of total firecounts showing the regions of peak fire occurrences in the pre-monsoon season. By overlaying the density map on the regional location map, regions of peak firecounts were identified as the national parks, wildlife reserves, forests and croplands in the plains and LH regions of Nepal. A field visit was conducted at 5 locations as shown in the density map to verify the vegetation types subjected to biomass burning during the period from February to March, 2014. I found that the mustard residues were subjected to burning in the croplands located in the plains. The residues of other crops such as wheat and rice were fed to the livestock while mustard residues was subjected to burning due to its less preference by the livestock. It was interesting to find that the grasslands and shrub lands within national parks and wildlife reserves were exposed to burning every year for regenerating new vegetation, which was essential for the animals feeding on the vegetation in those protected areas. In addition, local people revealed that the forests located at the foothills were subjected to burning as a result of human malice (regeneration of feed for cattle,

forest clearing for land encroachment, tapping of a legal loophole allowing the cut of trees after fire) and/or negligence (such as discarded burning cigarette butts, open camp fires).

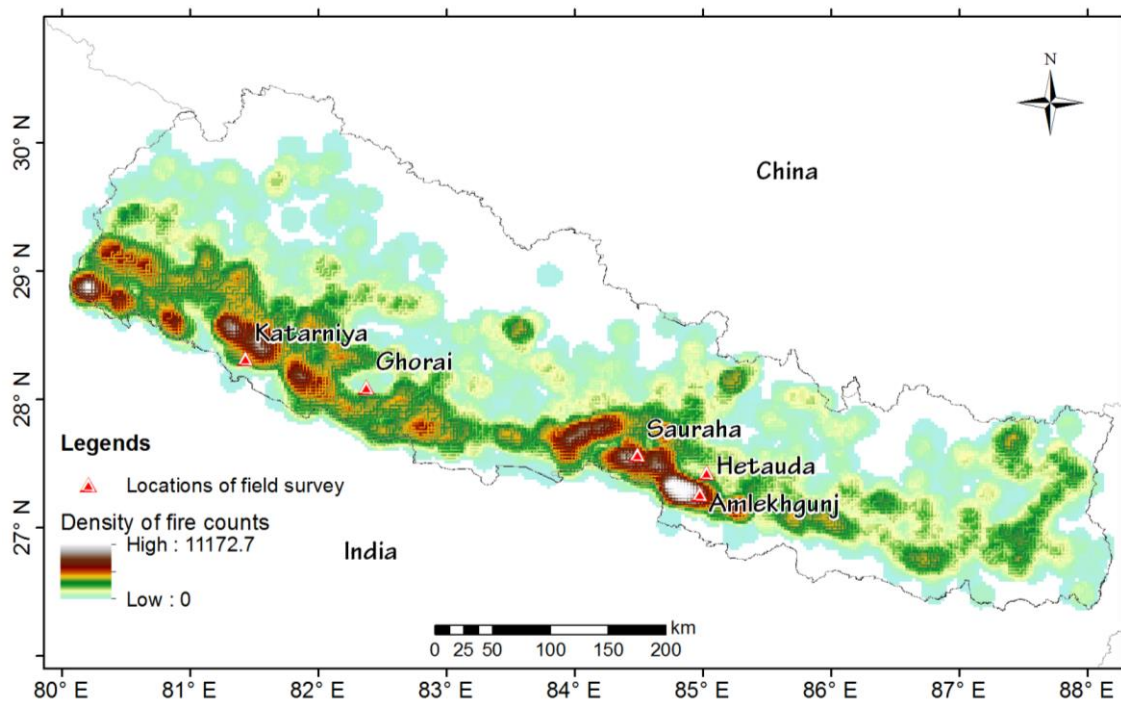


Figure 4-10 Density map of MODIS active firecounts showing biomass burning in pre-monsoon seasons in Nepal from 2005-2010. Symbols indicate location of field survey.

4.4.3. Influence of biomass burning in aerosol variations

To understand the influence of biomass burning in aerosol variations, at first, AP events characterized by significant increases in daily mean AOD values were identified. Figure 4-11 shows the time series in daily mean AOD and AP events in Simara and Kathmandu, calculated using the method described in section 4.3.2.2. For the entire time series, 153 AP events were identified for Simara and 145 AP events for Kathmandu, respectively. For Simara, AOD values in AP events ranged from 0.677 to 2.257 with an average of 1.06 and a standard deviation (SD) of 0.26. For Kathmandu, AOD values during AP events ranged from 0.552 to 1.96 with an average of 0.978 and a SD of 0.26. These values suggest that higher AOD values during AP events occurred in Simara in comparison to Kathmandu.

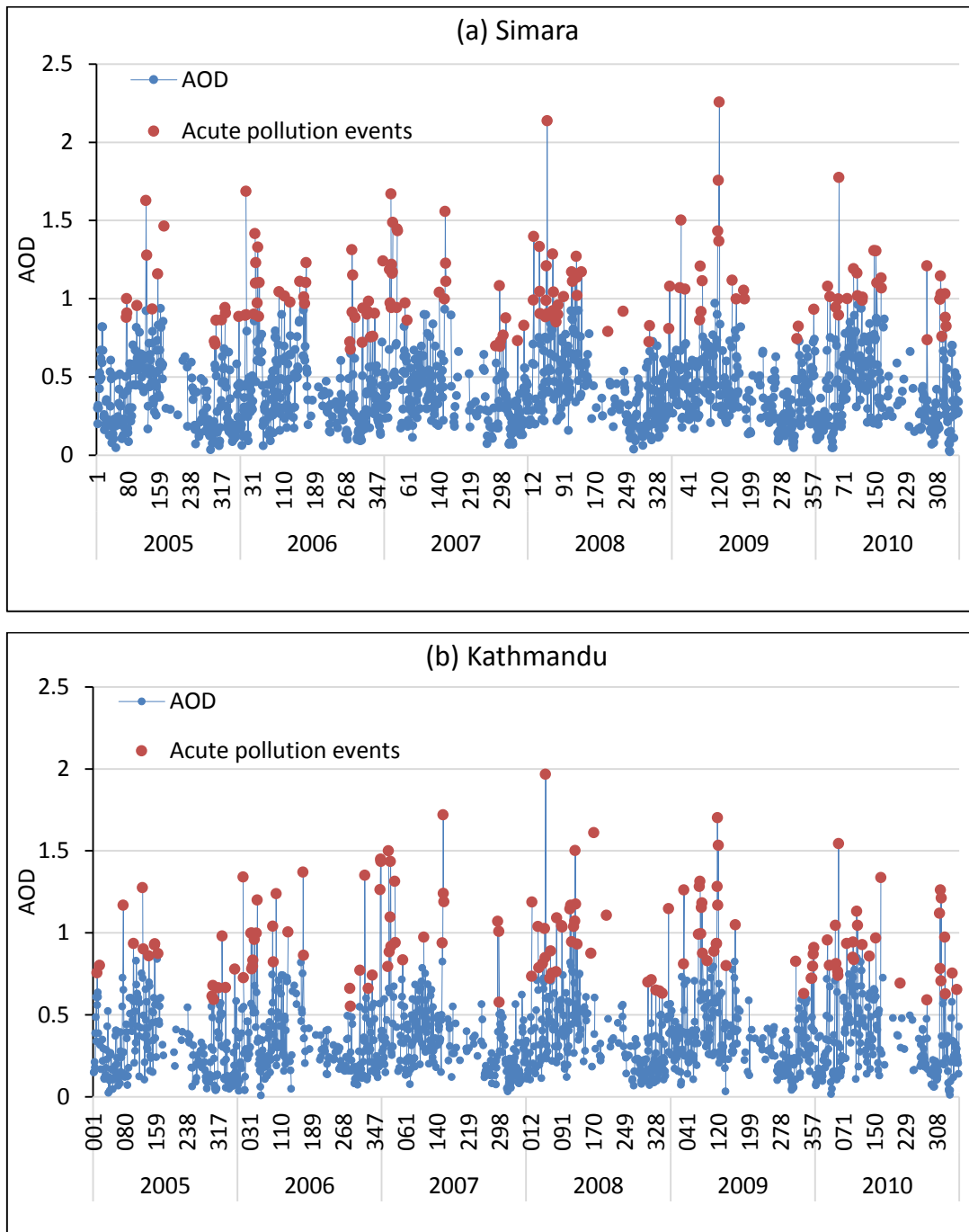


Figure 4-11 Time series of daily mean aerosol optical depth (AOD) and acute pollution events in (a) Simara and (b) Kathmandu from 2005 to 2010.

I further identified the trajectories that intercepted the firecounts occurring within and outside the boundary of Nepal before arriving Simara and Kathmandu. The trajectories are referred to as ‘biomass burning (BB) trajectories’ hereafter, and the days of arrival of BB trajectories at the two locations were identified using the method

described in section 4.3.2.4. Figure 4-12 shows monthly variations in firecounts intercepted by the trajectories arriving at Simara and Kathmandu from 2005 to 2010.

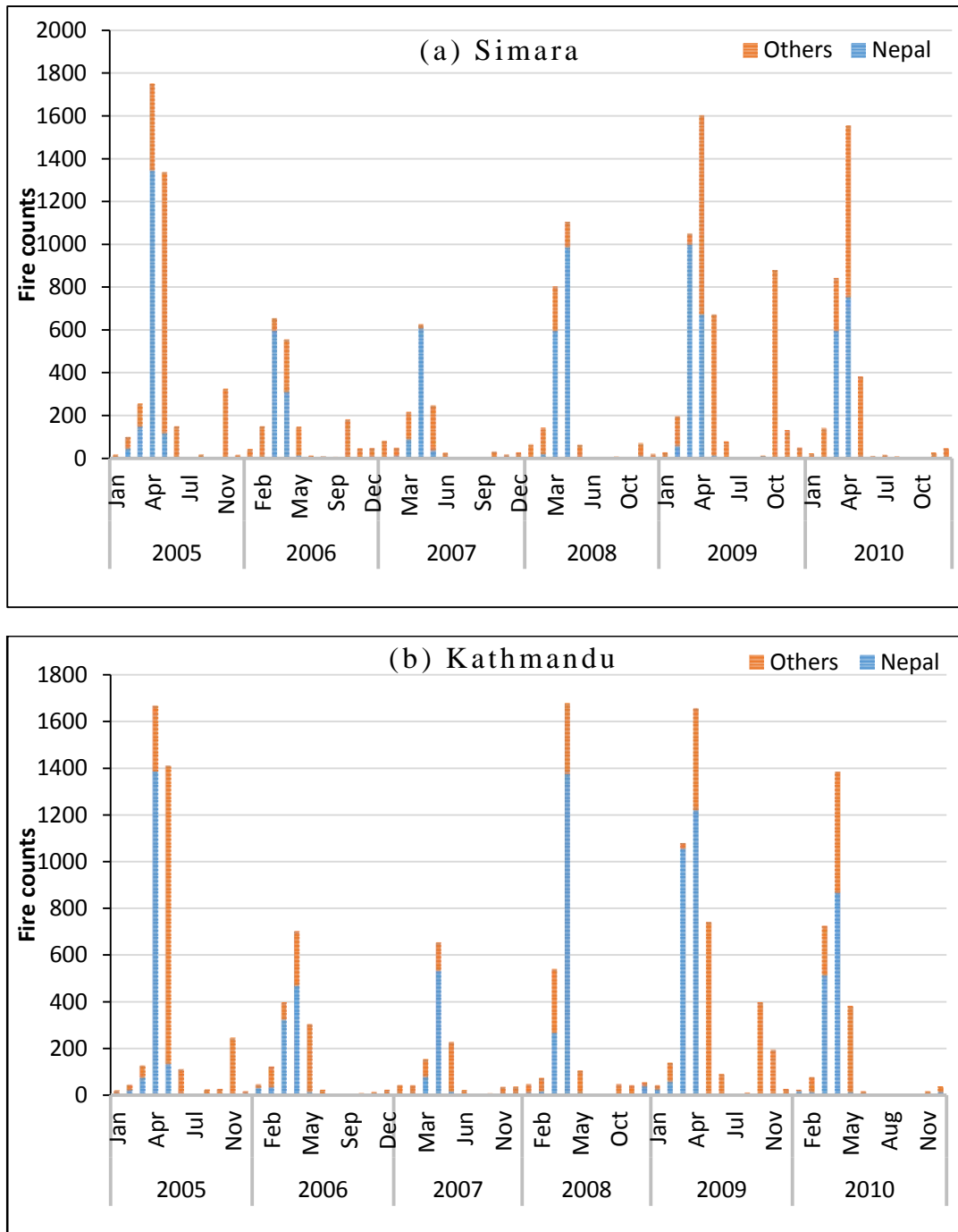


Figure 4-12 Monthly variations in firecounts intercepted by the trajectories arriving at (a) Simara and (b) Kathmandu from 2005 to 2010.

In the case of Simara, 80% of the firecounts were intercepted in the pre-monsoon season. Of the total firecounts intercepted by BB trajectories, 47% were within Nepal

while 53% were outside the boundary of Nepal. Similarly for Kathmandu, 86 % of the firecounts interception occurred in the same season. Of the total firecounts intercepted by BB trajectories for Kathmandu, 54% were within Nepal while 46% were outside the country. These estimates indicates that Kathmandu was influenced slightly more by the biomass burning occurring within Nepal while Simara was subjected more to trans-boundary influences of biomass burning. On average across the 6 years, the annual number of days with BB trajectories were 176 and 155 in Simara and Kathmandu, respectively.

To evaluate the possible contribution of biomass burning to the occurrence of AP events, I identified the days with simultaneous occurrences of both AP events and BB trajectories. Figure 4-13 shows the number of AP events possibly influenced by BB trajectories across the observation period. In Simara, out of the 153 AP events, 84 days (55% of AP events) were influenced by biomass burning occurring on a regional scale, referred to as ‘BB pollution events’. Seasonally, pre-monsoon season was highly influenced by BB trajectories particularly in the month of April, when 13 out of 15 AP events were influenced by biomass burning. In the case of Kathmandu, out of the 145 AP events, 87 days (60% of the AP events) were influenced by BB trajectories with highest influence in the pre-monsoon season. In April, 21 out of 22 AP events were influenced by biomass burning.

For each of the BB pollution events, it was important to identify the likely source regions of biomass burning to understand the influence from trans-boundary pollution. Figure 4-14 shows regional frequency of firecounts for different seasons during BB acute pollution events. At both the locations, it was evident that biomass burning occurring within Nepal could strongly influence the occurrence of highest AOD in pre-monsoon season, while trans-boundary biomass burning was dominant in all the other seasons, particularly in the post-monsoon season, which suggests that trans-boundary pollution by biomass burning plays a crucial role in causing peak AOD concentrations in Nepal.

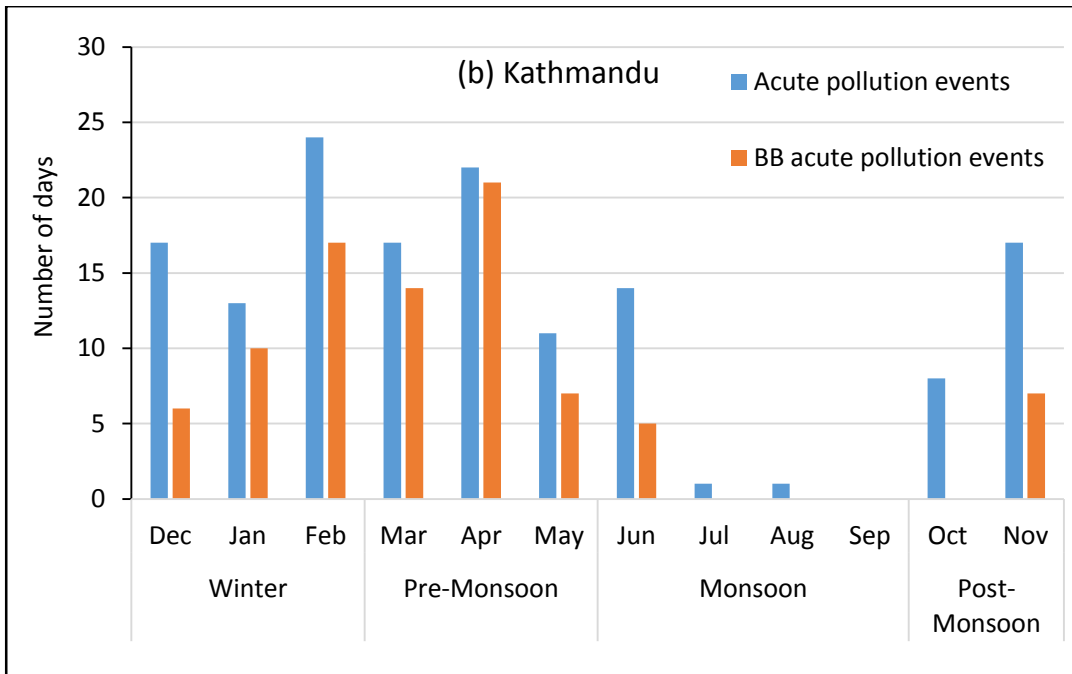
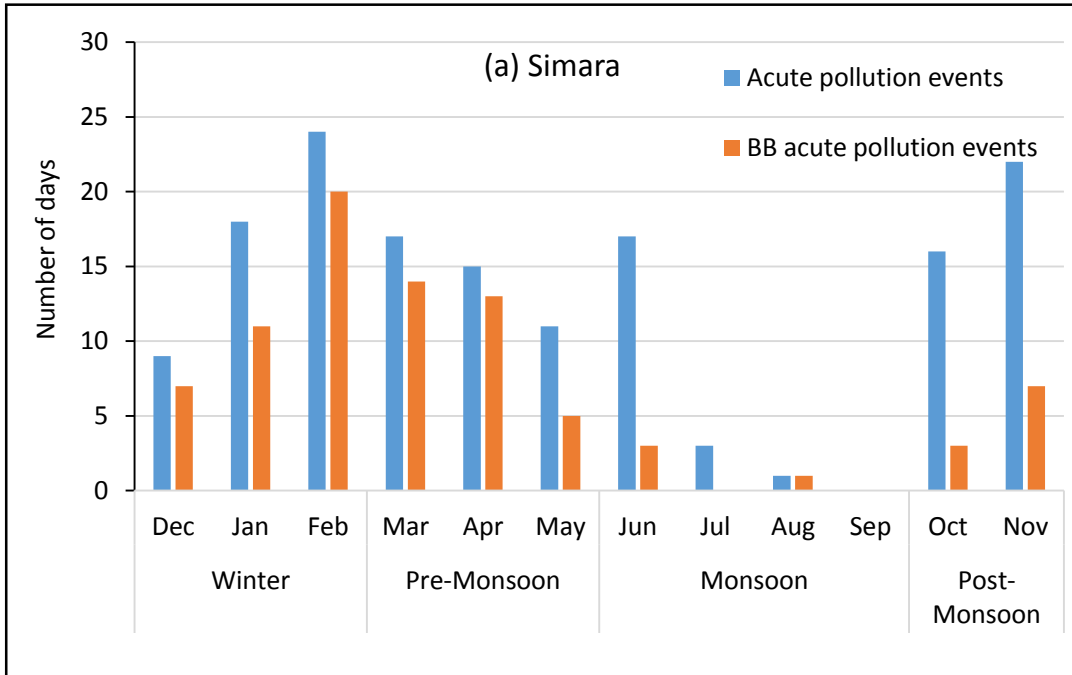


Figure 4-13 Number of acute pollution events possibly influenced by biomass burning in the region (a) Simara and (b) Kathmandu for the period 2005-2010.

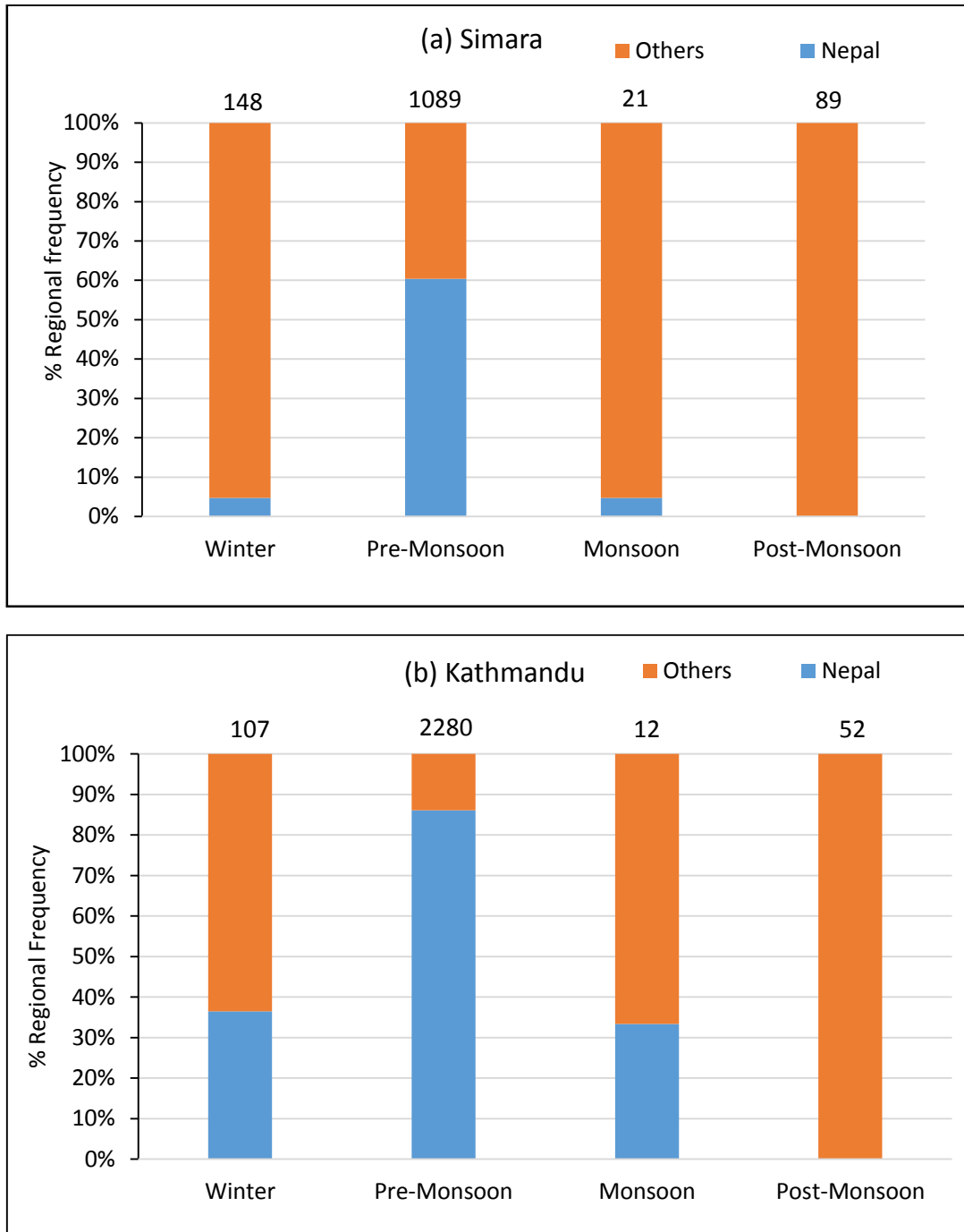


Figure 4-14 Regional frequency (%) of firecounts for different seasons during biomass burning (BB) pollution events (a) Simara and (b) Kathmandu across the observation period (2005-2010). Numbers at the top of each column indicate the total number of firecounts intercepted during BB pollution events.

4.4.4. Influence of long distance transport of polluted air mass on aerosol variations

The results described in the previous section shows that around 40% of the AP events in both the locations cannot be related to the identified biomass burning events, hence in this section I tried to identify the source locations that probably transported aerosols from local as well as long distance regions and contributed to peak AOD. By clustering the air mass backward trajectories arriving Kathmandu from 2005-2010, six clusters of air mass transport having different source of origins and different transport paths were identified as explained in section 4.3.2.5 (Figure 4-15).

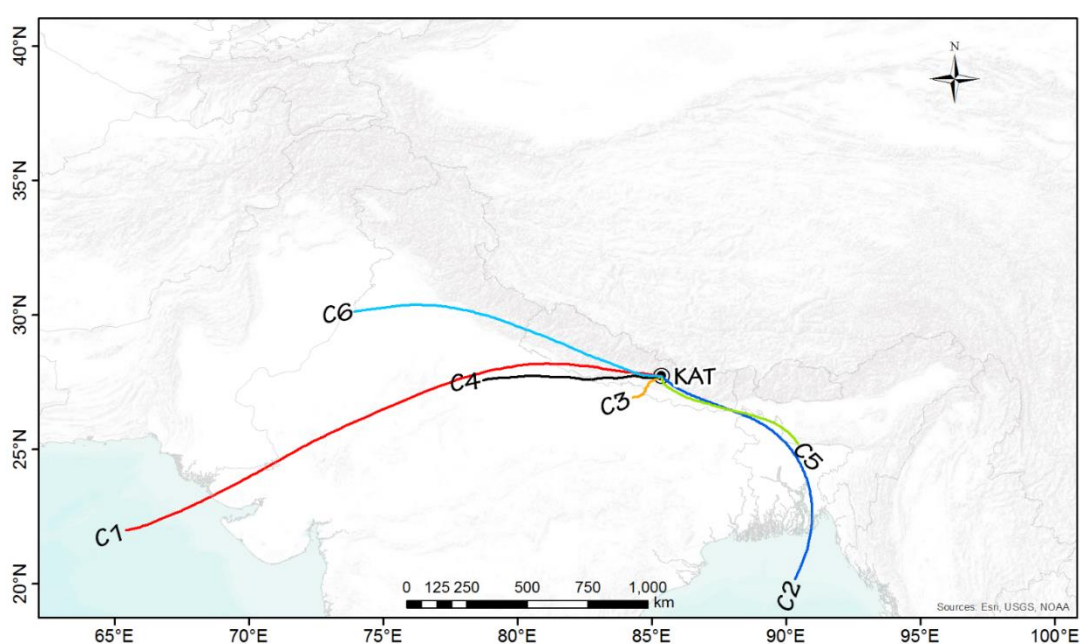


Figure 4-15 Mean backward trajectories for clusters 1 to 6 arriving at Kathmandu (KAT) across the period 2005-2010. See Appendix Fig. 3 for all the trajectories in each cluster.

Table 4-4 Seasonal frequency of each cluster reaching Kathmandu in 2005-2010.

Seasons	Mean clusters (%)					
	C1	C2	C3	C4	C5	C6
Winter	15.6	0.4	26.7	28.1	2.7	26.5
Pre-M	7.3	11.6	16.5	10.9	29.9	23.8
Monsoon	0.7	46.3	10.6	4.3	35.6	2.5
Post-M	1.6	3.3	55.8	8.4	22.8	8.1
Total	4.4	25.5	20.9	9.8	27.8	11.6

The seasonal and total frequencies of each cluster arriving Kathmandu from 2005 to 2010 are shown in Table 4-4 and the monthly variation in mean AOD matched with each cluster is presented in Figure 4-16.

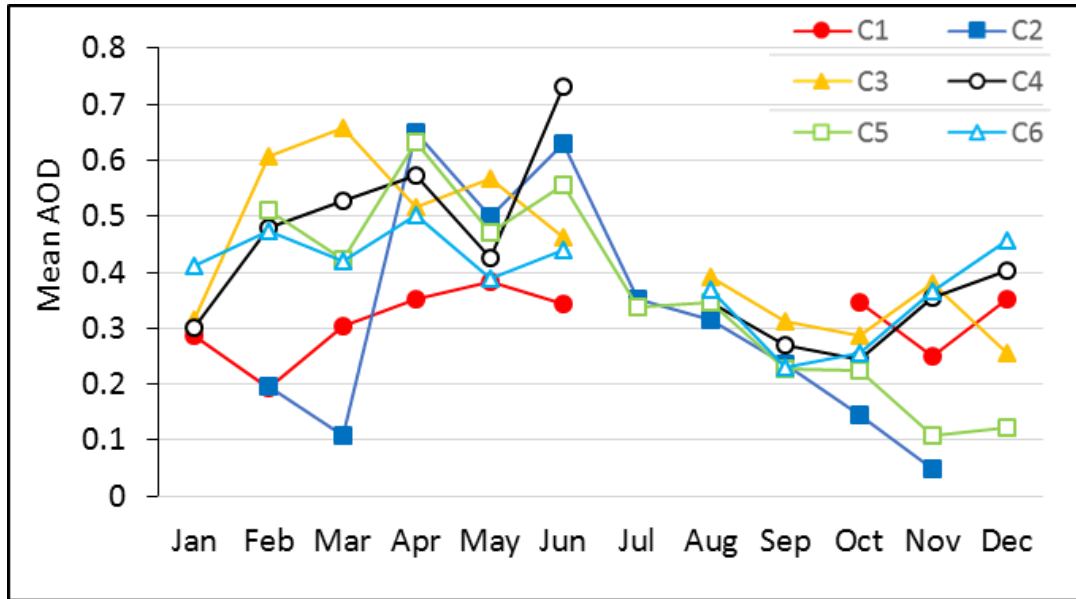


Figure 4-16 Monthly variation in mean AOD by trajectory clusters in Kathmandu in 2005-2010

Such clusters were prepared for air masses arriving Simara also (Figure 4-17). The pathways of the clusters were more or less the same for both the locations, therefore, only the description of the clusters and their pathways are given for Kathmandu.

Cluster 1 (C1) represents air masses that originated in the Arabian Sea, have passed through the Thar Desert and the IGP quickly before arriving at Kathmandu and has least contribution among all the clusters. Cluster 3 (C3), cluster 4 (C4) and cluster 6 (C6), all these 3 clusters comprising air masses from the IGP, were dominant in the winter season (accounted for 81.6% of all the air trajectories). Hence, the highest number of AP events (Figure 4-13a) and peak AOD in winter season can be attributed to the large-scale anthropogenic emissions (both of biomass and fossil fuel origins) from IGP. Cluster 5 (C5) encompasses the air mass that originated in one of the North-eastern states of India, Meghalaya. And C6, as mentioned earlier originated in northern state of IGP, Punjab. Both these clusters were dominant in the pre-monsoon season and had their pathways through the LH regions of Nepal, where biomass burning is dominant (Figure 4-10).

Meghalaya is dominated by slash and burn agriculture and Punjab is characterized by wheat residue burning in the pre-monsoon season (Vadrevu et al., 2013), these biomass burning might have made significant contribution to the peak AOD. Cluster 2 (C2) represented air masses originating in the Bay of Bengal, both C2 and C5 were dominant in the monsoon season (accounted for 81.9% of all the air trajectories in the season) and indicated the pathway of the ISM circulation. The peak AOD values in early June are related to the considerable amount of air pollutants brought by the ISM circulation (Shrestha et al., 2000). It should be noted that AOD values in C4 was the highest in June though it contributed only 4.3% in the monsoon season, which can be explained by the weakening or ‘break’ in the ISM circulation and dominance of westerly circulation (Marinoni et al., 2013). The air masses from C3 was dominant in the post-monsoon season and indicates the influence of local pollution. It is noteworthy that AOD values in C6 were similar to those in C3 despite small contribution of 8.1% of all the trajectories. This could be attributed to the polluted smoke of rice residue burning occurring on a large scale in Punjab of the northern IGP (Vadrevu et al., 2011).

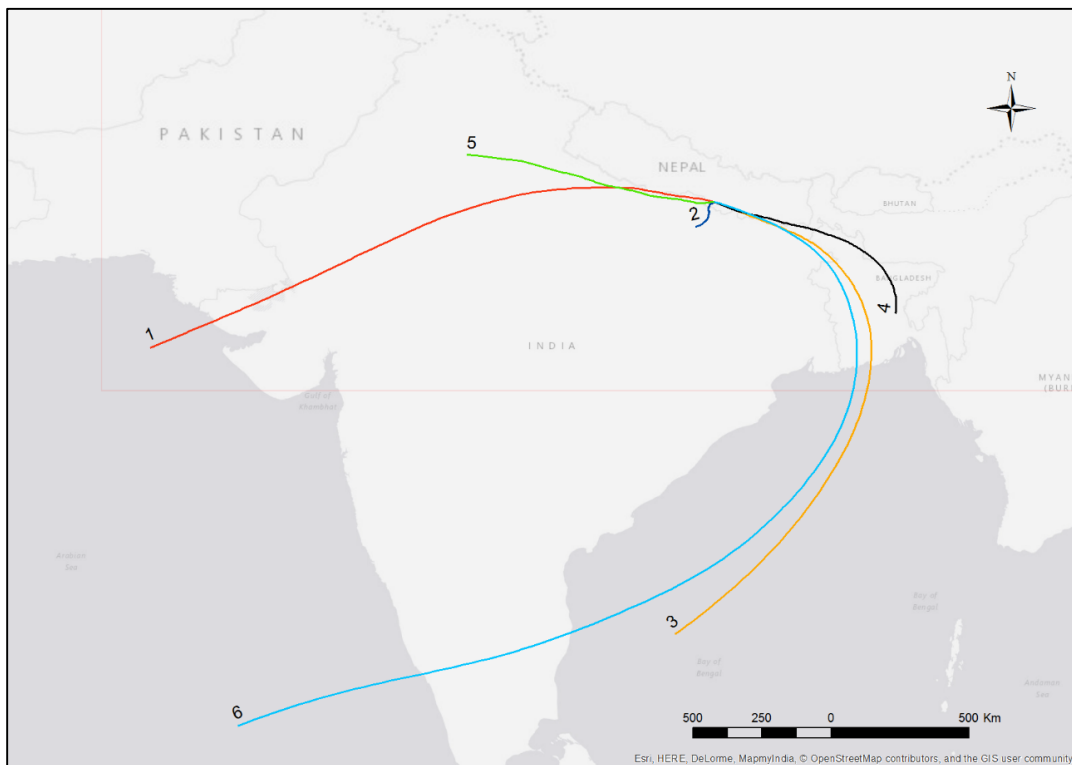


Figure 4-17 Mean backward trajectories for clusters 1 to 6 arriving at Simara (SIM) across the period 2005-2010.

4.5. Discussion

4.5.1. Aerosol optical depth variations in Nepal

Various satellite monitoring and field experiments have pointed the existence of atmospheric brown clouds (ABC) over South Asia, which is characterized by persistent thick tropospheric layers of aerosols with AOD values greater than 0.3 (Ramanathan et al., 2007a). In this study, 771 days (129 days per year) were identified across the observation period with exceedance of the standard AOD of 0.3 in Nepal. Further, AOD values greater than 0.3 had been reported for major cities with intense anthropogenic pollution in India and China (Li et al., 2009; Sarkar et al., 2006). The mean AOD of 0.35 observed for Nepal is much higher than the global mean AOD value of 0.12 ± 0.04 as reported by Ramanathan et al. (2005). The mean AOD values were particularly high during the pre-monsoon season, which is identified as the peak biomass burning season in Nepal. Vadrevu et al. (2011) reported mean AOD value of 0.6 in peak agricultural residue burning season in Punjab, exceeding 1.5 in most of the days in October and November during the period of rice residue burning (Badarinath, 2010; Kaskaoutis et al., 2014). Similarly, Pelon et al. (2008) recorded peak AOD values close to 2.0 from agricultural fires mainly in the dry season over Djougou, Benin, Africa. Eck (2003) reported strong peak of 2.0 in AOD values from tropical biomass burning in Brazil and Zambia. Eck et al. (2009) also reported AOD values of 0.70–0.98 during the peak biomass-burning season in the boreal forests, while MODIS AODs at the levels of 0.5–0.8 were retrieved over the Mediterranean due to severe Greek wildfires in August 2007 (Kaskaoutis et al., 2011). During BB pollution events mentioned in this study, AOD values were higher than 1.0, which is comparable to the AOD values recorded in those studies mentioned.

I attempted to compare MODIS-derived AOD values with the level 2 AERONET (Aerosol Robotic Network) ground-based observations of AOD. Unfortunately, AERONET stations are limited in Nepal and long-term data were unavailable. The AERONET derived AOD values of 0.54 for one of the stations, Hetauda (an inner valley in foothills), in April, 2009 closely matched with the MODIS derived AOD value of 0.60 for Simara (located at an aerial distance of 30 km from Hetauda) in the same month

and year. This suggests that MODIS-derived AOD values were consistent with the ground observations of AOD at AERONET stations.

4.5.2. Contribution of biomass burning to aerosol optical depth

Biomass burning has been recognized as an important source of several trace atmospheric components particularly black and organic carbon particles, which contributes to air quality degradation at local and global scales (Andreae and Merlet, 2001; Streets, 2003). The higher BC emissions compared to SO₂ emissions estimated in this study reflects the dominance of biomass burning aerosols in Nepal, which is consistent with the presence of high content of BC in Asian ABC, pointed earlier by Lelieveld et al. (2001). In this study, the peak AOD in different seasons were found to be influenced by biomass burning from within and outside the boundary of Nepal. On an average, approximately 50% of the firecounts intercepted by the trajectories arriving at the two locations were from outside the boundary of Nepal. However, larger number of firecounts does not necessarily mean higher aerosol emissions, since it largely depends on the severity and duration of fires as well as age of smoke plumes, dilution and mixing processes during its transport and boundary layer dynamics (Kaskaoutis et al., 2014). The lifetime of aerosols in the atmosphere vary from few minutes to several weeks, resulting in substantial spatial and temporal variations with peak concentrations near the source (Haywood and Boucher, 2000). Kaskaoutis et al. (2014) studied the mechanisms of transport of plumes arising from the agricultural fields in western IGP, and found larger AOD values in the western IGP progressively decreasing towards the eastern IGP, suggesting attenuation of the thickness of the smoke plumes along transport. Therefore, firecounts within Nepal could have made major contribution to the peak AOD, though a substantial number of firecounts outside the boundary of Nepal were intercepted by the trajectories particularly in the month of May, October and November (Figure 4-12).

Smoke plume heights from biomass burning are the key characteristics to determine the distance and direction the smoke will travel (Kahn et al., 2008). The height to which smoke plumes are injected significantly influences the AOD values since injection of plumes to higher altitudes enhances quick dilution with large scale circulations, while injection of plumes to lower altitudes are usually trapped within the planetary boundary

layer and are strongly influenced by the stability of the atmosphere (Kahn et al., 2007). For the Himalayan region, the minimum plume height of 2.8 km was observed for the smoke from biomass burning in April, suggesting lower smoke plume altitude (Vadrevu et al., 2011). Such plume heights are representative of young plumes and agriculture-forest fires (surface fires) in comparison to the plume heights of greater than 5 km from crown fires (Guan et al., 2010). These plume heights suggests that the emissions from biomass burning in Nepal are trapped within the planetary boundary layer, causing high AOD values in the pre-monsoon season. Further, during pre-monsoon in particular, the highest seasonal mixing layer heights are observed over South Asia (Vernekar et al., 2003), which may favor the transport of smoke plumes from the surface up to higher altitudes as observed by Marinoni et al. (2013) and Putero et al. (2014).

4.5.3. Contribution of atmospheric circulations and long range transport of pollutants to aerosol optical depth

The influence of long range transport of pollutants in Nepal is studied by analyzing the clusters of air masses arriving at Kathmandu as described in section 4.4.4. During the dry seasons (from October to May), westerly circulations are dominant while south-easterly flow from ISM is dominant in the monsoon season (Bonasoni et al., 2008; Shrestha et al., 2000). During dry seasons, the occurrence of dry meteorological conditions over South Asia and a prevalent westerly circulation over the Himalayas subject this region to the pollution and biomass-burning products that accumulate over the IGP (Ramanathan et al., 2007b). The persistent subsidence and trade wind inversion strongly inhibit the ventilation and dispersion of pollutants, favoring their buildup in the lower troposphere (Ramanathan et al., 2007a). The dry meteorological conditions also provide a conducive environment for the onset of wildfires and agricultural fires, which is an important additional source of carbonaceous aerosols in the atmosphere. The practice of rice residue burning during the post-monsoon season in western IGP and the transport of the smoke plumes towards the eastern IGP by the westerly circulations is well documented from the satellite images (Kaskaoutis et al., 2014; Singh and Kaskaoutis, 2014). These smoke plumes are typically funneled into the west-east IGP, tend to cause peak AOD in the plains and LH as indicated by C6 (Figure 4-15), but the Himalayan mountain range are little affected by low-level smoke air mass (plume height of 2-2.5km), which flows below the planetary boundary layer (Kaskaoutis et al., 2014).

In contrast, when the wheat residue burning occurs in western IGP during pre-monsoon season, weather patterns and rapid vertical mixing of air serve to dissipate smoke diffusely causing less influence to distant places (Singh and Kaskaoutis, 2014; Vernekar et al., 2003). This can also explain why the peak AOD in April is less contributed by the air masses from C6 and C5, and biomass burning within Nepal have a greater contribution as shown in Figure 4-14. On the other hand, a significant fraction (around 40%) of the pollution events during post monsoon and winter seasons were not explicitly linked with biomass burning (Figure 4-13). This could be attributed to the building up of the local emissions in the IGP during these seasons (Jaswal et al., 2013; Kaskaoutis et al., 2012) and its transport as indicated by C3, C4 and C6. During winter season in Kathmandu, Regmi et al. (2003) explained that the cooler southwesterly air mass from the IGP (indicated by C3 and C4) and northwesterly flows entering the valley from the west (indicated by C6), suppresses vertical mixing of air and leads to high air pollution episodes by decreasing the daytime ventilation of air mass over the valley.

With the arrival of the monsoon season, the atmospheric circulations change from westerly to south easterly flow of ISM (C2 and C5). In particular, the early monsoon season (in June) had the highest mean AOD of 0.50 (Figure 4-6) and appeared to be regularly affected by air pollution as indicated by the AP events (Figure 4-13). The scavenging effect of monsoon is evident in the months following June. This could be explained by the intra-seasonal variability of the ISM during its early stage. Barros and Lang (2003) reported that the onset of the monsoon circulation (usually from the end of May to the middle June) is characterized by weakening of the upper-level westerly circulation, and an increase in moisture and convective instability. These periods are referred to as “breaks”, which occurs due to weakening of the large scale monsoon circulation. During these breaks, the broad-scale monsoon trough moves northward and westerly dry winds prevail over Indian sub-continent indicated by C4, leading to atmospheric circulation and meteorological conditions similar to the pre-monsoon (Marinoni et al., 2013). Therefore, such episodes can potentially favor the transport of pollution to the Himalayas even in the monsoon season causing peak AOD values particularly in the month of June.

4.6. Conclusion

In summary, I found that the emissions from biomass burning exceeded the emissions from fossil fuel combustion in Nepal while considering two aerosol components, BC and SO₂. This study revealed that while biomass burning in Nepal is the major source of aerosols during pre-monsoon season, trans-boundary air pollution (both of biomass and fossil fuel origins) plays equally crucial role in causing peak AOD in other seasons. The dimming observed in Nepal caused by increase in anthropogenic aerosols particularly BC, will have profound impacts on agriculture and regional climate. The implications of findings from this study will be discussed in the next chapter.

Chapter 5

5. SYNTHESIS AND IMPLICATIONS

This study aimed to quantify the dimming in solar radiation (SR) and identify its possible drivers in Nepal. In addition, the sources of anthropogenic aerosols (detected as the major cause of dimming) were identified and the influences of biomass burning and trans-boundary air pollution on aerosol variations were studied. In this chapter, the findings of previous chapters are synthesized and also the implications of the findings are discussed with the main focus on impacts of the dimming and atmospheric brown clouds (ABC) on agriculture in Nepal.

5.1. Dimming and its possible drivers

This study analyzed long term changes in sunshine duration (SSD) and identified its possible drivers (Chapter 1, Chapter 2). SSD trends revealed the decline in Nepal at a rate of -0.20% per year across the period 1987-2010. Among the three physiographic regions: plains, low-hills (LH) and high-hills and mountains (HHM) as shown in Figure 2-1, the decline was particularly high in the plains at a rate of -0.56% per year when compared to the hilly regions (section 2.3.1). Further, the decline in the stations in the plains, which is the northernmost extension of the Indo-Gangetic plains (IGP), closely matched the decreasing trends observed at the stations lying in IGP (Soni et al., 2012), confirming the persistence of dimming over the region.

With the aim to identify possible driver of the observed dimming, SSD was classified into clear days (S_{clear}) and cloudy days (S_{cloudy}) and trends were observed in S_{clear} and S_{cloudy} . A significant decline was found in S_{clear} trends at a rate of -0.42% per year particularly at the stations located in the plains and the capital city, Kathmandu (section 3.3.1.1). This decline in S_{clear} is likely due to the increasing trend of the anthropogenic aerosols in the IGP (Lu et al., 2011; Sahu et al., 2008), causing a reduction in SR under clear days by scattering and absorbing SR through direct effect. Seasonally, the decline in S_{clear} was evident in all the dry seasons (October to May) in the plains (section 3.3.1.2), which suggests the increase in anthropogenic aerosols in all the dry seasons, mainly due to large scale fossil fuel and biomass combustion in the region (Kaskaoutis et al., 2012).

On the other hand, the trends in S_{cloudy} showed intense dimming at a rate of -3.27% per year with strong decline in all the three regions (section 3.3.1.1). Seasonally, the decline in S_{cloudy} occurred in monsoon and pre-monsoon seasons and was evident in all the three regions. The 8 times higher decline in S_{cloudy} compared to S_{clear} indicated that clouds play a larger role in the observed dimming than aerosols which could be likely due to the increasing trends in cloud amount. However, trends in total rainfall did not show any significant increase rather a significant decline was observed in total number of rainy days (NRD) as explained in section 3.3.2.1. Such anomalies in rainfall and NRD suggested a different phenomenon referred to as indirect effect of aerosols, in which the aerosols could enhance cloud amount and lifetime thereby reflects more SR, but at the same time suppresses light rainfall and NRD (Haywood and Boucher, 2000; Ramanathan et al., 2001; Rosenfeld, 2000). In this study indeed, a significant decline at a rate of -0.23% per year was observed in light rainfall ($R \leq 10\text{mm}$, $\text{NRD} \leq 10\text{ mm}$) (section 3.3.2.2). In addition, the decline in light rainfall was followed with a moderate increase in heavy rainfall (section 3.3.2.3). This can be explained by the phenomenon in which aerosol induced suppression of rainfall from shallow clouds could increase the rainfall from deep clouds in the later stage of cloud development (Philips et al., 2007; Qian et al., 2009; Rosenfeld et al., 2008; Tao et al., 2007). The aerosol-induced increase in shallow and deep clouds as reflected by the decrease in light rainfall and increase in heavy rainfall could be the most plausible explanation for the high dimming observed in S_{cloudy} in Nepal.

Hence, both direct and indirect effects of aerosols have been identified as the major driver of the dimming in plains while aerosol indirect effect plays a crucial role in the dimming in LH and HHM.

5.2. Major sources of aerosols, biomass burning and long-range transport of air pollutants

As aerosols were identified as the major driver of the decline in SSD, major sources of aerosols were sought out (section 4.4.1). Among the two major divisions of aerosol sources: biomass burning and fossil fuel combustion, the emissions from biomass burning were estimated to be approximately three times the emissions from fossil fuel combustion, contributing on average to 74% of the total emissions (BC and SO_2) in

Nepal. It has been pointed that Asian ABC has high content of BC contributed by biomass burning occurring on a wide scale in the IGP and the Himalayan region (Gustafsson et al., 2009; Lelieveld et al., 2001). The estimates from this study also confirm the dominance of BC emissions over SO₂ emissions in Nepal.

To understand aerosol variations and its relation to biomass burning, MODIS-derived firecounts and aerosol optical depth (AOD) were analyzed for the period 2005-2010 (section 4.4.2). The highest mean AOD values (0.495) and maximum firecounts (53% of total firecounts) both occurred in April and were found to be in peak values in pre-monsoon season, being consistent with the findings of Vadrevu et al. (2012) for the Himalayan region. With the aim to explore possible influence of biomass burning on aerosols variations (section 4.4.3), acute pollution (AP) events characterized by significant increase in AOD values were identified for two locations: Simara and Kathmandu (Figure 4-5). A coupling of air mass backward trajectory analysis with MODIS firecounts identified 55% of the AP events in Simara and 60% of the AP events in Kathmandu, respectively, to be influenced by biomass burning referred to as 'BB pollution events'. Regional frequency of firecounts for different seasons during BB pollution events suggested that biomass burning occurring in Nepal could strongly influence the occurrence of highest AOD in pre-monsoon season, while trans-boundary biomass burning was dominant in all the other seasons (Figure 4-14).

Cluster analysis of air mass backward trajectories indicated different source regions of aerosols for the trans-boundary transport to Nepal (Figure 4-15 and Figure 4-16). Of the six clusters arriving at Kathmandu (section 4.4.4), C3, C4 and C6 originated from the IGP and were dominant in winter season and contributed to the peak AOD associated with large-scale anthropogenic emissions (both of biomass and fossil fuel origins) from IGP (Jaswal et al., 2013; Kaskaoutis et al., 2012; Ramanathan and Ramana, 2005). The peak AOD in pre-monsoon season was significantly contributed by two clusters of trajectories. One of them was C5, originating in the North-eastern states of India, Meghalaya, dominated by slash and burn agriculture, and the other was C6, originating in Punjab, characterized by wheat residue burning (Vadrevu et al., 2013). C2 represented air masses originating in the Bay of Bengal, both C2 and C5 were dominant in the monsoon season and indicated the pathway of the ISM circulation, brings pollutants in early monsoon causing peak AOD in June. Weakening of ISM, also known as 'break'

periods was evident in air masses in C4, caused high AOD in June (A. Marinoni et al. 2013). The air masses from C6 (Punjab area) during post-monsoon season also contributed to peak AOD despite to the least extent among all the trajectories. This cluster can be attributed to the polluted smoke of rice residue burning occurring on a large scale in Punjab of the northern IGP (Badarinath, 2010; Vadrevu et al., 2011).

5.3. Implications of dimming and atmospheric brown clouds on agriculture in Nepal

Research in the past decades have highlighted critical importance of aerosol emissions on regional radiative forcing, precipitation, and monsoonal patterns (Ramanathan et al., 2005). In this study over Nepal, I also found the role of aerosols in the significant dimming in SSD, reduction in light rainfall, and a shift in rainfall rate from light to heavy rainfall. Among various aerosols, BC and tropospheric ozone have direct effects on crop yields beyond their indirect effects through climate such as changes in temperature and precipitation (Auffhammer et al., 2011; Bhatt et al., 2013). BC alters the quantity and nature of the solar radiation reaching the surface (Ramanathan and Carmichael, 2008), while higher ozone concentrations have been found to be detrimental to plants (Feng and Kobayashi, 2009; Sarkar and Agrawal, 2010).

Although the emissions of different kind of aerosols were not estimated separately in this study, the estimated higher emissions of BC and the steady increase in its emissions (Figure 4-2) suggest that BC among various aerosols might have played a significant role in the observed dimming in Nepal. This dimming has profound impact on agriculture, since SR input plays a key role in plant growth (Ballare et al., 2012) and crop production (Shuai et al., 2012; Yang et al., 2013). In a recent study conducted in Jiangsu province of China, Shuai et al. (2012) found that increasing aerosol concentrations and the resultant dimming offset the benefit of climate warming and caused a reduction of 0.16 t ha^{-1} in rice yields (approximately 1.8 %) from 1980 to 2008. Similarly, Yang et al. (2013) evaluated combined effect of global dimming and climate warming and explained that reduction in SR accounted for 74% of the simulated wheat yields reduction by 32% in the Chengdu region of China. In fact, modelling results pointed that the simultaneous reduction of ABC and GHGs (greenhouse gases) would

have increased rice harvests in India by 6.18% during 1966–1984 and 14.4% during 1985–1998 (Auffhammer et al., 2006).

Burney & Ramanathan (2014) presented for the first time the combined effects of climate (temperature and precipitation) changes and direct effect of aerosols (BC and ozone) on wheat and rice yields in India (major states lying in the IGP). They estimated that yields in 2010 were up to 36% lower in wheat and 20% lower in rice yields than they otherwise would have been without the climate change and pollutant effects. The plain regions of Nepal, lying in the IGP, are considered ‘bread basket’ of the country, where 38% of the land in the plains are cultivated (Bhatt et al., 2013). It is noteworthy that the main growing season (November to April) of wheat and dry season rice in the plains, coincides with the peak AOD values and significant dimming in S_{clear} observed in the winter and pre-monsoon seasons. Similarly the significant dimming observed in S_{cloudy} in monsoon season coincides with the rice growing season (July to October) in both plains and LH. The observed reduction in SR would significantly reduce the photosynthetic rate of the crops and other vegetation (forests, grasslands and shrublands) and lowers the productivity. Reduction in SR can also interfere with the grain filling in rice and wheat (Fischer, 1985; Yoshida and Hara, 1977). These losses of net-productivity in major crops resultant from the dimming in this region concern the livelihood and food security of a large population, who largely depend on wheat and rice production (Bhatt et al., 2013).

Despite growing concerns, aerosol related problems seem manageable mostly because aerosols are much shorter-lived climate pollutants (SLCPs) with residence time in the atmosphere being in the range from weeks to months. It is encouraging to note that the emission controls implemented in 2008 in China were successful in reducing Beijing emissions of BC by about 25%, as well as reducing the ratio of BC to SO_2 by about 20% (Wang et al., 2009). This exemplary case shows that if we restrict the known anthropogenic sources, mitigation is possible and relief can be realized in a very short period.

Higher contribution of biomass burning to the release of aerosols observed in my study suggests the need to address the issues related to open-biomass burning as well as use of fuel wood. At the national level, the mitigation efforts would include controlled fires in protected areas, use of improved cooking stoves, and awareness about the

implications of forest fires. Regarding the trans-boundary influx of aerosols, a larger international collaboration and cooperation will be required. Finally, it is important for governments and local and international agencies to be aware of the consequences of an increase in aerosol concentration. They should also be aware that the mitigation efforts (measures devoted to the reduction of aerosol emissions) represent a rewarding step for the food security and regional climate.

References:

- Abakumova, G., Feigelson, E., Russak, V., Stadnik, V., 1996. Evaluation of long-term changes in radiation, cloudiness, and surface temperature on the territory of the former Soviet Union. *Journal of Climatology* 9, 1319–1327.
- Abdalmogith, S.S., Harrison, R.M., 2005. The use of trajectory cluster analysis to examine the long-range transport of secondary inorganic aerosol in the UK. *Atmospheric Environment* 39, 6686–6695. doi:10.1016/j.atmosenv.2005.07.059
- Abrol, Y., Sangwan, S., Tiwari, M., Dadhwal, V., 2002. Land use / land cover in Indo-Gangetic Plains-history of changes, present concerns and future approaches, in: Mehrotra, J. (Ed.), *Land Use--Historical Perspectives: Focus on Indo-Gangetic Plains*. Allied Publishers, New Delhi, pp. 1–28.
- Ackerman, A.S., 2003. Enhancement of cloud cover and suppression of nocturnal drizzle in stratocumulus polluted by haze. *Geophysical Research Letters* 30, 1381. doi:10.1029/2002GL016634
- Akagi, S.K., Yokelson, R.J., Wiedinmyer, C., Alvarado, M.J., Reid, J.S., Karl, T., Crounse, J.D., Wennberg, P.O., 2011. Emission factors for open and domestic biomass burning for use in atmospheric models. *Atmospheric Chemistry and Physics* 11, 4039–4072. doi:10.5194/acp-11-4039-2011
- Alpert, P., 2005. Global dimming or local dimming?: Effect of urbanization on sunlight availability. *Geophysical Research Letters* 32, L17802. doi:10.1029/2005GL023320
- Andreae, M.O., Merlet, P., 2001. Emission of trace gases and aerosols from biomass burning. *Global Biogeochemical Cycles* 15, 955–966. doi:10.1029/2000GB001382
- ASDC, 2014. REL3.0 CLDPROPS 3HRLY [WWW Document]. Atmospheric Science Data Center, NASA. URL https://eosweb.larc.nasa.gov/project/srb/srb_rel3.0cldprops3_hrly_table (accessed 12.10.14).
- Auffhammer, M., Ramanathan, V., Vincent, J.R., 2006. Integrated model shows that atmospheric brown clouds and greenhouse gases have reduced rice harvests in

- India. *Proceedings of the National Academy of Sciences of the United States of America* 103, 19668–72. doi:10.1073/pnas.0609584104
- Auffhammer, M., Ramanathan, V., Vincent, J.R., 2011. Climate change, the monsoon, and rice yield in India. *Climatic Change* 111, 411–424. doi:10.1007/s10584-011-0208-4
- Badarinath, K.V.S., 2010. Impact of agriculture crop residue burning on atmospheric aerosol loading – a study over Punjab State, India. *Annales Geophysicae* 28, 367–379. doi:10.5194/angeo-28-367-2010
- Ballaré, C.L., Mazza, C.A., Austin, A.T., Pierik, R., 2012. Canopy light and plant health. *Plant Physiology* 160, 145–55. doi:10.1104/pp.112.200733
- Barros, A., Lang, T., 2003. Monitoring the monsoon in the Himalayas: Observations in central Nepal, June 2001. *Monthly Weather Review* 131, 1408–1427.
- Bhatt, D., Maskey, S., Babel, M.S., Uhlenbrook, S., Prasad, K.C., 2013. Climate trends and impacts on crop production in the Koshi River basin of Nepal. *Regional Environmental Change* 14, 1291–1301. doi:10.1007/s10113-013-0576-6
- Blue, D., Hsu, N.C., Sayer, A.M., Bettenhausen, C., Lee, J., Target, D., Levy, R.C., Mattoo, S., Munchak, L.A., Kleidman, R., 2014. Comparing MODIS C6 Deep Blue and Dark Target aerosol data, NASA Technical Reports. Greenbelt, MD United States. doi:10.1002/jgrd.50712.
- Bolch, T., Kulkarni, A., Kääb, A., Huggel, C., Paul, F., Cogley, J.G., Frey, H., Kargel, J.S., Fujita, K., Scheel, M., Bajracharya, S., Stoffel, M., 2012. The state and fate of Himalayan glaciers. *Science* 336, 310–314. doi:10.1126/science.1215828
- Bonasoni, P., Cristofanelli, P., Marinoni, A., Vuillermoz, E., Adhikary, B., 2012. Atmospheric pollution in the Hindu Kush–Himalaya region. *Mountain Research and Development* 32, 468–479. doi:10.1659/MRD-JOURNAL-D-12-00066.1
- Bonasoni, P., Laj, P., Angelini, F., Arduini, J., Bonafè, U., Calzolari, F., Cristofanelli, P., Decesari, S., Facchini, M.C., Fuzzi, S., Gobbi, G.P., Maione, M., Marinoni, A., Petzold, A., Roccatò, F., Roger, J.C., Sellegri, K., Sprenger, M., Venzac, H., Verza, G.P., Villani, P., Vuillermoz, E., 2008. The ABC-Pyramid Atmospheric Research Observatory in Himalaya for aerosol, ozone and halocarbon measurements.

- Science of the Total Environment 391, 252–261. doi:10.1016/j.scitotenv.2007.10.024
- Bonasoni, P., Laj, P., Angelini, F., Arduini, J., Bonafè, U., Calzolari, F., Cristofanelli, P., Villani, P., Vuillermoz, E., 2007. The ABC-Pyramid Atmospheric Research Observatory in Himalaya for aerosol, ozone and halocarbon measurements 1, 1–10. doi:10.1016/j.scitotenv.2007.10.024
- Bonasoni, P., Laj, P., Marinoni, a., Sprenger, M., Angelini, F., Arduini, J., Bonafè, U., Calzolari, F., Colombo, T., Decesari, S., Di Biagio, C., di Sarra, a. G., Evangelisti, F., Duchi, R., Facchini, M., Fuzzi, S., Gobbi, G.P., Maione, M., Panday, a., Roccato, F., Sellegri, K., Venzac, H., Verza, G., Villani, P., Vuillermoz, E., Cristofanelli, P., 2010. Atmospheric Brown Clouds in the Himalayas: first two years of continuous observations at the Nepal Climate Observatory-Pyramid (5079 m). Atmospheric Chemistry and Physics 10, 7515–7531. doi:10.5194/acp-10-7515-2010
- Bond, T.C., Streets, D.G., Yarber, K.F., Nelson, S.M., Woo, J.H., Klimont, Z., 2004. A technology-based global inventory of black and organic carbon emissions from combustion. Journal of Geophysical Research D: Atmospheres 109, D14203. doi:10.1029/2003JD003697
- Bontemps, S., Defourny, P., Bogaert, E. V., Arino, O., Kalogirou, V., Perez, J.R., 2011. GLOBCOVER 2009 Products Description and Validation Report. doi:10013/epic.39884.d016
- Bookhagen, B., Burbank, D.W., 2010. Toward a complete Himalayan hydrological budget: Spatiotemporal distribution of snowmelt and rainfall and their impact on river discharge. Journal of Geophysical Research 115, F03019. doi:10.1029/2009JF001426
- Boschetti, L., Roy, D., Hoffmann, A.A., Humber, M., 2013. MODIS Collection 5.1 Burned Area Product-MCD45. User's guide 35.
- Burney, J., Ramanathan, V., 2014. Recent climate and air pollution impacts on Indian agriculture. Proceedings of the National Academy of Sciences of the United States of America 111, 1–16. doi:10.1073/pnas.1317275111

- Carmichael, G.R., Adhikary, B., Kulkarni, S., D’Allura, A., Tang, Y., Streets, D., Zhang, Q., Bond, T.C., Ramanathan, V., Jamroensan, A., Marrapu, P., 2009. Asian aerosols: Current and year 2030 distributions and implications to human health and regional climate change. *Environmental Science & Technology* 43, 5811–5817. doi:10.1021/es8036803
- CBS, 2013. Statistical Year Book of Nepal. Central Beureau of Statistics, Nepal.
- Chung, C.E., Ramanathan, V., 2007. Relationship between trends in land precipitation and tropical SST gradient. *Geophysical Research Letters* 34, L16809. doi:10.1029/2007GL030491
- Dash, S.K., Kulkarni, M.A., Mohanty, U.C., Prasad, K., 2009. Changes in the characteristics of rain events in India. *Journal of Geophysical Research: Atmospheres* 114, D10109. doi:10.1029/2008JD010572
- Dessler, A.E., 2010. A determination of the cloud feedback from climate variations over the past decade. *Science* 330, 1523–1527. doi:10.1126/science.1192546
- Dey, S., 2004. Influence of dust storms on the aerosol optical properties over the Indo-Gangetic basin. *Journal of Geophysical Research* 109, D20211. doi:10.1029/2004JD004924
- Draxler, R.R., Hess, G.D., 1997. Description of the HYSPLIT_4 modeling system. NOAA Tech. Memo. ERL ARL-224, NOAA Air Resources Laboratory, Silver Spring, MD.
- Draxler, R.R., Hess, G.D., 1998. An overview of the HYSPLIT_4 modeling system of trajectories, dispersion, and deposition. *Australian Meteorological Magazine* 47, 295–308.
- Eck, T.F., 2003. High aerosol optical depth biomass burning events: A comparison of optical properties for different source regions. *Geophysical Research Letters* 30, 2035. doi:10.1029/2003GL017861
- Eck, T.F., Holben, B.N., Reid, J.S., Sinyuk, A., Hyer, E.J., O’Neill, N.T., Shaw, G.E., Vande Castle, J.R., Chapin, F.S., Dubovik, O., Smirnov, A., Vermote, E., Schafer, J.S., Giles, D., Slutsker, I., Sorokine, M., Newcomb, W.W., 2009. Optical properties of boreal region biomass burning aerosols in central Alaska and seasonal

- variation of aerosol optical depth at an Arctic coastal site. *Journal of Geophysical Research* 114, D11201. doi:10.1029/2008JD010870
- EEA, 2013. EMEP/EEA air pollutant emission inventory guidebook 2013: Technical guidance to prepare national emission inventories, EEA Technical report. European Environment Agency. doi:10.2800/92722
- El-Askary, H., Gautam, R., Singh, R.P., Kafatos, M., 2006. Dust storms detection over the Indo-Gangetic basin using multi sensor data. *Advances in Space Research* 37, 728–733. doi:10.1016/j.asr.2005.03.134
- ESRI, 2011. ArcGIS Desktop: Release 10.1. Environmental Systems Research Institute. Redlands, CA.
- Feng, Z., Kobayashi, K., 2009. Assessing the impacts of current and future concentrations of surface ozone on crop yield with meta-analysis. *Atmospheric Environment* 43, 1510–1519. doi:10.1016/j.atmosenv.2008.11.033
- Fischer, R.A., 1985. Number of kernels in wheat crops and the influence of solar radiation and temperature. *The Journal of Agricultural Science* 105, 447–461. doi:10.1017/S0021859600056495
- Forster, P., Ramaswamy, V., Artaxo, P., Berntsen, T., Betts, R., Fahey, D.W., Haywood, J., Lean, J., Lowe, D.C., Myhre, G., Nganga, J., Prinn, R., Raga, G., Schulz, M., Van Dorland, R., 2007. Changes in Atmospheric Constituents and in Radiative Forcing, in: Solomon, S., Qin, D., Manning, M., Chen, Z., Marquis, M., Averyt, K.B., Tignor, M., Miller, H.L. (Eds.), *Clim. Chang. 2007 Phys. Sci. Basis. Contrib. Work. Gr. I to Fourth Assess. Rep. Intergov. Panel Clim. Chang.* Cambridge University Press, United Kingdom and New York, NY, USA.
- Fortner, B., 1995. *The data handbook : A guide to understanding the organization and visualization of technical data.* Springer, New York. doi:10.1007/978-1-4612-2538-6
- Gautam, R., Hsu, N.C., Lau, K.-M., Kafatos, M., 2009a. Aerosol and rainfall variability over the Indian monsoon region: distributions, trends and coupling. *Annales Geophysicae* 27, 3691–3703. doi:10.5194/angeo-27-3691-2009

- Gautam, R., Hsu, N.C., Lau, K.-M., Tsay, S.-C., Kafatos, M., 2009b. Enhanced pre-monsoon warming over the Himalayan-Gangetic region from 1979 to 2007. *Geophysical Research Letters* 36, L07704. doi:10.1029/2009GL037641
- Gautam, R., Hsu, N.C., Tsay, S.C., Lau, K.M., Holben, B., Bell, S., Smirnov, A., Li, C., Hansell, R., Ji, Q., Payra, S., Aryal, D., Kayastha, R., Kim, K.M., 2011. Accumulation of aerosols over the Indo-Gangetic plains and southern slopes of the Himalayas: distribution, properties and radiative effects during the 2009 pre-monsoon season. *Atmospheric Chemistry and Physics* 11, 12841–12863. doi:10.5194/acp-11-12841-2011
- Giglio, L., Descloitres, J., Justice, C.O., Kaufman, Y.J., 2003. An enhanced contextual fire detection algorithm for MODIS. *Remote Sensing of Environment* 87, 273–282. doi:10.1016/S0034-4257(03)00184-6
- Good, E., 2009. Estimating daily sunshine duration over the UK from SEVIRI, in: *Proceedings of the EUMETSAT Meteorological Satellite Conference. EUMETSAT, 21-25 September, Bath, UK, pp. 1–6.*
- Griffith, D. A, Solak, M.E., Yorty, D.P., 2005. Is air pollution impacting winter orographic precipitation in Utah? *North American Weather Consultants, Inc.* 8.
- Guan, H., Esswein, R., Lopez, J., Bergstrom, R., Warnock, A., Follette-Cook, M., Fromm, M., Iraci, L.T., 2010. A multi-decadal history of biomass burning plume heights identified using aerosol index measurements. *Atmospheric Chemistry and Physics* 10, 6461–6469. doi:10.5194/acp-10-6461-2010
- Guhathakurta, P., Rajeevan, M., 2008. Trends in the rainfall pattern over India. *International Journal of Climatology* 28, 1453–1469. doi:10.1002/joc.1640
- Gustafsson, O., Kruså, M., Zencak, Z., Sheesley, R.J., Granat, L., Engström, E., Praveen, P.S., Rao, P.S.P., Leck, C., Rodhe, H., 2009. Brown clouds over South Asia: biomass or fossil fuel combustion? *Science* 323, 495–8. doi:10.1126/science.1164857
- Guttikunda, S.K., Carmichael, G.R., Calori, G., Eck, C., Woo, J.-H., 2003. The contribution of megacities to regional sulfur pollution in Asia. *Atmospheric Environment* 37, 11–22. doi:10.1016/S1352-2310(02)00821-X

- Hansen, J., Sato, M., Ruedy, R., 1997. Radiative forcing and climate response. *Journal of Geophysical Research* 102, 6831. doi:10.1029/96JD03436
- Haywood, J., Boucher, O., 2000. Estimates of the direct and indirect radiative forcing due to tropospheric aerosols: A review. *Reviews of Geophysics* 38, 513. doi:10.1029/1999RG000078
- Ichiyanagi, K., Yamanaka, M.D., Muraji, Y., Vaidya, B.K., 2007. Precipitation in Nepal between 1987 and 1996. *International Journal of Climatology* 27, 1753–1762. doi:10.1002/joc.1492
- IPCC, 2001. Climate change 2001: the scientific basis. In: Houghton, J., Ding, Y., Griggs, D., Noguer, M., van der Linden, P., Dai, X., Maskell, K., Johnson, C. (Eds.), *Climate Change 2001: The Scientific Basis. Contribution of Working Group I to the Third Assessment Report of the Intergovernmental Panel on Climate Change*. Cambridge University Press, Cambridge.
- Jaswal, A.K., 2009. Sunshine duration climatology and trends in association with other climatic factors over India for 1970–2006. *Mausam* 60, 437–454.
- Jaswal, A.K., Kumar, N., Prasad, A.K., Kafatos, M., 2013. Decline in horizontal surface visibility over India (1961–2008) and its association with meteorological variables. *Natural Hazards* 68, 929–954. doi:10.1007/s11069-013-0666-2
- Jhajharia, D., Singh, V.P., 2011. Trends in temperature, diurnal temperature range and sunshine duration in Northeast India. *International Journal of Climatology* 31, 1353–1367. doi:10.1002/joc.2164
- Jirak, I.L., Cotton, W.R., 2006. Effect of air pollution on precipitation along the front range of the Rocky Mountains. *Journal of Applied Meteorology and Climatology* 45, 236–245. doi:10.1175/JAM2328.1
- Jorba, O., Pérez, C., Roca-denbosch, F., and Baldasano, J., 2004. Cluster Analysis of 4-Day Back Trajectories Arriving in the Barcelona Area, Spain, from 1997 to 2002. *Journal of Applied Meteorology* 43, 887–901.

- Justice, C., Giglio, L., Boschetti, L., Roy, D., Csiszar, I., Morisette, J., Kaufman, Y., 2006. Algorithm Technical Background Document. MODIS FIRE PRODUCTS Version 2., 1–34.
- Kahn, R.A., Chen, Y., Nelson, D.L., Leung, F.-Y., Li, Q., Diner, D.J., Logan, J.A., 2008. Wildfire smoke injection heights: Two perspectives from space. *Geophysical Research Letters* 35, L04809. doi:10.1029/2007GL032165
- Kahn, R.A., Li, W.H., Moroney, C., Diner, D.J., Martonchik, J. V., Fishbein, E., 2007. Aerosol source plume physical characteristics from space-based multiangle imaging. *Journal of Geophysical Research: Atmospheres* 112, 1–20. doi:10.1029/2006JD007647
- Kaiser, D.P., Qian, Y., 2002. Decreasing trends in sunshine duration over China for 1954–1998: Indication of increased haze pollution? *Geophysical Research Letters* 29, 38–1–38–4. doi:10.1029/2002GL016057
- Kaskaoutis, D.G., Kharol, S.K., Sifakis, N., Nastos, P.T., Sharma, A.R., Badarinath, K.V.S., Kambezidis, H.D., 2011. Satellite monitoring of the biomass-burning aerosols during the wildfires of August 2007 in Greece: Climate implications. *Atmospheric Environment* 45, 716–726. doi:10.1016/j.atmosenv.2010.09.043
- Kaskaoutis, D.G., Kumar, S., Sharma, D., Singh, R.P., Kharol, S.K., Sharma, M., Singh, A.K., Singh, S., Singh, A., Singh, D., 2014. Effects of crop residue burning on aerosol properties, plume characteristics, and long-range transport over northern India. *Journal of Geophysical Research: Atmospheres* 119, 5424–5444. doi:10.1002/2013JD021357
- Kaskaoutis, D.G., Singh, R.P., Gautam, R., Sharma, M., Kosmopoulos, P.G., Tripathi, S.N., 2012. Variability and trends of aerosol properties over Kanpur, northern India using AERONET data (2001–10). *Environmental Research Letters* 7, 024003. doi:10.1088/1748-9326/7/2/024003
- Kaufman, Y.J., Justice, C.O., Flynn, L.P., Kendall, J.D., Prins, E.M., Giglio, L., Ward, D.E., Menzel, W.P., Setzer, A.W., 1998. Potential global fire monitoring from EOS-MODIS. *Journal of Geophysical Research* 103, 32215. doi:10.1029/98JD01644

- Kaufman, Y.J., Tanré, D., Remer, L. a., Vermote, E.F., Chu, a., Holben, B.N., 1997. Operational remote sensing of tropospheric aerosol over land from EOS moderate resolution imaging spectroradiometer. *Journal of Geophysical Research* 102, 17051. doi:10.1029/96JD03988
- Kitsara, G., Papaioannou, G., Papathanasiou, A., Retalis, A., 2012. Dimming/brightening in Athens: Trends in Sunshine Duration, Cloud Cover and Reference Evapotranspiration. *Water Resources Management* 27, 1623–1633. doi:10.1007/s11269-012-0229-4
- Lau, K.-M., Kim, K.-M., 2006. Observational relationships between aerosol and Asian monsoon rainfall, and circulation. *Geophysical Research Letters* 33, L21810. doi:10.1029/2006GL027546
- Lau, K.-M., Tsay, S.C., Hsu, C., Chin, M., Ramanathan, V., Wu, G.-X., Li, Z., Sikka, R., Holben, B., Lu, D., Chen, H., Tartari, G., Koudelova, P., Ma, Y., Huang, J., Taniguchi, K., Zhang, R., 2008. The Joint Aerosol–Monsoon Experiment: A New Challenge for Monsoon Climate Research. *Bulletin of the American Meteorological Society* 89, 369–383. doi:10.1175/BAMS-89-3-369
- Lelieveld, J., Crutzen, P.J., Ramanathan, V., Andreae, M.O., Brenninkmeijer, C.M., Campos, T., Cass, G.R., Dickerson, R.R., Fischer, H., de Gouw, J.A., Hansel, A., Jefferson, A., Kley, D., de Laat, A.T., Lal, S., Lawrence, M.G., Lobert, J.M., Mayol-Bracero, O.L., Mitra, A.P., Novakov, T., Oltmans, S.J., Prather, K.A., Reiner, T., Rodhe, H., Scheeren, H. a, Sikka, D., Williams, J., 2001. The Indian Ocean experiment: widespread air pollution from South and Southeast Asia. *Science (New York, N.Y.)* 291, 1031–6. doi:10.1126/science.1057103
- Levin, Z., Cotton, W.R. (Eds.), 2009. *Aerosol Pollution Impact on Precipitation: A scientific review*. Springer Netherlands, Dordrecht. doi:10.1007/978-1-4020-8690-8
- Levy, R.C., Mattoo, S., Munchak, L.A., Remer, L.A., Sayer, A.M., Patadia, F., Hsu, N.C., 2013. The Collection 6 MODIS aerosol products over land and ocean. *Atmospheric Measurement Techniques* 6, 2989–3034. doi:10.5194/amt-6-2989-2013

- Li, W., Hou, M., Xin, J., 2011. Low-cloud and sunshine duration in the low-latitude belt of South China for the period 1961–2005. *Theoretical and Applied Climatology* 104, 473–478. doi:10.1007/s00704-010-0360-1
- Li, Z., Zhao, X., Kahn, R., Mishchenko, M., Remer, L., Lee, K.-H., Wang, M., Laszlo, I., Nakajima, T., Maring, H., 2009. Uncertainties in satellite remote sensing of aerosols and impact on monitoring its long-term trend: a review and perspective. *Annales Geophysicae* 27, 2755–2770. doi:10.5194/angeo-27-2755-2009
- Liepert, B.G., 2002. Observed reductions of surface solar radiation at sites in the United States and worldwide from 1961 to 1990. *Geophysical Research Letters* 29, 61–61–61–4. doi:10.1029/2002GL014910
- Liepert, B.G., Feichter, J., Lohmann, U., Roeckner, E., 2004. Can aerosols spin down the water cycle in a warmer and moister world? *Geophysical Research Letters* 31, L06207. doi:10.1029/2003GL019060
- Lohani, S.N.S.N., Eco, A., 2007. Climate change in Nepal – shall we wait until bitter consequences? *Journal of Agriculture and Environment* 8, 38–45. doi:10.3126/aej.v8i0.725
- Lu, Z., Zhang, Q., Streets, D.G., 2011. Sulfur dioxide and primary carbonaceous aerosol emissions in China and India, 1996–2010. *Atmospheric Chemistry and Physics* 11, 9839–9864. doi:10.5194/acp-11-9839-2011
- Maplecroft, 2010. *Climate Change Vulnerability Map 2011*. Maplecroft, CCVI Bath, UK.
- Marinoni, A., Cristofanelli, P., Laj, P., Duchi, R., Calzolari, F., Decesari, S., Sellegri, K., Vuillermoz, E., Verza, G.P., Villani, P., Bonasoni, P., 2010. Aerosol mass and black carbon concentrations, a two year record at NCO-P (5079 m, Southern Himalayas). *Atmospheric Chemistry and Physics* 10, 8551–8562. doi:10.5194/acp-10-8551-2010
- Marinoni, A., Cristofanelli, P., Laj, P., Duchi, R., Putero, D., Calzolari, F., Landi, T.C., Vuillermoz, E., Maione, M., Bonasoni, P., 2013. High black carbon and ozone concentrations during pollution transport in the Himalayas: Five years of

- continuous observations at NCO-P global GAW station. *Journal of Environmental Sciences* 25, 1618–1625. doi:10.1016/S1001-0742(12)60242-3
- McGowan, H., and Clark, A., 2008. Identification of dust transport pathways from Lake Eyre, Australia using Hysplit. *Atmospheric Environment* 42, 6915–6925.
- Norris, J.R., Wild, M., 2007. Trends in aerosol radiative effects over Europe inferred from observed cloud cover, solar “dimming” and solar “brightening”. *Journal of Geophysical Research: Atmospheres* 112, D08214. doi:10.1029/2006JD007794
- Norris, J.R., Wild, M., 2009. Trends in aerosol radiative effects over China and Japan inferred from observed cloud cover, solar “dimming,” and solar “brightening.” *Journal of Geophysical Research: Atmospheres* 114, D00D15. doi:10.1029/2008JD011378
- Padma Kumari, B., Goswami, B.N., 2010. Seminal role of clouds on solar dimming over the Indian monsoon region. *Geophysical Research Letters* 37, L06703. doi:10.1029/2009GL042133
- Padma Kumari, B., Londhe, A.L., Daniel, S., Jadhav, D.B., 2007. Observational evidence of solar dimming: Offsetting surface warming over India. *Geophysical Research Letters* 34, L21810. doi:10.1029/2007GL031133
- Pant, P., Hegde, P., Dumka, U.C., Sagar, R., Satheesh, S.K., Moorthy, K.K., Saha, A., Srivastava, M.K., 2006. Aerosol characteristics at a high-altitude location in central Himalayas: Optical properties and radiative forcing. *Journal of Geophysical Research* 111, D17206. doi:10.1029/2005JD006768
- Pelon, J., Mallet, M., Mariscal, A., Goloub, P., Tanré, D., Bou Karam, D., Flamant, C., Haywood, J., Pospichal, B., Victori, S., 2008. Microlidar observations of biomass burning aerosol over Djougou (Benin) during African Monsoon Multidisciplinary Analysis Special Observation Period 0: Dust and Biomass-Burning Experiment. *Journal of Geophysical Research* 113, D00C18. doi:10.1029/2008JD009976
- Philips, V.T.J., Donner, L.J., Garner, S.T., 2007. Nucleation Processes in Deep Convection Simulated by a Cloud-System-Resolving Model with Double-Moment

- Bulk Microphysics. *Journal of the Atmospheric Sciences* 64, 738–761. doi:10.1175/JAS3869.1
- Putero, D., Landi, T.C., Cristofanelli, P., Marinoni, A., Laj, P., Duchi, R., Calzolari, F., Verza, G.P., Bonasoni, P., 2014. Influence of open vegetation fires on black carbon and ozone variability in the southern Himalayas (NCO-P, 5079 m a.s.l.). *Environmental Pollution* 184, 597–604. doi:10.1016/j.envpol.2013.09.035
- Qian, Y., Gong, D., Fan, J., Leung, L.R., Bennartz, R., Chen, D., Wang, W., 2009. Heavy pollution suppresses light rain in China: Observations and modeling. *Journal of Geophysical Research* 114, D00K02. doi:10.1029/2008JD011575
- Qian, Y., Kaiser, D.P., Leung, L.R., Xu, M., 2006. More frequent cloud-free sky and less surface solar radiation in China from 1955 to 2000. *Geophysical Research Letters* 33, L01812. doi:10.1029/2005GL024586
- Qian, Y., Wang, W., Leung, L.R., Kaiser, D.P., 2007. Variability of solar radiation under cloud-free skies in China: The role of aerosols. *Geophysical Research Letters* 34, L12804. doi:10.1029/2006GL028800
- Radke, L., Coakley, J., King, M., 1989. Direct and remote sensing observations of the effects of ships on clouds. *Science* 246, 10–13.
- Raichijk, C., 2012. Observed trends in sunshine duration over South America. *International Journal of Climatology* 32, 669–680. doi:10.1002/joc.2296
- Ramana, M. V., Ramanathan, V., Feng, Y., Yoon, S.-C., Kim, S.-W., Carmichael, G.R., Schauer, J.J., 2010. Warming influenced by the ratio of black carbon to sulphate and the black-carbon source. *Nature Geoscience* 3, 542–545. doi:10.1038/ngeo918
- Ramana, M. V., Ramanathan, V., Podgorny, I.A., Pradhan, B.B., Shrestha, B., 2004. The direct observations of large aerosol radiative forcing in the Himalayan region. *Geophysical Research Letters* 31, L05111. doi:10.1029/2003GL018824
- Ramanathan, V., Carmichael, G., 2008. Global and regional climate changes due to black carbon. *Nature Geoscience* 1, 221–227. doi:10.1038/ngeo156
- Ramanathan, V., Chung, C., Kim, D., Bettge, T., Buja, L., Kiehl, J.T., Washington, W.M., Fu, Q., Sikka, D.R., Wild, M., 2005. Atmospheric brown clouds: impacts

- on South Asian climate and hydrological cycle. *Proceedings of the National Academy of Sciences of the United States of America* 102, 5326–5333. doi:10.1073/pnas.0500656102
- Ramanathan, V., Crutzen, P.J., Kiehl, J.T., Rosenfeld, D., 2001. Aerosols, climate, and the hydrological cycle. *Science* 294, 2119–2124. doi:10.1126/science.1064034
- Ramanathan, V., Li, F., Ramana, M. V., Praveen, P.S., Kim, D., Corrigan, C.E., Nguyen, H., Stone, E.A., Schauer, J.J., Carmichael, G.R., Adhikary, B., Yoon, S.C., 2007a. Atmospheric brown clouds: Hemispherical and regional variations in long-range transport, absorption, and radiative forcing. *Journal of Geophysical Research* 112, D22S21. doi:10.1029/2006JD008124
- Ramanathan, V., Ramana, M. V., 2005. Persistent, widespread, and strongly absorbing haze over the Himalayan foothills and the Indo-Gangetic Plains. *Pure and Applied Geophysics* 162, 1609–1626. doi:10.1007/s00024-005-2685-8
- Ramanathan, V., Ramana, M. V., Roberts, G., Kim, D., Corrigan, C., Chung, C., Winker, D., 2007b. Warming trends in Asia amplified by brown cloud solar absorption. *Nature* 448, 575–8. doi:10.1038/nature06019
- Regmi, R., Kitada, T., Kurata, G., 2003. Numerical simulation of late wintertime local flows in Kathmandu valley, Nepal: Implication for air pollution transport. *Journal of Applied Meteorology* 42, 389–403.
- Roberts, J.J., Best, B.D., Dunn, D.C., Treml, E.A., Halpin, P.N., 2010. Marine Geospatial Ecology Tools: An integrated framework for ecological geoprocessing with ArcGIS, Python, R, MATLAB, and C++. *Environmental Modelling and Software* 25, 1197–1207. doi:10.1016/j.envsoft.2010.03.029
- Rosenfeld, D., 2000. Suppression of rain and snow by urban and industrial air pollution. *Science* 287, 1793–1796. doi:10.1126/science.287.5459.1793
- Rosenfeld, D., Dai, J., Yu, X., Yao, Z., Xu, X., Yang, X., Du, C., 2007. Inverse relations between amounts of air pollution and orographic precipitation. *Science* 315, 1396–8. doi:10.1126/science.1137949

- Rosenfeld, D., Givati, A., 2006. Evidence of Orographic Precipitation Suppression by Air Pollution–Induced Aerosols in the Western United States. *Journal of Applied Meteorology and Climatology* 45, 893–911. doi:10.1175/JAM2380.1
- Rosenfeld, D., Lohmann, U., Raga, G.B., O’Dowd, C.D., Kulmala, M., Fuzzi, S., Reissell, A., Andreae, M.O., 2008. Flood or drought: how do aerosols affect precipitation? *Science* 321, 1309–13. doi:10.1126/science.1160606
- Roy, D.P., Jin, Y., Lewis, P.E., Justice, C.O., 2005. Prototyping a global algorithm for systematic fire-affected area mapping using MODIS time series data. *Remote Sensing of Environment* 97, 137–162. doi:10.1016/j.rse.2005.04.007
- Sahu, S.K., Beig, G., Sharma, C., 2008. Decadal growth of black carbon emissions in India. *Geophysical Research Letters* 35, L02807. doi:10.1029/2007GL032333
- Sanchez-Lorenzo, A., Calbó, J., Martin-Vide, J., 2008. Spatial and temporal trends in sunshine duration over western Europe (1938–2004). *Journal of Climate* 21, 6089–6098. doi:10.1175/2008JCLI2442.1
- Sarkar, A., Agrawal, S.B., 2010. Identification of ozone stress in Indian rice through foliar injury and differential protein profile. *Environmental Monitoring and Assessment* 161, 205–15. doi:10.1007/s10661-008-0738-z
- Sarkar, S., Chokngamwong, R., Cervone, G., Singh, R.P., Kafatos, M., 2006. Variability of aerosol optical depth and aerosol forcing over India. *Advances in Space Research* 37, 2153–2159. doi:10.1016/j.asr.2005.09.043
- Seiler, W., Crutzen, P., 1980. Estimates of gross and net fluxes of carbon between the biosphere and the atmosphere from biomass burning. *Climatic Change* 2, 207–247.
- Shrestha, A., Wake, C.P., Dibb, J.E., Mayewski, P.A., 2000. Precipitation fluctuations in the Nepal Himalaya and its vicinity and relationship with some large scale climatological parameters. *International Journal of Climatology* 20, 317–327. doi:10.1002/(SICI)1097-0088(20000315)20:3<317::AID-JOC476>3.0.CO;2-G
- Shrestha, A.B., Wake, C.P., Dibb, J.E., Mayewski, P.A., Whitlow, S.I., Carmichael, G.R., Ferm, M., 2000. Seasonal variations in aerosol concentrations and compositions in the Nepal Himalaya. *Atmospheric Environment* 34, 3349–3363. doi:10.1016/S1352-2310(99)00366-0

- Shrestha, A.B., Wake, C.P., Mayewski, P.A., Dibb, J.E., 1999. Maximum temperature trends in the Himalaya and its vicinity: An analysis based on temperature records from Nepal for the period 1971-94. *Journal of Climate* 12, 2775–2786. doi:10.1175/1520-0442(1999)012<2775:MTTITH>2.0.CO;2
- Shrestha, D., Singh, P., Nakamura, K., 2012. Spatiotemporal variation of rainfall over the central Himalayan region revealed by TRMM precipitation radar. *Journal of Geophysical Research* 117, D22106. doi:10.1029/2012JD018140
- Shrestha, P., Barros, a. P., 2010. Joint spatial variability of aerosol, clouds and rainfall in the Himalayas from satellite data. *Atmospheric Chemistry and Physics* 10, 8305–8317. doi:10.5194/acp-10-8305-2010
- Shuai, J., Zhang, Z., Liu, X., Chen, Y., Wang, P., Shi, P., 2012. Increasing concentrations of aerosols offset the benefits of climate warming on rice yields during 1980–2008 in Jiangsu Province, China. *Regional Environmental Change* 13, 287–297. doi:10.1007/s10113-012-0332-3
- Sigdel, M., Ikeda, M., 2012. Seasonal contrast in precipitation mechanisms over Nepal deduced from relationship with the large-scale climate patterns. *Nepal Journal of Science and Technology* 13, 115–123. doi:10.3126/njst.v13i1.7450
- Singh, R.P., 2004. Variability of aerosol parameters over Kanpur, northern India. *Journal of Geophysical Research* 109, D23206. doi:10.1029/2004JD004966
- Singh, R.P., Kaskaoutis, D.G., 2014. Crop residue burning: A threat to south Asian air quality. *Eos, Transactions American Geophysical Union* 95, 333–334. doi:10.1002/2014EO370001
- Sirois, A., Bottenheim, J.W., 1995. Ambient air concentrations at Kejimikujik National Park, Nova Scotia. *Journal of Geophysical Research* 100, 2867-2881. doi:10.1029/94JD02951
- Soni, V.K., Pandithurai, G., Pai, D.S., 2012. Evaluation of long-term changes of solar radiation in India. *International Journal of Climatology* 32, 540–551. doi:10.1002/joc.2294
- Stanhill, G., Cohen, S., 2001. Global dimming: a review of the evidence for a widespread and significant reduction in global radiation with discussion of its

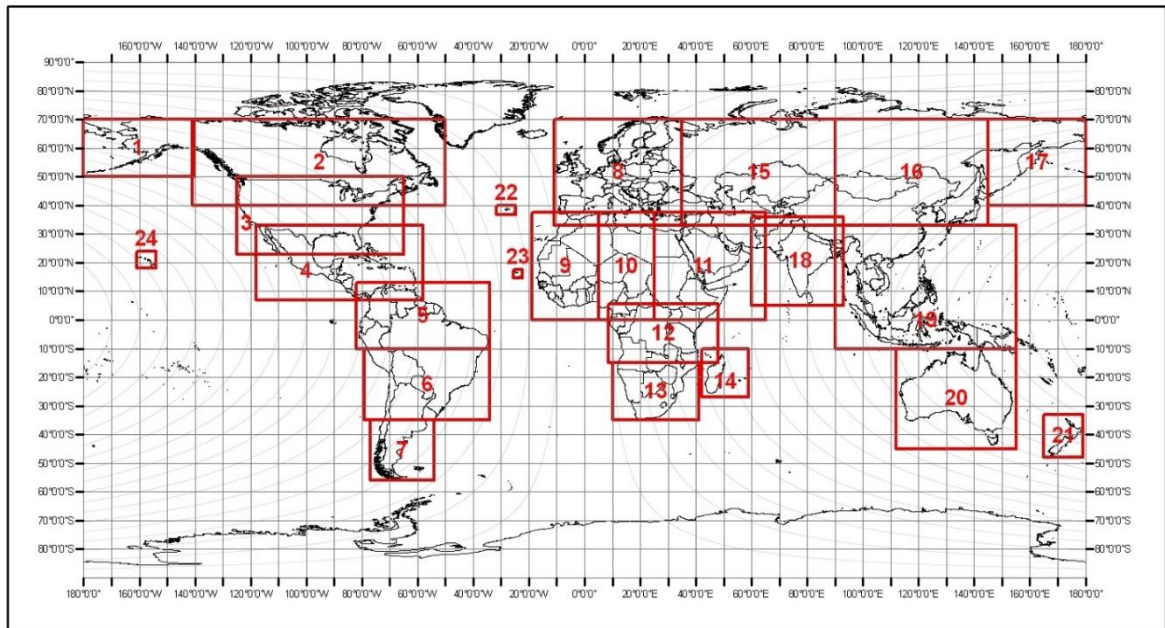
- probable causes and possible agricultural consequences. *Agricultural and Forest Meteorology* 107, 255–278. doi:10.1016/S0168-1923(00)00241-0
- Streets, D.G., 2003. An inventory of gaseous and primary aerosol emissions in Asia in the year 2000. *Journal of Geophysical Research* 108, 8809. doi:10.1029/2002JD003093
- Streets, D.G., Yan, F., Chin, M., Diehl, T., Mahowald, N., Schultz, M., Wild, M., Wu, Y., Yu, C., 2009. Anthropogenic and natural contributions to regional trends in aerosol optical depth, 1980–2006. *Journal of Geophysical Research* 114, D00D18. doi:10.1029/2008JD011624
- Su, L., Yuan, Z., Fung, J. C. H., and Lau, A. K. H., 2015. A comparison of HYSPLIT backward trajectories generated from two GDAS datasets. *Science of the Total Environment* 506-507, 527–537.
- Tang, H., Liu, G., Zhu, J., Han, Y., Kobayashi, K., 2013. Seasonal variations in surface ozone as influenced by Asian summer monsoon and biomass burning in agricultural fields of the northern Yangtze River Delta. *Atmospheric Research* 122, 67–76. doi:10.1016/j.atmosres.2012.10.030
- Tao, W.-K., Li, X., Khain, A., Matsui, T., Lang, S., Simpson, J., 2007. Role of atmospheric aerosol concentration on deep convective precipitation: Cloud-resolving model simulations. *Journal of Geophysical Research* 112, D24S18. doi:10.1029/2007JD008728
- Tripathi, S.N., Pattnaik, A., Dey, S., 2007. Aerosol indirect effect over Indo-Gangetic plain. *Atmospheric Environment* 41, 7037–7047. doi:10.1016/j.atmosenv.2007.05.007
- Twomey, S., 1977. The influence of pollution on the shortwave albedo of clouds. *Journal of the Atmospheric Sciences* 34, 1149-1152.
- Vadrevu, K.P., Ellicott, E., Badarinath, K.V.S., Vermote, E., 2011. MODIS derived fire characteristics and aerosol optical depth variations during the agricultural residue burning season, north India. *Environmental Pollution* 159, 1560–9. doi:10.1016/j.envpol.2011.03.001

- Vadrevu, K.P., Ellicott, E., Giglio, L., Badarinath, K.V.S., Vermote, E., Justice, C., Lau, W.K.M., 2012. Vegetation fires in the Himalayan region – Aerosol load, black carbon emissions and smoke plume heights. *Atmospheric Environment* 47, 241–251. doi:10.1016/j.atmosenv.2011.11.009
- Vadrevu, K.P., Giglio, L., Justice, C., 2013. Satellite based analysis of fire–carbon monoxide relationships from forest and agricultural residue burning (2003–2011). *Atmospheric Environment* 64, 179–191. doi:10.1016/j.atmosenv.2012.09.055
- Vernekar, K.G., Sinha, S., Sadani, L.K., Sivaramakrishnan, S., Parasnis, S.S., Mohan, B., Saxena, S., Dharmaraj, T., Patil, M.N., Pillai, J.S., Murthy, B.S., Debaje, S.B., Bagavathsingh, A., 2003. An overview of the land surface processes experiment (LASPEX) over a semi-arid region of India. *Boundary-Layer Meteorology* 106, 561–572. doi:10.1023/A:1021283503661
- Wang, F., Chen, D. S., Cheng, S. Y., Li, J. B., Li, M. J., and Ren, Z. H., 2010. Identification of regional atmospheric PM10 transport pathways using HYSPLIT, MM5-CMAQ and synoptic pressure pattern analysis. *Environmental Modelling and Software* 25, 927–934.
- Wang, Y., Hao, J., McElroy, M.B., Munger, J.W., Ma, H., Chen, D., Nielsen, C.P., 2009. Ozone air quality during the 2008 Beijing Olympics: effectiveness of emission restrictions. *Atmospheric Chemistry and Physics* 9, 5237–5251. doi:10.5194/acp-9-5237-2009
- Wang, Y., Yang, Y., Han, S., Wang, Q., Zhang, J., 2013. Sunshine dimming and brightening in Chinese cities (1955-2011) was driven by air pollution rather than clouds. *Climate Research* 56, 11–20. doi:10.3354/cr01139
- Wang, Y.Q., Zhang, X.Y., Draxler, R.R., 2009. TrajStat: GIS-based software that uses various trajectory statistical analysis methods to identify potential sources from long-term air pollution measurement data. *Environmental Modelling and Software* 24, 938–939. doi:10.1016/j.envsoft.2009.01.004
- WECS, 2010. Energy Sector Synopsis Report. Kathmandu, Nepal.

- Wild, M., 2009. Global dimming and brightening: A review. *Journal of Geophysical Research* 114, D00D16. doi:10.1029/2008JD011470
- Wild, M., 2012. Enlightening global dimming and brightening. *Bulletin of the American Meteorological Society* 93, 27–37. doi:10.1175/BAMS-D-11-00074.1
- Wild, M., Gilgen, H., Roesch, A., Ohmura, A., Long, C.N., Dutton, E.G., Forgan, B., Kallis, A., Russak, V., Tsvetkov, A., 2005. From dimming to brightening: decadal changes in solar radiation at Earth's surface. *Science* 308, 847–850. doi:10.1126/science.1103215
- Wild, M., Trüssel, B., Ohmura, A., Long, C.N., König-Langlo, G., Dutton, E.G., Tsvetkov, A., 2009. Global dimming and brightening: An update beyond 2000. *Journal of Geophysical Research* 114, D00D13. doi:10.1029/2008JD011382
- WMO, 2003. Equipment and methods of observation, in: *Manual on the Global Observing System: Volume 1 “Global Aspects.”* World Meteorological Organization, Geneva, pp. III–16–III–20.
- WMO, 2011. Characterizing climate from datasets, in: *Guide to Climatological Practices* WMO-NO. 100. World Meteorological Organization, Geneva, pp. 4–1–4–18.
- Xia, X., 2010. Spatiotemporal changes in sunshine duration and cloud amount as well as their relationship in China during 1954–2005. *Journal of Geophysical Research* 115, D00K06. doi:10.1029/2009JD012879
- Yang, X., Asseng, S., Wong, M.T.F., Yu, Q., Li, J., Liu, E., 2013. Quantifying the interactive impacts of global dimming and warming on wheat yield and water use in China. *Agricultural and Forest Meteorology* 182-183, 342–351. doi:10.1016/j.agrformet.2013.07.006
- Yasunari, T.J., Tan, Q., Lau, K.-M., Bonasoni, P., Marinoni, A., Laj, P., Ménégoz, M., Takemura, T., Chin, M., 2013. Estimated range of black carbon dry deposition and the related snow albedo reduction over Himalayan glaciers during dry pre-monsoon periods. *Atmospheric Environment* 78, 259–267. doi:10.1016/j.atmosenv.2012.03.031

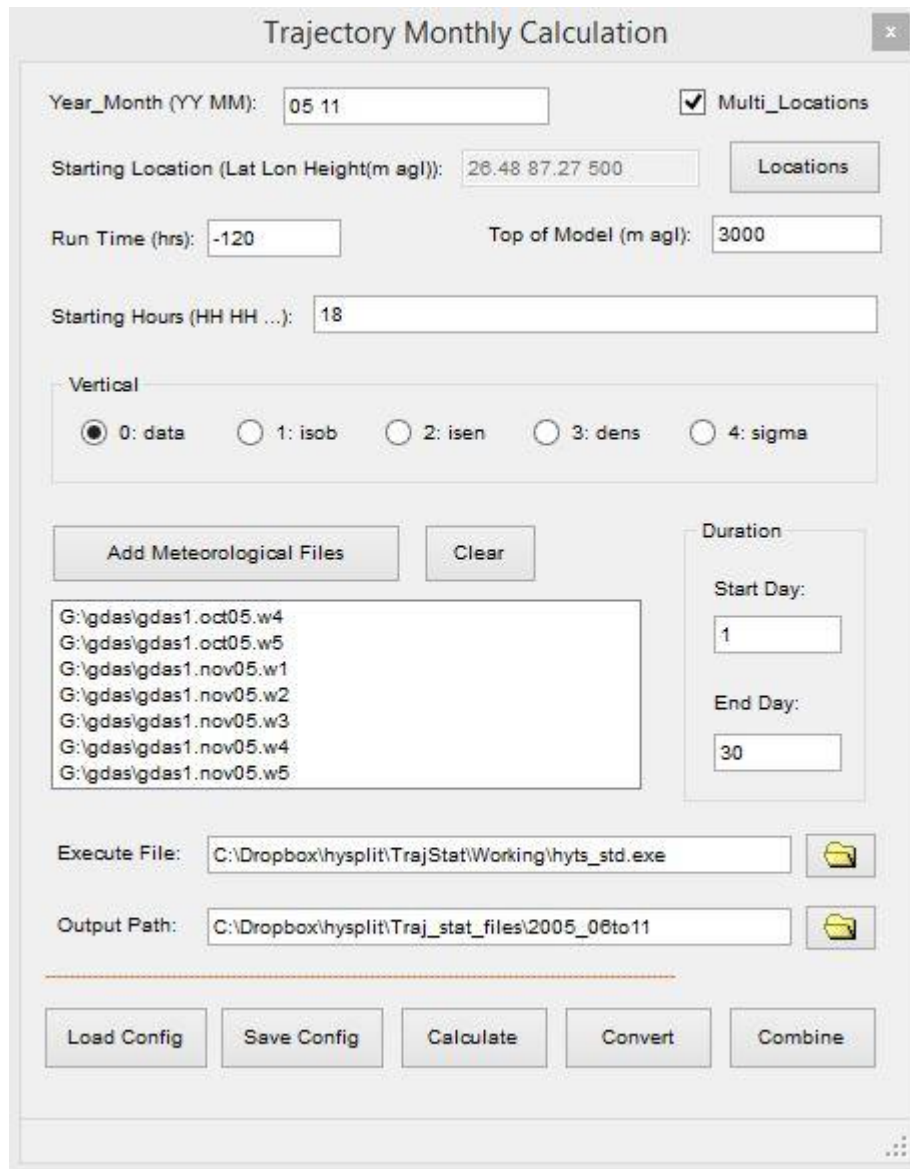
- Ye, J., Li, F., Sun, G., Guo, A., 2009. Solar dimming and its impact on estimating solar radiation from diurnal temperature range in China, 1961–2007. *Theoretical and Applied Climatology* 101, 137–142. doi:10.1007/s00704-009-0213-y
- Yokelson, R.J., Burling, I.R., Gilman, J.B., Warneke, C., Stockwell, C.E., de Gouw, J., Akagi, S.K., Urbanski, S.P., Veres, P., Roberts, J.M., Kuster, W.C., Reardon, J., Griffith, D.W.T., Johnson, T.J., Hosseini, S., Miller, J.W., Cocker III, D.R., Jung, H., Weise, D.R., 2013. Coupling field and laboratory measurements to estimate the emission factors of identified and unidentified trace gases for prescribed fires. *Atmospheric Chemistry and Physics* 13, 89–116. doi:10.5194/acp-13-89-2013
- Yoshida, S., Hara, T., 1977. Effects of air temperature and light on grain filling of an Indica and a Japonica rice (*Oryza sativa* L.) under controlled environmental conditions. *Soil Science and Plant Nutrition* 23, 93-107. doi:10.1080/00380768.1977.10433026

Appendices

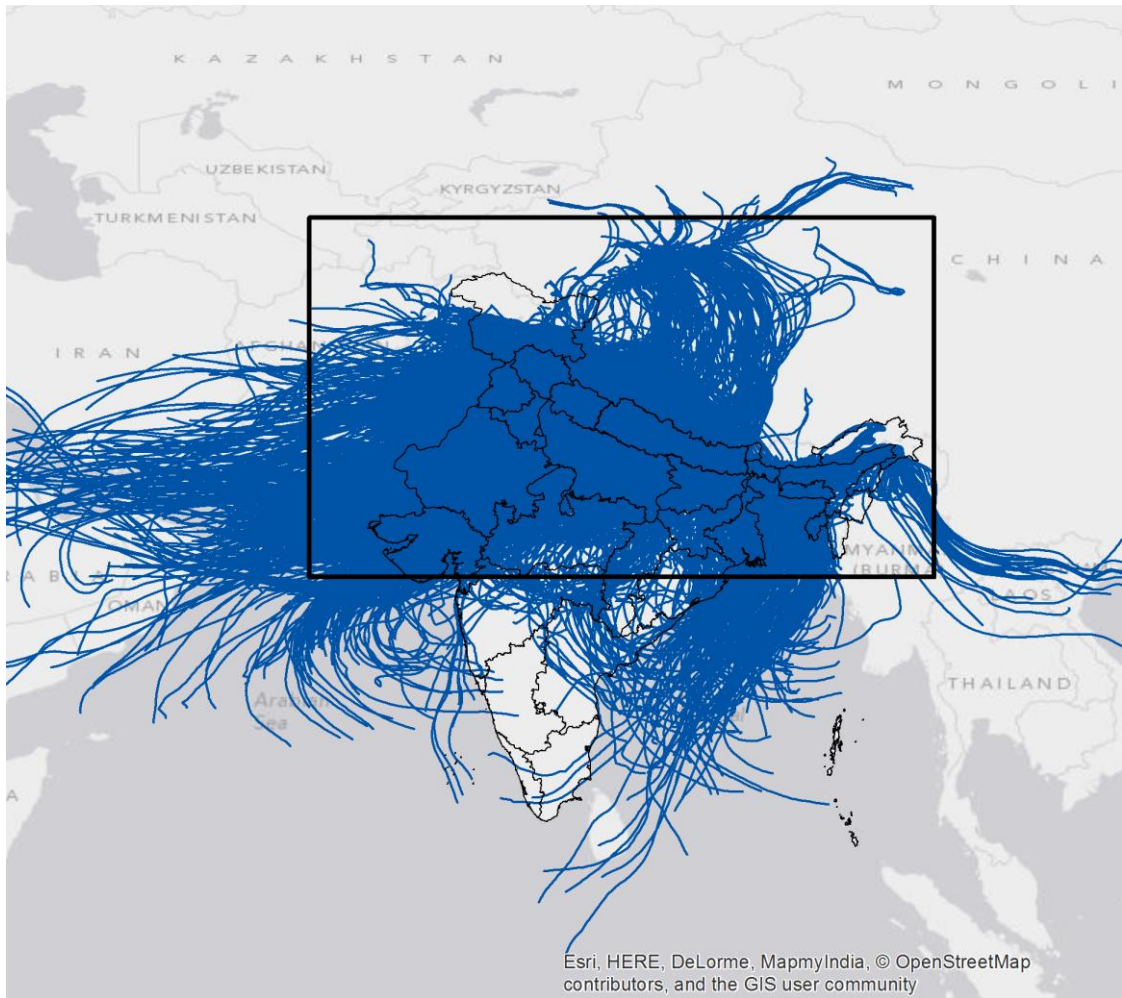


Window Number	Coverage	Min Lon.	Max Lon.	Min Lat.	Max Lat.
18	South Asia	60	93	5	36

Appendix Fig. 1 Coverage of the subset windows used to obtain the MODIS burnt area product.



Appendix Fig. 2 Screen capture of HYSPLIT graphical interface showing parameter settings



Appendix Fig. 3 Daily 5-day backward trajectories of air masses arriving Kathmandu from 2005-2010

Appendix Table 1 All-Nepal inter-annual trends in rainfall (R) ranging from 2 mm to 50 mm across the stations and physiographic regions for the period 1980-2009.

Stations	R<=2mm	R<=5mm	R<=10mm	R>=10mm	R>=15mm	R>=20mm	R>=30mm	R>=35mm	R>=40mm	R>=45mm	R>=50mm
Biratnagar	0.43	0.86*	0.18	0.02	0.14	0.03	-0.04	0.15	0.25	-0.01	0.06
Bhairawaha	0.58	-0.15	-0.05	-0.47	-0.47	-0.61	-0.64	-0.67	-0.87	-0.93	-0.95
Simara	-0.59	-0.59	0.06	0.24	0.29	0.34	0.40	0.45	0.38	0.41	0.19
Dhangadi	0.63	0.05	-0.01	0.73	0.72	0.76	0.93^	1.10^	0.93	1.22^	1.14
Plains	0.25	0.05	0.05	0.15	0.19	0.15	0.19	0.28	0.20	0.21	0.11
Dipayal	0.27	-0.58	-0.83*	-0.42	-0.21	0.19	-0.20	-0.33	-0.08	-0.23	0.00
Surkhet	-0.06	-0.69^	-0.55	0.05	0.09	0.05	0.46	0.44	0.22	-0.08	-0.30
Pokhara	0.22	-0.17	0.09	0.15	0.15	0.26	0.37	0.48	0.54	0.38	0.39
Dhankuta	-0.15	-0.44	-0.40	-0.07	-0.11	-1.41	0.00	-0.13	0.33	0.48	0.72
Kathmandu	-0.81*	0.13	-0.05	0.31	0.43	0.68	0.62	0.46	0.56	1.03	0.74
Low-hills	-0.13	-0.33*	-0.32*	0.07	0.11	0.23	0.33	0.35	0.42	0.32	0.16
Okhaldhunga	-0.61	-0.13	0.02	0.51	0.63	0.71	0.76	0.68	0.97	1.34^	0.99
Taplejung	-0.32	0.32	-0.20	-0.09	-0.18	-0.18	-0.30	-0.24	-0.32	0.00	-0.07
Dadeldhura	-0.56	-0.77*	-0.83*	-0.27	-0.21	-0.21	-0.19	0.06	0.42	0.89	0.90
Jumla	0.44	-0.36	-0.30	-0.79	-0.92	-0.49	-0.48	0.21	-0.20	-0.16	-2.37
High-hills and M	-0.24	-0.19	-0.30*	-0.02	0.01	0.09	0.11	0.22	0.41	0.79	0.13
All-Nepal	-0.09	-0.19^	-0.23*	0.07	0.12	0.17	0.23	0.30	0.33	0.34	0.27

^a Statistical significance of the trends are shown by *** for P<0.001, ** for P<0.01, * for P<0.05 and ^ for P<0.10. Trends with no asterisks were not significantly different from zero.

Appendix Table 2 All-Nepal inter-annual trends in number of rainy days (NRD) with rainfall ranging from 2 mm to 50 mm across the stations and physiographic regions for the period 1980-2009.

Stations	NRD<=2 mm	NRD<=5 mm	NRD<=10 mm	NRD>=10 mm	NRD>=15 mm	NRD>=20 mm	NRD>=30 mm	NRD>=35 mm	NRD>=40 mm	NRD>=45 mm	NRD>=50 mm
Biratnagar	0.27	0.50 [^]	0.33	-0.11	0.28	0.03	-0.13	0.26	0.46	0.00	0.14
Bhairawaha	0.16	-0.15	-0.12	-0.23	-0.13	-0.44	-0.42	-0.45	-0.81	-0.93	-0.97
Simara	-1.16 ^{**}	-0.93 ^{**}	-0.55 [^]	0.12	0.31	0.44	0.67	0.85	0.74	0.85	0.49
Dhangadi	1.13 [*]	0.70 [^]	0.50	0.48	0.37	0.40	0.73	1.04 [*]	0.69	1.21 [*]	1.06
Plains	0.09	0.03	0.04	0.07	0.21	0.12	0.23	0.45	0.30	0.33	0.14
Dipayal	0.49	0.06	-0.15	-0.87 [^]	-0.48	0.23	-0.44	-0.75	-0.51	-0.84	-0.59
Surkhet	-1.94 ^{***}	-1.51 ^{***}	-1.23 ^{***}	-0.02	0.09	0.03	0.93 [^]	1.00 [^]	0.79	0.48	0.25
Pokhara	0.11	-0.12	-0.04	-0.18	-0.24	0.01	0.17	0.38	0.49	0.18	0.18
Dhankuta	-1.05 ^{**}	-0.90 ^{***}	-0.79 ^{***}	-0.14	-0.30	-0.37	-0.13	-0.47	0.02	0.36	0.75
Kathmandu	-0.67 [*]	-0.30	-0.27	0.04	0.22	0.67	0.57	0.32	0.45	1.09 [^]	0.67
Low-hills	-0.62 ^{***}	-0.54 ^{***}	-0.48 ^{***}	-0.20	-0.13	0.11	0.27	0.31	0.43	0.26	0.31
Okhaldhunga	-0.55	-0.35	-0.21	0.20	0.47	0.61	0.64	0.46	0.86	1.43	0.90
Taplejung	0.10	0.31	0.06	0.03	-0.13	-0.10	-0.29	-0.18	-0.31	0.19	0.14
Dadeldhura	0.12	-0.15	-0.34	-0.53	-0.51	-0.63	-0.86	-0.65	-0.28	0.26	0.09
Jumla	0.31	-0.08	-0.14	-0.82 [^]	-1.16 [^]	-0.61	-0.60	0.35	-0.10	-0.03	-2.64
High-hills and M	-0.01	-0.05	-0.14	-0.17	-0.16	-0.04	-0.12	-0.04	0.18	0.70	0.58
All-Nepal	-0.23 [*]	-0.23 ^{**}	-0.23 ^{***}	-0.12	-0.03	0.07	0.17	0.29 [^]	0.33 [^]	0.37 [^]	0.25

^a. Statistical significance of the trends are shown by ^{***} for P<0.001, ^{**} for P<0.01, ^{*} for P<0.05 and [^] for P<0.10. Trends with no asterisks were not significantly different from zero.